Identification and Adaptive Control for High-performance AC Drive Systems

by

David M. Reed

A dissertation submitted in partial fulfillment
of the requirements for the degree of
Doctor of Philosophy
(Electrical Engineering: Systems)
in The University of Michigan
2016

Doctoral Committee:

Associate Professor Heath Hofmann, Co-chair
Professor Jing Sun, Co-chair
Professor Jessy Grizzle
Professor Ilya Kolmanovsky

In loving memory of my uncle Davi,
for inspiring my love of science and interest in electrical engineering.

And to my family,
for all of your love, support, and understanding.

ACKNOWLEDGEMENTS

I would like to begin by expressing my deep gratitude to my advisors, Professors Jing Sun and Heath Hofmann, for their support, guidance, and mentorship over the past four-plus years. While it took me some time to adapt (pun intended) to her advising style, I am grateful for Professor Sun's persistence and patience while pushing me to realize my potential as an academic researcher more fully. I also greatly appreciate her use of controls themed analogies in our weekly discussions.

Additionally, I owe a great deal of thanks to Professor Hofmann for bringing me to Michigan and allowing me the freedom to pursue my research interests, even when they tilted more towards controls than power and energy. I first starting working with Heath back when I was a master's student at Penn State, before I even knew what a Lyapunov function was, and I am glad that I was able to earn my PhD under his supervision as well.

I also wish to thank Professor Jessy Grizzle, not only for serving on my committee, but also for answering my questions and offering advice over the past few years. From letting me borrow his office phone to call campus security when I locked myself out of the lab after hours, to engaging in insightful discussions regarding my research (and sometimes just controls in general). I am fortunate to have had the opportunity to take his Nonlinear Systems and Control course, and have surely benefited from his presence here at Michigan.

Additionally, I would like to thank Professor Ilya Kolmanovsky for serving on my dissertation committee, as well as for his helpful suggestions and discussions throughout the process. I don't think I could have found a better cognate member for my dissertation committee.

I am also grateful to Professors Necmiye Ozay and Ian Hiskens for letting me pick their brains from time to time. I was fortunate to have had the opportunity to GSI Linear Systems Theory during my time at Michigan, working with Professor Ozay. While time consuming, it was a very rewarding experience.

I would also like to express my sincere gratitude to Rebecca "Becky" Turanski and Michele "Shelly" Feldkamp for all of their help, hard work, and just generally making the department a more pleasant place to work.

Throughout my studies at Michigan, as well as Penn State, I was lucky to have had so many excellent teachers - Professors Jim Freudenberg, Jessy Grizzle, Laura Balzano, Chris Rahn, Jack Langelaan, Jeff Schiano, Jack Mitchell, and Javier Gómez-Calderón, to name just a few.

I am also grateful for the help of my labmates, particularly Kan Zhou, Abdi Zenyu, and Jun Hou, who spent a considerable amount of time helping collect data for the induction machine work presented in this dissertation. And also Vicky Cheung, who has been the best undergraduate lab assistant one could ask for.

I would be remiss not to acknowledge the many friends and classmates here at Michigan who have made the process of completing this degree not only more bearable, but enjoyable - Mai Le, Aaron Stein, Ian Beil, Rob Vandermeulen, Nick Asendorf, Madison McGaffin, Matt Prelee, JJ Lipor, Mads Almassalkhi, Hamid Ossareh (who was also the best GSI I've ever had), Steph Crocker, Greg Ledva, as well as the members of the RACElab group (for all of their helpful feedback on papers and presentations). I am also grateful to the "Snarky Comments" crew for welcoming me into their group and the continuing friendships. My time in the Mitten would not have been the same without Formal Tailgates, Snarky Christmas, and other gatherings which left me sore from laughter.

Finally, I would like to thank my family for all of their love and support.

*My sincere apologies to anyone I have forgotten!

TABLE OF CONTENTS

LIST OF FIGURES

Figure

LIST OF TABLES

Table

ABSTRACT

Identification and Adaptive Control for High-performance AC Drive Systems
by
David M. Reed

Co-Chairs: Heath Hofmann and Jing Sun

High-performance AC machinery and drive systems can be found in a variety of applications ranging from motion control to vehicle propulsion. Such applications typically require high-bandwidth and tight regulation of position, speed and/or torque over a wide range of operating conditions. However, machine parameters can vary significantly with electrical frequency, flux levels, and temperature, degrading the performance of the drive system. While adaptive control techniques can be used to estimate machine parameters online, it is sometimes desirable to estimate certain parameters offline. Additionally, parameter identification and control are typically conflicting objectives with identification requiring plant inputs which are rich in harmonics, and control objectives often consisting of regulation to a constant set-point. In this dissertation, we present research which seeks to address these issues for high-performance AC machinery and drive systems.

The first part of this dissertation concerns the offline identification of induction machine parameters. Specifically, we have developed a new technique for induction machine parameter identification which can easily be implemented using a voltage-source inverter. The proposed technique is based on fitting steady-state experimental data to the circular stator current locus in the stator flux linkage reference-frame for varying steady-state slip frequencies, and provides accurate estimates of the magnetic parameters, as well as the rotor resistance and core loss conductance. This approach allows leakage inductance and rotor resistance to be accurately estimated while avoiding the difficulties associated with inverter-based implementations of the standard locked-rotor test. Experimental results for a 43 kW induction machine are

provided which demonstrate the utility of the proposed technique by characterizing the machine over a wide range of flux levels, including magnetic saturation.

The remainder of this dissertation concerns the development of generalizable design methodologies for Simultaneous Identification and Control (SIC) of overactuated systems via case studies with Permanent Magnet Synchronous Machines (PMSMs). Specifically, we present two different approaches to the design of adaptive controllers for PMSMs which exploit overactuation to achieve identification and control objectives simultaneously. The first approach, termed "Adaptive Excitation Decoupling", utilizes a disturbance decoupling control law to prevent the excitation input from perturbing the regulated output. Machine parameters used in the control law are updated online via a normalized gradient estimator. The second approach uses a Lyapunov-based inner-loop adaptive controller to constrain the states to the output error-zeroing manifold, defined by the torque output mapping, on which they are varied to provide excitation for parameter identification. Finally, the issue of input selection (i.e., excitation input design and control allocation) is addressed for the Lyapunov-based design by incorporating a receding-horizon control allocation which includes a metric for generating persistently exciting reference trajectories. While both approaches are shown to achieve the SIC objective, and each hold promise for generalization, the Lyapunov-based design has robustness and stability advantages over the Adaptive Excitation Decoupling approach.

CHAPTER I

Introduction

This dissertation describes a series of related research efforts aimed at advancing the state-of-the-art in identification and control for high-performance AC motor drive systems, with the secondary goal of developing control methodologies for simultaneous identification and control of overactuated systems. Motivated by the rising interest in electric propulsion for vehicular applications, as well as the desire to fully utilize the capabilities of the AC machines used in such applications, we consider the problems of offline identification of induction machine parameters and simultaneous identification and torque regulation of Permanent Magnet Synchronous Machines (PMSMs). In particular, Simultaneous Identification and Control (SIC) of PMSMs will serve as a testbed for SIC methodologies for overactuated systems.

1.1 Motivation and Overview

These days, high-performance AC machinery and drive systems can be found in a variety of applications ranging from motion control (servo drives) to vehicle propulsion (traction drives). The distinguishing feature of high-performance drives, as opposed to lower performance industrial drives (e.g., for pumps and fans), is the need for high-bandwidth (i.e., fast response times) and tight (i.e., high accuracy) regulation of position, speed and/or torque [12]. While the low cost of electronic components, particularly powerful microprocessors, continues to make electric drives a cost-effective alternative for applications once dominated by mechanical systems, there are other advantages as well. For instance, the dynamics of electrical systems are typically much faster than those of mechanical systems, and the routing of wiring for electrical power (and control signals) is often easier than lines for fuel and hydraulic fluid. Furthermore, when properly designed, electrical systems are typically more reliable than mechanical systems due to a reduction in moving parts which are susceptible

to wear-and-tear. Additionally, high-performance AC machinery and drive systems are capable of delivering impressive performance, particularly in terms of low-speed torque (see Figure 1.1 for an example), making AC machines an attractive alternative to SI engines for vehicle propulsion.

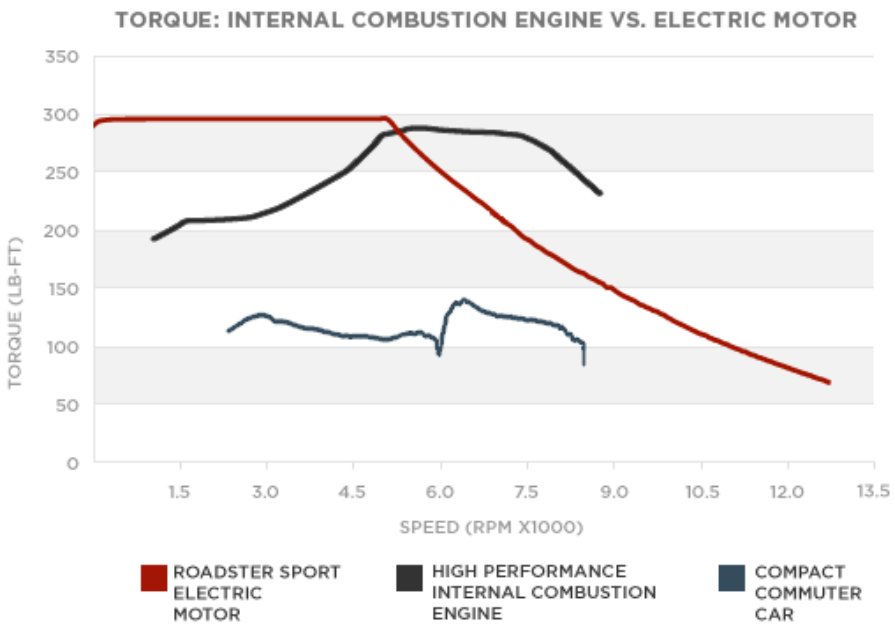

Figure 1.1: Comparison of torque-speed curves for Tesla induction motor and conventional IC engines [1].

Interest in hybrid and electric vehicles has increased greatly over the past decade due to the rising cost of energy along with environmental concerns and government mandates. While electric drives are a fairly mature technology, their use in vehicle propulsion applications presents some unique challenges when it comes to maintaining a high level of performance over a very wide speed range, and under a variety of operating conditions (loads, temperatures, etc.). Machine parameters can vary significantly [7, 38, 40, 41] with electrical frequency, flux levels, and temperature. For instance, resistance can increase by as much as 100% with temperature [39], while inductances vary significantly when high flux levels cause magnetic saturation. Additionally, the sensitivity of the permanent magnet flux linkage to a 100°C rise in temperature in ferrite, neodymium, and samarium cobalt magnets are -19%, -12%, and -3%, respectively, from nominal [39]. These variations tend to "detune" the electric drive's control system, degrading its performance. In particular, since torque isn't

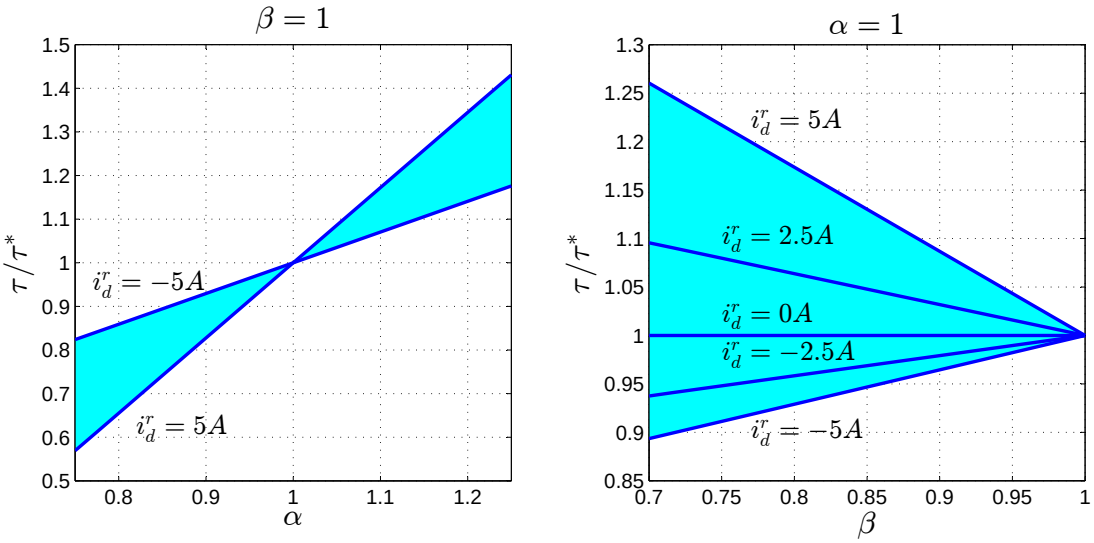

Figure 1.2: Example of steady-state torque errors (ratio) in a PMSM drive for variations in the permanent magnet flux linkage (left) and quadrature-axis self-inductance (right) for a variety of direct-axis currents. The following machine parameters were used to generate these plots: $L_d = 212.3\,\mu$H, $L_q = 1.274\,$mH, and $\Lambda_{PM} = 12.644\,$m-Vsec.

directly measured due the impracticality[1] of fielding torque sensors, the accuracy of the regulated torque is therefore sensitive to variations in parameters which appear in the torque output mapping (e.g., inductance and permanent magnet flux linkage). For example [39], the ratio of the regulated torque output, τ, of a PMSM drive to its reference, τ^*, is given by

$$\frac{\tau}{\tau^*} = \frac{(L_d - \beta L_q) i_d^r + \alpha \Lambda_{PM}}{(L_d - L_q) i_d^r + \Lambda_{PM}}, \tag{1.1}$$

where i_d^r is the direct-axis current, L_d is the direct-axis inductance, L_q is the quadrature-axis current, and Λ_{PM} is the permanent magnet flux linkage. The scalars α and β are introduced to represent errors in the permanent magnet flux linkage and quadrature-axis inductance, respectively. This ratio (1.1) is plotted in Figure 1.2 for a range of uncertainty and direct-axis currents, using machine parameters provided in the caption. Thus, accurate knowledge of machine parameters, including their variations, is key to maintaining high-performance in electric drive systems. This is particularly true in all-electric vehicles where it is desirable to run the machine in maximally-efficient operation points which depend upon the parameters of the machine.

[1]Torque transducers are expensive and their calibration is sensitive to environmental conditions, making them unsuitable for use in field applications (e.g., electric vehicles).

While parameter identification and adaptive control are mature fields of study, their application in practice still tends to be challenging. In particular, the need for inputs to the system under identification and/or control to be *persistently exciting* fundamentally conflicts with typical control objectives (e.g., set-point regulation), particularly in transportation applications where rider comfort would be negatively impacted by any large perturbations. In applications where accurate parameter knowledge is important, it is therefore of interest to ensure that the system is persistently excited while eliminating, or at least minimizing, the impact of that excitation on the regulated outputs. Overactuated systems[2] provide an opportunity to achieve persistent excitation and output regulation objectives simultaneously. In AC machines, the reduced-order two-phase equivalent models have two control inputs, the direct and quadrature-axis voltages, and a single performance output, electromagnetic torque, to be regulated. Thus, AC machines are an example of an overactuated system.

In this dissertation, we present research which seeks to address many of these issues for high-performance AC machinery and drive systems, as well as investigation of methodologies for simultaneous identification and control of overactuated systems. Previous research of the authors demonstrated the use of an adaptive rotor resistance estimator for improving the performance of direct field-oriented torque regulation for induction machines in the presence of rotor resistance variations [63, 65]. While this dissertation will not cover field-oriented control of induction machines, the need for accurate parameter knowledge in such controllers motivates our first research project; a new offline technique for improved identification of induction machine parameters over a wide range of operating conditions [64]. In particular, our offline technique provides accurate estimates of the magnetic induction machine parameters as well as the rotor resistance and core loss conductance, which may be used in a field-oriented controller to achieve high-performance torque regulation over a wide operating range that includes magnetic saturation. The remainder of this dissertation covers research which concerns the development of simultaneous identification and control methodologies for overactuated systems via case studies with Permanent Magnet Synchronous Machines (PMSMs) [66, 67]. More specifically, we will present two different approaches, the first of which utilizes a disturbance decoupling control law to prevent excitation for parameter identification from perturbing the regulated output. The second approach uses an inner-loop Lyapunov-based adaptive controller to ensure

[2]We use the term "overactuated" to refer to systems which have strictly more inputs than outputs to be controlled.

that the states asymptotically track persistently exciting filtered reference commands generated by a static control allocation based on the torque output mapping, thereby constraining the states to the manifold described by the output mapping. Finally, the second approach is modified to use a receding horizon control allocation which generates persistently exciting reference trajectories while also ensuring that the output regulation objective is achieved.

Since the research to be discussed in this dissertation concerns the application of system identification and adaptive control techniques to electric machinery and drive systems, some basic background in these areas will be discussed. Following the general background discussions, we will discuss the state-of-the-art in offline induction machine parameter identification, as well as simultaneous identification and control. Additional literature pertaining to adaptive control of PMSMs in general, will be discussed at the beginning of Chapter 3. Finally, we will outline the open issues which will be addressed as well as the specific contributions of this dissertation.

1.2 Background and the State of the Art

1.2.1 Background on Electric Machinery and Drive Systems

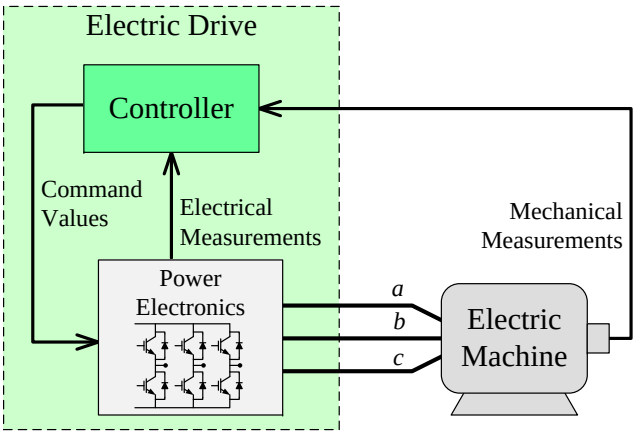

Figure 1.3: Drive system architecture.

The term "electric drive" generally refers to the power electronics, controller and electrical sensors required to operate an electric machine in applications where tight control over torque and/or speed is desired. The basic motor drive system architecture is shown in Figure 1.3. It should be noted that, while the focus of this dissertation is the identification and adaptive control of 3-phase AC machines, the control techniques used are based on a two-phase equivalent model. The use of two-phase models is

common practice, as it leads to reduced order models which are easier to work with, and may be extended to higher-than-three-phase machines as well.

Assuming that the machine is balanced in its construction, the 3-phase stator currents sum to zero, and so the machine dynamics are adequately captured by two electrical states, rather than three. Intuitively, the main principle of operation in (rotating) electric machines is the generation of a rotating magnetic field, which only requires two phases to achieve. The reason three phases are used in practice is that it eliminates the need for a fourth "return" conductor in the AC distribution system. The mapping from 3-phase $(a-b-c)$ variables to equivalent 2-phase $(d-q)$ is generally referred to as the Clarke transform, named after Edith Clarke [14]:

$$\begin{bmatrix} x_d \\ x_q \\ x_0 \end{bmatrix} = \begin{bmatrix} 2/3 & -1/3 & -1/3 \\ 0 & \sqrt{3}/3 & -\sqrt{3}/3 \\ 1/3 & 1/3 & 1/3 \end{bmatrix} \begin{bmatrix} x_a \\ x_b \\ x_c \end{bmatrix} = \mathbf{T}_{23} \begin{bmatrix} x_a \\ x_b \\ x_c \end{bmatrix} . \tag{1.2}$$

Likewise, the inverse Clark transform is given by

$$\begin{bmatrix} x_a \\ x_b \\ x_c \end{bmatrix} = \begin{bmatrix} 1 & 0 & 1 \\ -1/2 & \sqrt{3}/2 & 1 \\ -1/2 & -\sqrt{3}/2 & 1 \end{bmatrix} \begin{bmatrix} x_d \\ x_q \\ x_o \end{bmatrix} = \mathbf{T}_{23}^{-1} \begin{bmatrix} x_d \\ x_q \\ x_o \end{bmatrix} = \mathbf{T}_{32} \begin{bmatrix} x_d \\ x_q \\ x_o \end{bmatrix} . \tag{1.3}$$

However, a simplification can be made by noting that the zero sequence component (x_o) is equal to zero under our assumption of balanced construction and operation. This leads to the following mapping referred to as the Modified Clark transform (1.4)

$$\begin{bmatrix} x_d \\ x_q \end{bmatrix} = \begin{bmatrix} 1 & 0 \\ \frac{\sqrt{3}}{3} & \frac{2\sqrt{3}}{3} \end{bmatrix} \begin{bmatrix} x_a \\ x_b \end{bmatrix} . \tag{1.4}$$

Additionally, we note that the transform used in this dissertation is scaled such that the *peak values* of the 3-phase sinusoidal electrical variables are preserved in the 2-phase representation.

In this dissertation, the machines are assumed to be fed by a Voltage Source Inverter (VSI) (see Figure 1.4), which generates Pulse-Width Modulated (PWM) (see Figure 1.5) versions of the sinusoidal voltages commanded by the control algorithm. The primary advantage of using PWM voltages is a large reduction in converter losses since the VSI transistors, which serve as "switches", are never operated in their "linear" region for an extended period of time, but instead alternate between "ON" and "OFF" states. The drawbacks are the generation of Electromagnetic Interference

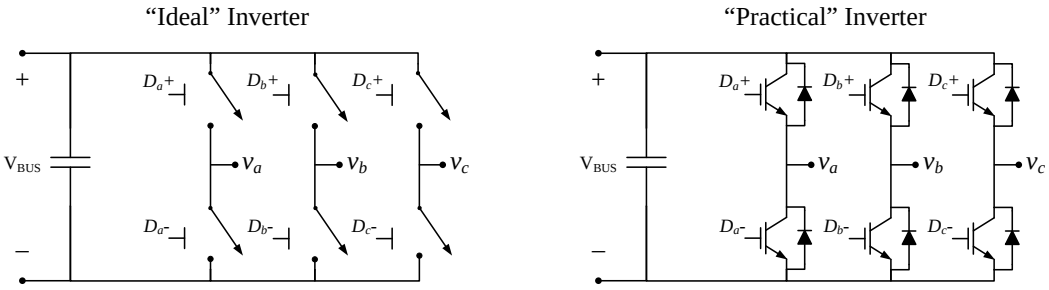

Figure 1.4: Ideal (left) and practical (right) three-phase VSIs.

(EMI), and that *hard-switching* (i.e., switching when there is an overlap in voltage across the device and current through it) increases stress on switching devices, winding insulation, and even machine bearings. By synchronizing the switching of the transistors and the sampling of the Analog-to-Digital Converters (ADCs), we avoid any spurious measurements due to EMI; while other design choices can help mitigate the other issues associated with hard-switching (e.g., using a motor with inverter-duty rated insulation).

The inverter is typically treated as "ideal" when designing the control algorithm in that current harmonics generated by switching are neglected, save the desired fundamental frequency, as well as the dead-time effect and voltage limitations. The justification for this comes from average-value modeling [69], which holds provided that the switching frequency, f_{sw}, is sufficiently higher than that of the maximum fundamental frequency, f_{max}. A typical rule-of-thumb is that $f_{sw} \geq 21 f_{max}$ [57]. In terms of control, the VSI may be viewed as the actuator used to control the AC

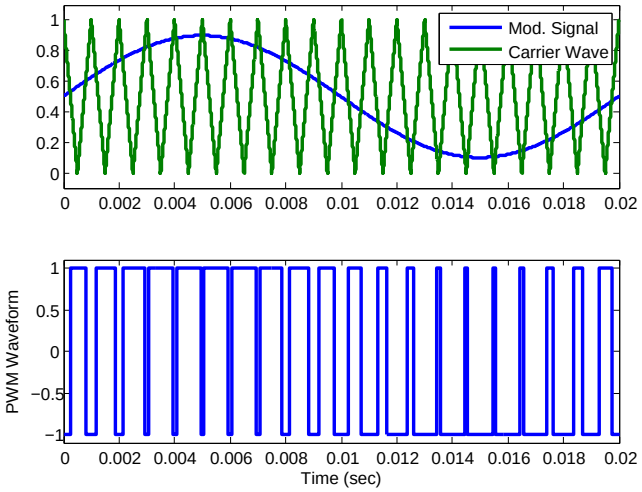

Figure 1.5: Generation of sinusoidal PWM waveform.

machine, and our dynamic AC machine models will therefore take the stator voltages to be the *inputs* to the dynamics, while currents and/or flux linkages will serve as the *states*. Our *measured outputs* will typically be the stator currents, as well as the rotor speed and/or position. Electromagnetic torque will generally serve as our *performance* (or *regulated*) *output*, which is unmeasured due to the impracticality of measuring torque.

Finally, it is noted that modern control of AC machines is typically based on what are referred to as Field-Oriented Control (FOC) techniques. The basic premise of FOC is to perform the actual control (e.g., current regulation) in a rotating reference frame. This approach has several advantages:

1. Sinusoidal electrical variables are transformed into constant values in such reference frames under steady-state conditions. This allows the use of conventional control techniques, such as PI compensation, to regulate the stator currents of the machine.

2. Further simplification of the AC machine dynamics. For example, in synchronous machines, representing the dynamics in a reference frame aligned with the rotor position eliminates nonlinear terms associated with the EMF.

3. Additionally, for both synchronous and induction (a.k.a. asynchronous) machines, the expressions relating electrical variables (e.g., currents and flux linkages) to the electromagnetic torque are simplified, which is advantageous as these expressions are used to generate the command values for regulating the electrical states in order to achieve a desired torque.

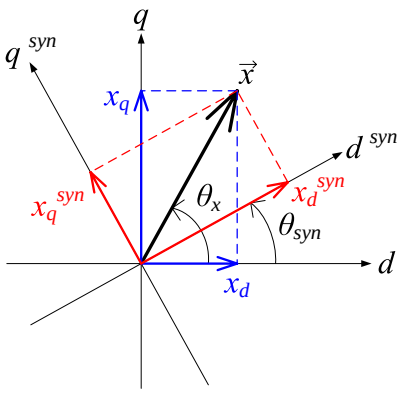

Figure 1.6: Vector diagram depicting the Park transform of an arbitrary vector.

The projection of electrical variables into a rotating reference frame (Figure 1.6) is typically referred to as the Park transform, named for R.H. Park who published the first papers in 1929 [59] detailing the application of reference frame theory to the analysis of AC machines. Starting from two-phase equivalent variables and using notation from Fig. 1.6, the Park transform is simply given by,

$$\vec{x}^{syn} = \begin{bmatrix} x_d^{syn} \\ x_q^{syn} \end{bmatrix} = \begin{bmatrix} \cos(\theta_{syn}) & \sin(\theta_{syn}) \\ -\sin(\theta_{syn}) & \cos(\theta_{syn}) \end{bmatrix} \begin{bmatrix} x_d \\ x_q \end{bmatrix} = e^{-\mathbf{J}\theta_{syn}} \vec{x}, \tag{1.5}$$

where $\mathbf{J}$ is the 90° counter-clockwise (CCW) rotation matrix:

$$\mathbf{J} = \begin{bmatrix} 0 & -1 \\ 1 & 0 \end{bmatrix}.$$

For completeness, the inverse Park transform is simply given by,

$$\vec{x} = \begin{bmatrix} x_d \\ x_q \end{bmatrix} = \begin{bmatrix} \cos(\theta_{syn}) & -\sin(\theta_{syn}) \\ \sin(\theta_{syn}) & \cos(\theta_{syn}) \end{bmatrix} \begin{bmatrix} x_d^{syn} \\ x_q^{syn} \end{bmatrix} = e^{\mathbf{J}\theta_{syn}} \vec{x}^{syn}. \tag{1.6}$$

1.2.2 State-of-the-Art in Offline Identification of Induction Machine Parameters

Historically, induction machines have been the industrial workhorse while permanent magnet machines have dominated high-performance applications. However, advancements in their design and control have made induction machines a viable alternative to permanent magnet machines in automotive applications (e.g., the Tesla Model S) where ruggedness and the absence of expensive rare-earth magnets are desirable characteristics. Nevertheless, the challenge remains that high-performance control techniques for induction machines, such as field-oriented control, require accurate knowledge of the machine parameters [41].

Over the past few decades, a considerable amount of attention has been given to the online identification of the rotor time constant and/or rotor resistance, e.g. [32, 42, 55, 63, 75, 81, 85], as these parameters can vary significantly with temperature, leading to severe detuning in both direct and indirect field-oriented controllers [7, 41]. In addition to the rotor time constant, online techniques have been proposed for other machine parameters as well, e.g., [25, 50, 61, 73]. However, the added complexity and design difficulty of adaptive parameter estimation might not be appropriate for some applications. Furthermore, since the variations in some machine parameters, such as

the inductances, may be modeled as functions of known or measurable variables such as flux linkage magnitude [24], offline identification of such machine parameters for non-adaptive control methodologies is a viable alternative.

The IEEE standard for induction machine parameter identification [2] uses no-load and locked-rotor tests for offline parameter identification. However, accurate parameter estimation using the standard requires special equipment to conduct these tests. For example, it is recommended that locked-rotor tests be conducted at electrical frequencies close to typical slip frequencies (e.g., 25% of rated frequency) to obtain accurate leakage inductance and rotor resistance estimates. While a voltage-source inverter could be used to generate voltages with such a frequency, the presence of switching harmonics in the output voltage complicates voltage measurements, unless the inverter has a significant output filter. An alternative to measuring the voltage is to calculate the voltage from the inverter duty cycles and bus voltage. However, transistor voltage drops and the deadtime effect [7] make it difficult to accurately determine output voltages when they are small, as in the case of the locked-rotor test.

Alternatives to the IEEE standard for offline identification of induction machine parameters have been proposed, which can generally be categorized as using either transient measurements (e.g., [21, 35, 46, 68, 70, 80]) for parameter identification, or steady-state measurements (e.g., [3,4,43,58]), like the technique proposed in this dissertation. In [3], an adaptive (search boundary) genetic algorithm is used to identify machine parameters, while a more recent paper [4] has proposed using the Levenberg-Marquardt algorithm, commonly used to solve nonlinear least-squares problems, to estimate induction machine parameters. Other approaches have been proposed as well [43, 58] which use variable frequency tests at a standstill (i.e., zero rotor speed) to estimate parameters. However, none of these papers [3,4,21,35,43,46,58,68,70,80] considers core loss in their parameter identification, which can influence the accuracy of estimated parameters [8, 79]. Nor is the characterization of magnetic saturation considered beyond noting that it can have an influence on the accuracy of estimated parameters [35, 43, 46, 58, 68, 70]. Finally, the value-added by estimating the core loss conductance and saturation characteristics is that knowledge of these parameters, and their variations, may be used in the control law (e.g., [24] for inclusion of saturation, and [79] for core loss) as well as for loss estimation and/or minimization (e.g., [23]).

1.2.3 Background on Parameter Identification and Adaptive Control

Model-based control requires reasonably accurate knowledge of the plant parameters. While there are a number of ways to determine the plant parameters, a common approach is to fit an input-output model of the plant to experimental data obtained by exciting the plant dynamics with a known input and measuring the output response. This identification process may be done "offline" when the plant parameters either a) don't vary significantly, or b) vary in a known or repeatable manner. As mentioned in the previous section, the inductances of an AC machine can be modeled as nonlinear functions of flux linkage magnitude to capture saturation effects. The saturation characteristics don't vary significantly with temperature or time, and can therefore be identified offline and "hard-coded" in the controller. The plant parameters may also be identified "online" in real-time when there is an immediate need or use for that information, such as condition monitoring and fault detection, for example.

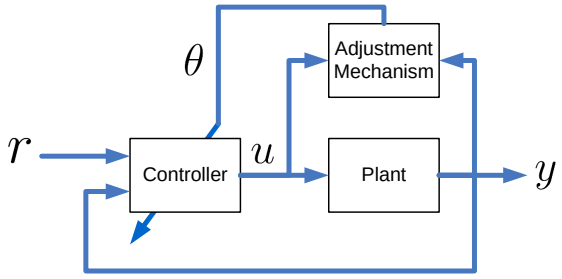

Figure 1.7: Typical structure of adaptive controllers.

Online identification is typically performed in the context of adaptive control. As used in this document, the term *adaptive control* refers to a control methodology in which control law parameters are updated in real-time via a parameter identification algorithm. The typical structure of an adaptive controller is shown in Figure 1.7. A common design approach for adaptive control, which we have used in our research, is the so-called *certainty equivalence principle* in which the control law is designed first assuming that the plant parameters are known, and then an adaptive law is designed to estimate those parameters. Thus, as the parameter estimates converge to their true values, the performance of the adaptive controller tends to the desired performance of the certainty equivalence design.

To identify the plant parameters, linear parametric models of the following form are often used,

$$z(t) = \theta^T \phi(t), \tag{1.7}$$

where z and ϕ consist of measurable signals, and θ consists of the plant parameters

we want to identify. Note that in general z is a vector (often a scalar), while ϕ and θ are either vectors or matrices, depending on the particular application. Additionally, it should be noted that z and ϕ often contain time-differentiated versions of measured signals, which are typically "estimated" by filtering [28]; this will be discussed in more detail later when it is needed. Identifying the plant parameters can be thought of as an optimization problem which seeks to find the estimated parameters, $\hat{\theta}$, which minimize the difference between the measured signal, z, and its estimated value $\hat{z} = \hat{\theta}^T\phi$ (assuming z and ϕ are bounded), e.g.:

$$\min_{\hat{\theta}} \frac{1}{2}\|z - \hat{\theta}^T\phi\|_2^2 \tag{1.8}$$

Parameter estimates are often obtained using the familiar gradient-descent and least-squares algorithms [28]. However, an important sufficient condition for the estimated parameters to converge to their true values (i.e., $\hat{\theta} \to \theta$ as $t \to \infty$) is that the regressor $\phi(t)$ be *persistently exciting*:

Definition I.1. (Persistence of Excitation (PE) [28]): A piecewise continuous signal vector $\phi : \mathbb{R}^+ \mapsto \mathbb{R}^n$ is said to be **persistently exciting** in $\mathbb{R}^n$ with a level of excitation $\alpha_0 > 0$ if there exist constant scalars $\alpha_1, T_0 > 0$ such that

$$\alpha_1\mathbf{I} \geq \frac{1}{T_0}\int_t^{t+T_0} \phi(\sigma)\phi^\top(\sigma)d\sigma \geq \alpha_0\mathbf{I}, \quad \forall\, t \geq 0. \tag{1.9}$$

While we won't get into the details here, the persistence of excitation condition on the regressor is key to proving that the parameter error, $\tilde{\theta} = \hat{\theta} - \theta$, goes to zero. A rule of thumb is that the input to the system under identification must contain at least one distinct frequency component for every two parameters to be identified; this condition is referred to as *sufficient richness* [28].

Analysis of closed-loop adaptive control systems tends to be rather challenging since even when the plant under control is linear-time invariant (LTI), the closed-loop system under adaptive control is nonlinear. This is particularly true when the control law and parameter estimator are designed separately, and then simply "plugged" together to form an adaptive controller. So, even though combining, say, a least-squares parameter estimator with a particular control law to form an adaptive controller is an intuitive and easy design approach, it is typically very challenging to prove closed-loop stability for such a design.

An alternative approach is to formulate a control law based on the certainty equivalence principle, and then design the parameter estimator (or update law) such that it ensures the closed-loop system is stable in the presence of parameter uncertainty, using a Lyapunov stability analysis. Essentially, what happens is that the adaptive law is designed to cancel the indefinite terms which appear when the Lyapunov function candidate is differentiated with respect to time, ensuring that the derivative of the Lyapunov function is negative semi-definite for all time, t, and that the closed-loop system is therefore stable in the sense of Lyapunov. Barbalat's lemma [28, 33, 71] is then typically used to prove asymptotic stability of the closed-loop adaptive control system. While this design approach is generally more involved than the "plug-and-play" approach using linear parametric models and least-squares (or gradient descent) algorithms, it has the advantage of coming with a stability proof. However, the difficulty associated finding a Lyapunov function, if possible, limits the general applicability of this approach.

1.2.4 State-of-the-Art in Simultaneous Identification and Control

As noted earlier, identification and control are typically conflicting objectives. For identification, we need to select plant inputs such that the plant dynamics are persistently excited, which typically involves signals which are rich in harmonic content. However, for output regulation, we are typically interested in tracking some reference value, often a constant set-point, which may not provide sufficient excitation for parameter convergence. For single-input single-output (SISO) systems, this is an unavoidable trade-off between output regulation and parameter identification.

One approach to handling this trade-off is the so-called "dual control", introduced by Feldbaum in 1960 [15]. The dual control input is derived by solving a stochastic optimal control problem which seeks to balance the trade-off between maintaining tight control and small parameter estimation errors. A key characteristic of dual control is that the control law is a function of the estimated parameters as well as their uncertainties, similar to how a Kalman filter estimates states along with the noise covariance. However, analysis requires nonlinear stochastic control theory, and solutions to the optimal dual control problem are challenging if not impossible to find for all but simple problems [84]. For this reason, there has been a fair amount of interest in finding approximate (or sub-optimal) approaches to achieving the dual control objective, e.g., [5, 11, 16, 19, 20, 22, 30, 37, 49, 54, 62, 72, 82].

Receding Horizon Control (RHC) (a.k.a. Model Predictive Control (MPC)[3]) [52],

[3]In this dissertation, the terms RHC and MPC will be used interchangeably.

which has seen a rapid growth in popularity in recent years, provides a natural platform for alternative dual control (i.e., simultaneous identification and control) strategies due in part to its inherent optimization and constraint handling. In fact, most of the papers cited in the preceding paragraph use MPC as a basis for implementation [5, 11, 19, 20, 22, 37, 54, 62, 72, 82]. Within the MPC framework, a metric for excitation is incorporated into the optimization problem to ensure the generation of persistently exciting control signals along with the usual control metrics. The trade-off between identification and control may then be managed by tuning the weighting (or penalties) placed on excitation and regulation metrics. For example, in [19, 54] the metric for persistent excitation is included as an inequality constraint in the MPC formulation, whereas [37] includes it in the cost function. However, while a trade-off is unavoidable in SISO systems, overactuated systems provide an opportunity to circumvent this trade-off.

In an overactuated system, there is no unique input vector which yields a particular output. Thus, overactuated systems provide an opportunity to achieve persistent excitation and output regulation objectives simultaneously, potentially without trade-off, when the excitation is constrained to the "null-space" of the system. While this idea has been explored for specific applications in recent years [10, 45, 83], the problem has yet to be treated in a more general framework. In [45], [83] the authors exploit the redundancy in a spacecraft with an overactuated reaction wheel array by restricting the optimized excitation signal to the "null-motion" of craft in order to estimate actuator misalignments. Similarly, in [10], the authors exploit the actuation redundancy in an electric vehicle with separate drives for the front and rear wheels, to generate sufficiently rich input signals for road friction coefficient identification without affecting the vehicle motion.

1.3 Open Issues and Contributions

1.3.1 Open Issues

The open issues in identification and control for high-performance AC drive systems which we will address in this dissertation are as follows:

- *Accurate offline identification of induction machine parameters using a voltage-source inverter and over a wide operating range* - The IEEE standard for induction machine parameter identification [2] uses no-load and locked-rotor tests for offline parameter identification. However, accurate parameter estimation us-

ing the standard requires special equipment to conduct these tests. While a voltage-source inverter could be used, the presence of switching harmonics in the output voltage complicates voltage measurements, unless the inverter has a significant output filter. Thus, there is a need for an alternative to the IEEE standard for offline induction machines parameter identification, which can be implemented in VSI-driven systems and is capable of characterizing machines over a wide range of operating conditions. While alternatives to the IEEE standard have been proposed in the literature (see Section 1.2.2), these techniques do not consider core loss or the characterization of magnetic saturation, both of which can significantly affect the accuracy of the estimated parameters, and knowledge of which may be used to improve controller performance.

- *Development of methodologies for simultaneous identification and control of overactuated systems* - Adaptive control is often used to obtain high-performance when controlling uncertain systems. However, while steady-state tracking can typically be guaranteed, regardless of the accuracy of the estimated parameters, transient performance, as well as the regulation of unmeasured outputs, can suffer in the presence of inaccurate parameter estimates. Furthermore, accurate parameter knowledge is vital to secondary objectives such as loss minimization (e.g., in AC machines) and condition monitoring, as well as ensuring that constraints are satisfied in predictive control designs. While parameter identification and output regulation are typically conflicting objectives, overactuated systems such as AC machines provide an opportunity to achieve these objectives simultaneously in real-time without compromise. Dual control and alternatives have been introduced to manage this trade-off, typically for SISO systems. However, currently no general methodology exists which specifically exploits overactuation for simultaneous identification and control.

1.3.2 Summary of Contributions and Innovations

This dissertation seeks to address the open issues described in the previous section, and more, via the following contributions:

- *A novel technique for offline identification of induction machine parameters* - We have developed a new technique for induction machine parameter identification which can easily be implemented using a voltage-source inverter [64]. The proposed technique is based on fitting steady-state experimental data to the circular stator current locus in the stator flux linkage reference-frame for varying

steady-state slip frequencies, and provides accurate estimates of the magnetic parameters, as well as the rotor resistance and core loss conductance. This approach allows accurate leakage inductance and rotor resistance estimation while avoiding the difficulties associated with inverter-based implementations of the locked-rotor test. Experimental results for a 43 kW induction machine are provided which demonstrate the utility of the proposed technique by characterizing the machine over a wide range of flux levels, including magnetic saturation;

- *The development of generalizable design methodologies for simultaneous identification and control of overactuated systems via case studies with permanent magnet synchronous machines* - Specifically, this dissertation will present two different approaches to the design of adaptive controllers for PMSMs which exploit overactuation to achieve identification and control objectives simultaneously by ensuring that excitation signals introduced for parameter identification have a minimal impact on the regulated torque output. The first approach, termed "Adaptive Excitation Decoupling" [67], utilizes a disturbance decoupling control law to prevent the excitation input from perturbing the regulated output, while machine parameters used in the control law are updated online via a normalized gradient estimator. The second approach [66] uses a Lyapunov-based inner-loop adaptive controller to constrain the states to the output error-zeroing manifold, defined by the torque output mapping, on which they are varied to provide excitation for parameter identification. Finally, the issue of input selection (i.e., excitation input design and control allocation) is addressed for the Lyapunov-based design by incorporating a receding-horizon control allocation which includes a metric for generating persistently exciting reference trajectories. While both approaches are shown to achieve the SIC objective, and each hold promise for generalization, the Lyapunov-based design has robustness and stability advantages over the Adaptive Excitation Decoupling approach.

- *The development of numerical tools for analysis and design of high-performance AC drive systems* - Specifically, we have developed Simulink® models for single and three-phase inverters with dead-time effect and center-based PWM, sampled-data controller models which account for time delays as well as single and twice-per-period sampling schemes, and finally AC machine models which allow parameters to be varied;

- *Construction of a physical testbed for electric drives with hybrid energy storage* - Finally, we have constructed a testbed for the purpose of experimentally validating advanced control algorithms for high-performance AC drive systems, as well as energy cycling using hybrid energy storage. While it won't be discussed in detail here, the development of the testbed has been documented in [26].

1.4 Reader's Guide

The remainder of this dissertation is organized as follows:

Chapter 2: Offline Identification of Induction Machine Parameters presents a new technique for offline identification of induction machine parameters using a voltage-source inverter. The stator current locus representation in the stator flux linkage reference frame is first derived, and next, the estimation technique is discussed. Following a discussion of the stator flux linkage estimator, simulation and experimental results demonstrating the effectiveness of the proposed technique are presented.

Chapter 3: Adaptive Excitation Decoupling Approach to Simultaneous Identification and Control of Permanent Magnet Synchronous Machines begins our discussion of simultaneous identification and control of permanent magnet synchronous machines. The proposed technique utilizes a disturbance decoupling control law to prevent the excitation input, introduced to ensure that conditions for persistency of excitation are satisfied, from perturbing the regulated (i.e., electromagnetic torque) output. A normalized gradient-based identifier is used to estimate the machine parameters and update the excitation (i.e., disturbance) decoupling control law. Simulations are used to verify the resulting closed-loop adaptive excitation decoupling controller.

Chapter 4 Simultaneous Identification and Control of Permanent Magnet Synchronous Machines via Adaptive 2-DOF Lyapunov Design presents an alternative adaptive control design for PMSMs which achieves the simultaneous identification and control objective using a Lyapunov-based design. By regulating the states to the output error-zeroing manifold, we ensure that perturbations to the torque output (due to the presence of an excitation signal) are minimized while still providing excitation for parameter identification. This approach has the advantages that the stator currents (i.e., the states)

are directly regulated, closed-loop stability is proven, and analysis of sufficient conditions for parameter convergence is tractable.

Chapter 5 Receding Horizon Control Allocation for Simultaneous Identification and Control of PMSMs extends the approach presented in Chapter 4 to use an optimization-based control allocation, rather than the fixed allocation used in Chapter 4. A receding-horizon optimization, which includes a metric for encouraging the generation of persistently exciting signals, is used to generate the command current trajectories for a given command torque, which are fed to the inner-loop adaptive current regulator derived in Chapter 4. This work address the limitations of the work presented in Chapter 4 in that specialized knowledge (i.e., intuition) of the plant is not needed to design the control allocation, and the design of persistently exciting signals is guided by a rigorous metric; these points, the control allocation and design of persistently exciting signals, are handled automatically by the receding-horizon optimization.

Chapter 6 Conclusions and Future Work summarizes the results of this research and makes suggestions for future research directions.

CHAPTER II

Offline Identification of Induction Machine Parameters

2.1 Introduction

This chapter presents a new technique for induction machine parameter identification using steady-state current measurements. The proposed technique is based on fitting experimental data to the circular stator current locus in the stator flux linkage reference-frame for varying steady-state slip frequencies, and provides accurate estimates of the magnetic parameters, as well as the rotor resistance and core loss conductance. Numerical simulation results evaluating the accuracy of the estimated parameters in the presence of non-ideal effects are presented, and experimental results for a 43 kW induction machine are provided which demonstrate the utility of the proposed technique by characterizing the machine over a wide range of flux levels, including magnetic saturation.

2.2 The Steady-State Stator Current Locus

In this work, the induction machine is modeled as having a smooth air-gap (i.e., slotting effects are neglected) in addition to the following simplifying assumptions:

A1. a quasi-linear magnetics model;

A2. the machine is balanced in its construction with sinusoidally-distributed magnetomotive force (mmf);

This chapter is based on a previously published conference paper [64] which has been expanded and submitted to a journal and is currently under review:
D. M. Reed, H. F. Hofmann, and J. Sun, "Offline Identification of Induction Machine Parameters with Core Loss Estimation using the Stator Current Locus," *Under review,* 2015.

A3. a 1:1 effective turns ratio;

A4. the core loss is modeled as a resistive shunt just after the stator winding resistance (see Figure 2.1).

The first assumption, **A1**, permits variations in the magnetic parameters with operating conditions, while **A2** justifies the use of a 2-phase equivalent model and transformation from 3-phase to 2-phase using the Clarke transform [14]. The third assumption, **A3**, is common for squirrel-cage induction machines, which do not have physical rotor windings. Finally, while core loss is typically modeled as a resistance in parallel with the mutual inductance [17], this placement is somewhat arbitrary as leakage flux also travels through the machine iron. **A4** simplifies the analysis while still capturing the nature of the core loss (i.e., electrical power which is not converted into mechanical power). Finally, a list of induction machine notation is provided in Table 2.1.

Table 2.1: List of induction machine notation.

Symbol	Description
$\vec{v}_s(t) = [v_{sd}(t)\ v_{sq}(t)]^\top$	Stator Voltage Vector
$\vec{i}_s(t) = [i_{sd}(t)\ i_{sq}(t)]^\top$	Stator Current Vector
$\vec{\lambda}_s(t) = [\lambda_{sd}(t)\ \lambda_{sq}(t)]^\top$	Stator Flux Linkage Vector
R_s	Stator Winding Resistance
L_s	Stator Winding Self-Inductance
M	Mutual Inductance
G_c	Core Loss Conductance
ω_e	Electrical Frequency
$\vec{i}_r(t) = [i_{rd}(t)\ i_{rq}(t)]^\top$	Rotor Current Vector
$\vec{\lambda}_r(t) = [\lambda_{rd}(t)\ \lambda_{rq}(t)]^\top$	Rotor Flux Linkage Vector
R_r	Rotor Resistance
L_r	Rotor Self-Inductance
ω_r	Rotor Angular Velocity
P	Number of Poles
$\omega_{re} = \frac{P}{2}\omega_r$	Rotor Electrical Angular Velocity
$\omega_{se} = \omega_e - \omega_{re}$	Electrical Slip Frequency

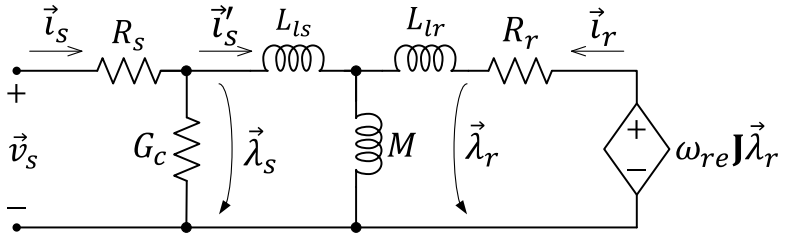

Figure 2.1: Dynamic 2-phase equivalent circuit model for an induction machine.

The desired expressions for the steady-state stator currents in the stator flux linkage reference-frame are developed starting from the flux linkage dynamics in the stationary reference-frame for the 2-phase equivalent induction machine model:

$$\frac{d\vec{\lambda}_s}{dt} = -R_s\vec{i}_s + \vec{v}_s, \tag{2.1}$$

$$\frac{d\vec{\lambda}_r}{dt} = -R_r\vec{i}_r + \omega_{re}\mathbf{J}\vec{\lambda}_r, \tag{2.2}$$

where $\vec{\lambda}_s = [\lambda_{sd}\ \lambda_{sq}]^\top$ is the stator flux linkage vector, $\vec{\lambda}_r = [\lambda_{rd}\ \lambda_{rq}]^\top$ is the rotor flux linkage vector, $\vec{i}_s = [i_{sd}\ i_{sq}]^\top$ is the stator current vector, $\vec{i}_r = [i_{rd}\ i_{rq}]^\top$ is the rotor current vector, $\vec{v}_s = [v_{sd}\ v_{sq}]^\top$ is the stator voltage vector, and $\mathbf{J}$ is the 90° CCW rotation matrix. These expressions (2.1)-(2.2) are easily derived by applying Kirchhoff's and Faraday's laws to the equivalent circuit model provided in Fig. 2.1. Additionally, the following flux linkage/current relationships, which hold for arbitrary reference-frames (denoted by the superscript x), are needed

$$\vec{\lambda}_s^x = L_s\vec{i}_s^x + M\vec{i}_r^x, \tag{2.3}$$

$$\vec{\lambda}_r^x = M\vec{i}_s^x + L_r\vec{i}_r^x, \tag{2.4}$$

where $L_s = L_{ls} + M$ and $L_r = L_{lr} + M$.

To represent (2.2) in the stator flux linkage reference-frame, we use the Park transform [59],

$$\vec{x}^{\,\lambda_s} = e^{-\mathbf{J}\theta_{\lambda_s}}\vec{x}, \tag{2.5}$$

where the superscript λ_s is used to designate variables which are being represented in the stator flux linkage reference-frame, the angle of which is denoted by θ_{λ_s}. Applying (2.5) to the stationary-frame electrical variables in (2.2) yields

$$\frac{d\vec{\lambda}_r^{\lambda_s}}{dt} = -R_r\vec{i}_r^{\lambda_s} + \omega_{se}\mathbf{J}\vec{\lambda}_r^{\lambda_s}, \tag{2.6}$$

where $\omega_{se} = \omega_e - \omega_{re}$ is the electrical slip frequency. At steady-state[1] (2.6) gives us the following expression for the steady-state rotor currents

$$\vec{I}_r^{\lambda_s} = -\frac{\Omega_{se}}{R_r}\mathbf{J}\vec{\Lambda}_r^{\lambda_s}, \tag{2.7}$$

where Ω_{se} is the steady-state electrical slip frequency. From (2.3)-(2.4) it can be shown that

$$\vec{\lambda}_r^x = \frac{\sigma^2}{L_s}\vec{i}_r^x + \frac{M}{L_s}\vec{\lambda}_s^x, \tag{2.8}$$

where $\sigma^2 = L_s L_r - M^2$. Plugging (2.8) into (2.7) and solving for the rotor current, $\vec{I}_r^{\lambda_s}$, we obtain the following expression for the steady-state rotor currents in the stator flux linkage reference-frame as a function of slip frequency and stator flux linkage:

$$\vec{I}_r^{\lambda_s} = -\frac{\frac{\Omega_{se}}{R_r}\frac{M}{L_s}}{1+\left(\frac{\Omega_{se}}{R_r}\frac{\sigma^2}{L_s}\right)^2}\left[\frac{\Omega_{se}}{R_r}\frac{\sigma^2}{L_s}\mathbf{I} + \mathbf{J}\right]\vec{\Lambda}_s^{\lambda_s}, \tag{2.9}$$

where $\mathbf{I}$ is the 2×2 identity matrix.

Finally, using the stator current relationship with the core loss conductance (as defined in Fig. 2.1),

$$\vec{i}_s = G_c\frac{d\vec{\lambda}_s}{dt} + \vec{i}_s', \tag{2.10}$$

which, at steady-state and when represented in the stator flux linkage reference-frame, is given by

$$\vec{I}_s^{\lambda_s} = G_c\Omega_e\mathbf{J}\vec{\Lambda}_s^{\lambda_s} + \vec{I}_s^{\lambda_s'}, \tag{2.11}$$

along with the fact that

$$\vec{I}_s^{\lambda_s'} = \frac{1}{L_s}\left(\vec{\Lambda}_s^{\lambda_s} - M\vec{I}_r^{\lambda_s}\right), \tag{2.12}$$

we obtain the desired scalar form expressions for the steady-state direct, $I_{sd}^{\lambda_s}$, and quadrature, $I_{sq}^{\lambda_s}$, stator currents in the stator flux linkage reference-frame in which the direct-axis is aligned with the stator flux linkage vector (i.e., $\vec{\lambda}_s^{\lambda_s} = [||\vec{\lambda}_s||\ \ 0]^\top$):

$$I_{sd}^{\lambda_s} = \left[1 + \left(\frac{M}{\sigma}\right)^2 \frac{\left(\Omega_{se}/\Omega_{se,max}^{\lambda_s}\right)^2}{1+\left(\Omega_{se}/\Omega_{se,max}^{\lambda_s}\right)^2}\right]\frac{||\vec{\Lambda}_s||}{L_s}, \tag{2.13}$$

$$I_{sq}^{\lambda_s} = \left(\frac{M}{\sigma}\right)^2 \frac{\left(\Omega_{se}/\Omega_{se,max}^{\lambda_s}\right)}{1+\left(\Omega_{se}/\Omega_{se,max}^{\lambda_s}\right)^2}\frac{||\vec{\Lambda}_s||}{L_s} + G_c\Omega_e||\vec{\Lambda}_s||, \tag{2.14}$$

[1]Steady-state variables are denoted by capital letters.

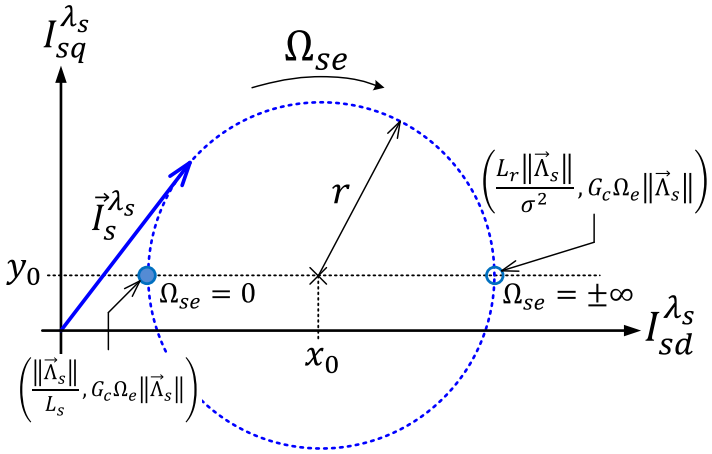

Figure 2.2: Parameterized steady-state stator current locus in the stator flux linkage reference-frame.

where Ω_e is the steady-state electrical frequency, $||\vec{\Lambda}_s||$ is the stator flux linkage magnitude and $\Omega_{se,max}^{\lambda_s} = \frac{R_r L_s}{\sigma^2}$ is the slip frequency which maximizes torque for a given stator flux linkage magnitude.

When plotted as a function of slip frequency, (2.13) and (2.14) produce the circular stator current locus in Figure 2.2. The parameterized stator current locus circle is given by

$$\left(I_{sd}^{\lambda_s} - x_o\right)^2 + \left(I_{sq}^{\lambda_s} - y_o\right)^2 = r^2, \tag{2.15}$$

where,

$$x_o = \frac{1}{2}\left(\frac{1}{L_s} + \frac{L_r}{\sigma^2}\right)||\vec{\Lambda}_s||, \tag{2.16}$$

$$y_o = G_c\Omega_e||\vec{\Lambda}_s||, \tag{2.17}$$

$$r = \frac{M^2}{2\sigma^2 L_s}||\vec{\Lambda}_s||. \tag{2.18}$$

The stator current locus in Fig. 2.2 can therefore be used to identify the magnetic parameters of the induction machine (i.e., L_s,L_r, and M), as well as the core loss conductance, G_c, by fitting the parametric circle (2.15) to experimental data (i.e., $I_{sd}^{\lambda_s}(\Omega_{se})$ and $I_{sq}^{\lambda_s}(\Omega_{se})$) which forms the stator current locus, provided that the stator flux linkage magnitude is held constant (i.e., regulated) during data collection. Once estimates of the center location, $(\hat{x}_o, \hat{y}_o)$, and radius, $\hat{r}$, have been computed, the core loss and magnetic parameters are calculated assuming that the inductance ratio, $\frac{L_s}{L_r}$, is known[2]. This assumption gives us three equations with three unknowns, $L_{s,r}$,

[2]If the NEMA-design letter is known, this ratio can be found in IEEE Standard 112; otherwise

M, and G_c. Once we have estimates of the magnetic parameters and the core loss conductance, (2.13) and (2.14) along with the corresponding slip frequencies, are used to estimate the rotor resistance, R_r.

Since the magnetic parameters are obtained from the parameterization of the fitted locus circle, their estimates are independent of the rotor resistance, which will vary with temperature. Other benefits of the proposed technique are a reduction in the dimension of the estimation problem by identifying magnetic parameters (and core loss conductance) separately from the rotor resistance, the use of multiple data points in estimating parameters, and the ability to characterize the machine over a wide range of operating points which include magnetic saturation.

2.3 Proposed Parameter Estimation Technique

2.3.1 Fitting the Parameterized Stator Current Locus Circle to Data

Using the stator current locus presented in the previous section, the magnetic parameters, as well as the core loss conductance, are identified by fitting the parameterized circle (Fig. 2.2) to experimental data. The fitting is achieved by solving a reasonably simple minimization problem. According to the theory, the zero-slip data point and the center of the stator current locus should be aligned horizontally. While it may seem simplistic to use the zero-slip data point to fix the center of the estimate stator current locus (circle), it works well in practice, as will be demonstrated in our numerical analysis.

Enforcing the condition that the zero-slip data point determines the vertical offset in the locus circle, we see that

$$\hat{y}_o = I_{sq}(\Omega_{se} = 0). \tag{2.19}$$

The magnetic parameters are then computed by solving the following minimization problem

$$(\hat{x}_o, \hat{r}) = \arg \min_{(x,r)>0} J_{scl}(x, r), \tag{2.20}$$

where the cost function, $J_{scl}(x, r)$, is given by,

$$J_{scl} = \sum_{n=1}^{N} \left[r^2 - \left(\left(I_{sd,n}^{\lambda_s} - x \right)^2 + \left(I_{sq,n}^{\lambda_s} - \hat{y}_o \right)^2 \right) \right]^2, \tag{2.21}$$

assume $L_s/L_r = 1$.

where $I_{sd,n}^{\lambda_s}$ and $I_{sq,n}^{\lambda_s}$ are the n^{th} measurements of the steady-state direct and quadrature stator currents in the stator flux linkage reference-frame. This approach (2.20)-(2.21) is sometimes referred to as a "pure least-squares" solution [76]. In our work, we chose to solve this minimization problem numerically using MATLAB's *fmincon* constrained nonlinear programming algorithm.

Given estimates of the center location, $(\hat{x}_o, \hat{y}_o)$, and radius, $\hat{r}$, the stator self-inductance is given by

$$\hat{L}_s = \frac{||\vec{\Lambda}_s||}{\hat{x}_o - \hat{r}}. \tag{2.22}$$

Next, we assume that the stator and rotor inductances are the same (i.e. $\hat{L}_s/\hat{L}_r = 1$) and compute the leakage term:

$$\hat{\sigma}^2 = \frac{\hat{L}_r \hat{L}_s ||\vec{\Lambda}_s||}{2\hat{L}_s \hat{x}_o - ||\vec{\Lambda}_s||}. \tag{2.23}$$

Once the self-inductance and leakage terms are known, the mutual inductance is calculated:

$$\hat{M} = \sqrt{\hat{L}_s \hat{L}_r - \hat{\sigma}^2}. \tag{2.24}$$

Finally, the estimate of the core loss conductance is given by

$$\hat{G}_c = \frac{\hat{y}_o}{\Omega_e ||\vec{\Lambda}_s||}. \tag{2.25}$$

To estimate the rotor resistance, we will minimize the sum-of-squares error between the experimental data points (i.e., $I_{sd}^{\lambda_s}(\Omega_{se})$ and $I_{sq}^{\lambda_s}(\Omega_{se})$) and those predicted by the steady-state model of the stator current locus (in the stator flux linkage reference-frame). Again, the parameter estimation is obtained by solving a constrained minimization problem:

$$\hat{R}_r = \underset{R_r \in [R_{r,min}, R_{r,MAX}]}{\arg\min} J_{R_r}(R_r) \tag{2.26}$$

where the cost function, $J_{R_r}(R_r)$, is given by,

$$J_{R_r}(R_r) = \sum_{n=1}^{N} \left(\left(I_{sd,n}^{\lambda_s} - \hat{I}_{sd,n}^{\lambda_s} \right)^2 + \left(I_{sq,n}^{\lambda_s} - \hat{I}_{sq,n}^{\lambda_s} \right)^2 \right), \tag{2.27}$$

where $\hat{I}^{\lambda_s}_{sd,n}$ and $\hat{I}^{\lambda_s}_{sq,n}$ are functions of R_r derived from (2.13) and (2.14):

$$\hat{I}^{\lambda_s}_{sd,n} = \left[1 + \frac{\hat{M}^2}{\hat{\sigma}^2} \frac{\left(\hat{\sigma}^2 \Omega_{se,n}\right)^2}{\left(R_r \hat{L}_s\right)^2 + \left(\hat{\sigma}^2 \Omega_{se,n}\right)^2}\right] \frac{||\vec{\Lambda}_s||}{\hat{L}_s}, \tag{2.28}$$

$$\hat{I}^{\lambda_s}_{sq,n} = \frac{\hat{M}^2}{\hat{\sigma}^2} \frac{R_r \hat{L}_s \hat{\sigma}^2 \Omega_{se,n}}{\left(R_r \hat{L}_s\right)^2 + \left(\hat{\sigma}^2 \Omega_{se,n}\right)^2} \frac{||\vec{\Lambda}_s||}{\hat{L}_s} + \hat{G}_c \Omega_{e,n} ||\vec{\Lambda}_s||. \tag{2.29}$$

Note that a non-zero stator flux linkage magnitude and non-zero slips are required for identification of the rotor resistance. This amounts to a rather intuitive persistent excitation condition [63], in that it suggests rotor currents must be present in order to determine the rotor resistance. While this cost function (2.27)-(2.29) is globally non-convex, it is convex for practical rotor resistance values (e.g., positive values) with a unique minimum at the true resistance. Therefore, we enforce constraints when solving the minimization problem, requiring that $R_r \in [0.1R_s,\ 10R_s]$. Once again, we use MATLAB's *fmincon* constrained nonlinear programming algorithm to solve the minimization problem.

2.3.2 Procedure for Data Collection

In order to generate the experimental stator current locus, the measured stator currents must be projected into the stator flux linkage reference-frame using the Park transform (2.5). Additionally, the stator flux linkage magnitude must be held constant while the steady-state direct and quadrature stator currents are recorded for various steady-state (i.e., constant) slip frequencies, Ω_{se}. To ensure that the flux linkage magnitude remains constant, a Proportional-Integral (PI) regulator is used to drive the error between the commanded stator flux magnitude, $||\tilde{\Lambda}_s||$, and estimated flux magnitude, $||\hat{\Lambda}_s||$, to zero. The output of the PI regulator is the stator excitation voltage magnitude, $||\vec{v}_s||$, as depicted in Figure 2.3. The slip frequency is varied by either fixing the electrical frequency, Ω_e, of the stator excitation voltage and varying the regulated rotor speed of the load machine, or vice versa.

Selection of the electrical excitation frequency, Ω_e, is somewhat arbitrary. In general, running at higher speeds (and thus, higher electrical frequencies) will reduce the influence of stator resistance variations, as well as inverter non-ideal effects like dead-time, by increasing voltage levels in the machine. Additionally, the electrical frequency should be high enough that the effects of integrator approximations are negligible. Similar to electrical frequency, the use of higher stator flux linkage magnitudes

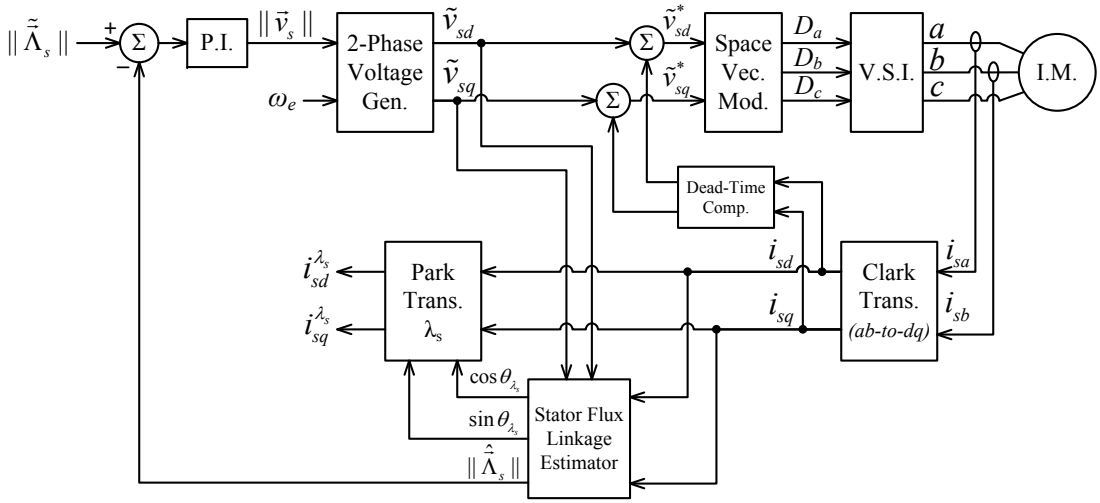

Figure 2.3: Data acquisition controller block diagram for the proposed parameter estimation technique.

will also help to minimize the influence of stator resistance variations and inverter non-ideal effects (e.g., dead-time). However, it is advisable to consider multiple flux linkage magnitudes during data collection, to check at what point the machine (iron) begins to saturate. The nominal (or rated) specifications from the manufacturer are a good starting point for selecting the electrical frequency and stator flux linkage magnitude.

2.3.3 Dead-time Compensation

In practical implementations, it is desirable to avoid the use of stator voltage measurements due to the added cost and complexity involved in processing the pulse-width modulated (PWM) voltage waveforms. Instead of measured voltages, our algorithm (Fig. 2.3) uses the commanded stator voltages to estimate the stator flux linkage. However, use of the commanded voltages requires compensation of non-ideal inverter characteristics such as the dead-time effect [7], which lead to distortions in the stator current locus, as depicted in Figure 2.4. In other words, the stator current locus is not circular in the presence of the dead-time effect. For this reason, first-harmonic dead-time compensation is employed to ensure that the actual voltages applied to the machine terminals closely resemble the commanded values used to estimate the stator flux linkage. In discrete-time and in the stationary reference-frame, the compensated voltage command, $\tilde{\vec{v}}^{*}_{s,k} = [\tilde{v}^{*}_{sd,k} \;\; \tilde{v}^{*}_{sq,k}]^{\top}$, at time-step "$k$" is

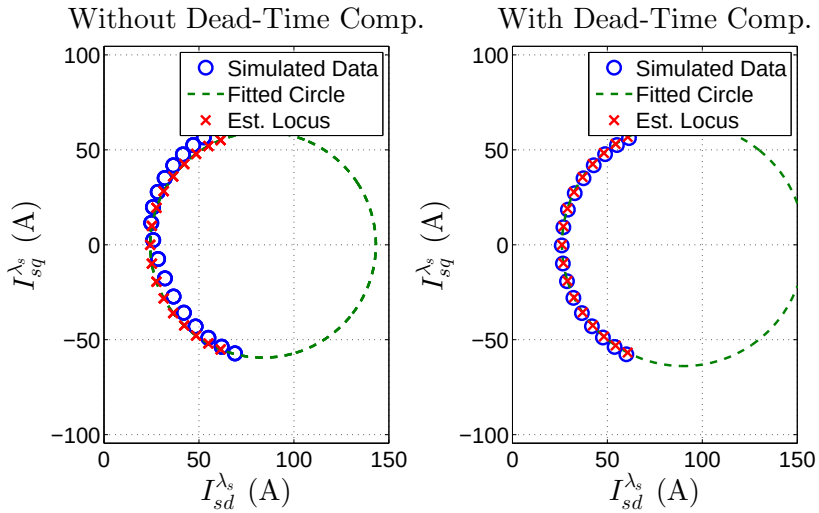

Figure 2.4: Simulation of the proposed data acquisition procedure depicting the distortion in the stator current locus due to dead-time effect(left) and improvement using first-harmonic dead-time compensation (right).

given by:

$$\tilde{\vec{v}}_{s,k}^{*} = \tilde{\vec{v}}_{s,k} + \frac{4}{\pi} V_{bus} t_d f_{sw} \left(e^{\mathbf{J}(1.5 T_s \Omega_e)} \frac{\vec{i}_{s,k}}{||\vec{i}_{s,k}||} \right). \tag{2.30}$$

where $\tilde{\vec{v}}_{s,k} = [\tilde{v}_{sd,k} \ \tilde{v}_{sq,k}]^\top$ is the ideal (commanded) stator voltage vector, $\vec{i}_{s,k} = [i_{sd,k} \ i_{sq,k}]^\top$ is the measured stator current vector, t_d is the dead-time, f_{sw} is the switching frequency of the power electronics (in Hertz) and V_{bus} is the DC bus voltage. The sinusoidal first-harmonic of the square-wave dead-time voltage is used to avoid introducing the additional harmonic content associated with the *sign* function.

Finally, we note that the exponential term in (2.30) is used to compensate for the time delay present in the experimental sampled-data implementation. While a stator current predictor could be employed to compensate the time delay, it would require accurate knowledge of the machine parameters (which we are trying to identify). Instead, we simply advance the normalized stator current vector by 1.5 times the angular distance traveled by the stator current vector over one sample period. The factor of 1.5 is used to center the prediction over the next sample period, which was found to provide improved performance in numerical simulations.

2.4 Stator Flux Linkage Estimation

Accurate estimation of the stator flux linkage is necessary for the proposed parameter identification technique, as well as for field-oriented control techniques in

general. In particular, consideration must be given to the sampled-data nature of modern controller implementations, which include a time delay between when stator currents are sampled and when the computed duty cycle is executed.

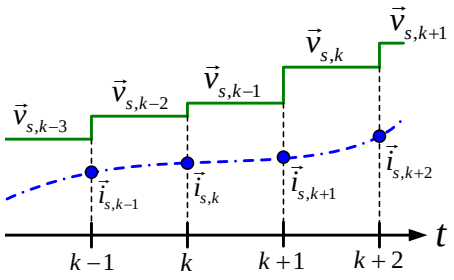

Figure 2.5: Timing relationships for sampled-data implementation with unit delay.

Typically, the stator flux linkage is estimated by integrating the stator flux linkage dynamics (2.1). In general, the stator flux linkage vector at time t_k is given by

$$\vec{\lambda}_{s,k} = \vec{\lambda}_{s,k-1} + \int_{t_{k-1}}^{t_k} \left(\vec{v}_s(t) - R_s \vec{i}_s(t) \right) dt. \tag{2.31}$$

We will assume that the voltage applied to the stator terminals is constant over a given sample period, T_s, which is true in an average-value sense, and that there is a one sample-period delay before a computed voltage is applied, as depicted in Figure 2.5. In other words, the voltage/duty cycle computed at time index k is applied at $k+1$. Under these assumptions, the discrete-time estimate of the stator flux linkage at time k is given by

$$\hat{\vec{\lambda}}_{s,k} = \hat{\vec{\lambda}}_{s,k-1} + T_s \vec{e}_{s,k}, \tag{2.32}$$

with

$$\vec{e}_{s,k} = \tilde{\vec{v}}_{s,k-2} - \frac{R_s}{2} \left(\vec{i}_{s,k} + \vec{i}_{s,k-1} \right), \tag{2.33}$$

where $\tilde{\vec{v}}_{s,k-2}$ denotes the *commanded* voltage computed at time index $k-2$ (which is implemented at $k-1$), $\vec{i}_{s,k}$ and $\vec{i}_{s,k-1}$ denote the *measured* stator current at time index k and $k-1$, respectively. In the z-domain, (2.32) may be represented by the following transfer function

$$\hat{\vec{\lambda}}_{s,k} = \left\{ \frac{zT_s}{z-1} \right\} \vec{e}_{s,k}. \tag{2.34}$$

Note that $\vec{e}_{s,k}$ is essentially an input to the discrete-time integrator in (2.34). However, the use of a pure integrator is undesirable in practice, as it can lead to drift and instabilities. Instead, we use a discrete-time approximation of a stable second-order continuous-time integrator approximation.

To reject DC biases in the measured currents, and achieve a faster phase transition (to 90°) we employ a second-order integrator approximation [63],

$$\hat{\vec{\lambda}}_s = \left\{ \frac{s}{s^2 + 2\zeta\omega_n s + \omega_n^2} \right\} \left(\vec{v}_s - R_s \vec{i}_s \right), \tag{2.35}$$

where "s" is the Laplace variable, $\zeta > 0$ is the damping constant, ω_n sets the corner frequency of the integrator approximation, and the brackets, e.g., $\{F(s)\}$, are used to indicate a dynamic operator with transfer function $F(s)$. To ensure accurate estimates of the stator flux linkage, ω_n should be set as low as possible[3] (i.e., $\omega_n \leq 0.01\,\Omega_e$) while still providing stable flux linkage estimates. While the discussion of continuous-time representations is conceptually convenient, discrete-time implementations must be derived for experimental implementation on a microcontroller.

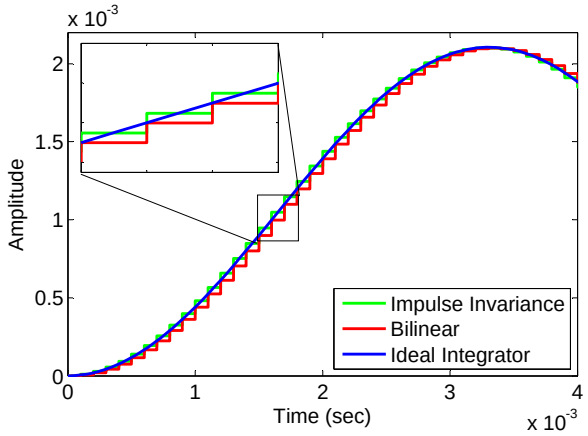

Figure 2.6: Comparison of bilinear and impulse invariance discrete-time second order integrator approximations with ideal continuous-time integrator.

Two common methods for deriving discrete-time approximations of continuous-time transfer functions are the bilinear transform and the impulse invariance method [60]. While the bilinear transform is generally favored for filter design, it leads to a small delay in our application, which is avoided by using the impulse invariance method, as shown in Figure 2.6. Using the impulse invariance method, the following discrete-time integrator approximation is obtained for $\zeta = 0.4$ and $\omega_n = 5$ rad/sec

$$\hat{\vec{\lambda}}_{s,k} = \left\{ \frac{0.0001z^2 - 0.0001z}{z^2 - 2z + 0.9999} \right\} \vec{e}_{s,k}, \tag{2.36}$$

where the coefficients are computed using MATLAB's *c2d* command, which converts

[3]Note that $F(s) \approx \frac{1}{s}$ for $\omega >> \omega_n$.

continuous-time system models to a discrete-time equivalent using the method specified (e.g., '*impulse*' for the impulse invariance method).

2.5 Numerical Analysis

Numerical simulations implemented in MATLAB/Simulink are used to evaluate the proposed parameter identification methodology's accuracy in the presence of non-ideal effects which are encountered in experimental implementations. Specifically, our simulations include non-ideal inverter characteristics such as dead-time, switch resistance, and diode voltage drops, as well as the sampled-data nature of experimental implementations, which include a one-time-step delay. Additionally, zero-mean Gaussian noise, of amplitude (i.e., variance) comparable to what we have observed in our experimental test-bed, is added to the three-phase stator current measurements.

To capture the sampled-data nature of the experimental system, our algorithm is implemented in a triggered subsystem in Simulink, while the machine dynamics are simulated in a continuous-time environment using MATLAB's *ode45* solver. To reduce simulation times, an "average-value" inverter model is used. That is, we do not model the switching nature of the inverter, since the switching frequency is high enough that its impact on performance is negligible. We do, however, model the dead-time effect and other non-ideal effects (resistive and diode voltage drops of the IGBT switches) by appropriately modifying the voltage commands produced by the identification algorithm before they are fed to the induction machine model.

The methodology for data collection and data acquisition controller (Fig. 2.3) with stator flux linkage estimation, described in the prequel, were used to generate the numerical data from MATLAB/Simulink at various slip frequencies. The simulated data was generated at a variety of flux linkage magnitudes ranging from 0.06 V-sec to 0.14 V-sec, closely mimicking the experimental conditions (same bus voltage, sampling frequency, etc.) and using machine parameter values similar to those of the test machine. An electrical base frequency of 153.33 Hz was used, which corresponds to a zero-slip rotor speed of 4600 rpm (i.e., the rated rotor speed of the experimental test machine). The simulated data was then used to compute the machine parameters in the same fashion that the experimental data is processed, using the proposed technique discussed earlier. The resulting parameter errors are plotted in Figure 2.7 as a function of flux linkage magnitude.

Inspection of the simulation results in Fig. 2.7 reveals that the proposed parameter identification methodology is capable of estimating the magnetic parameters and rotor

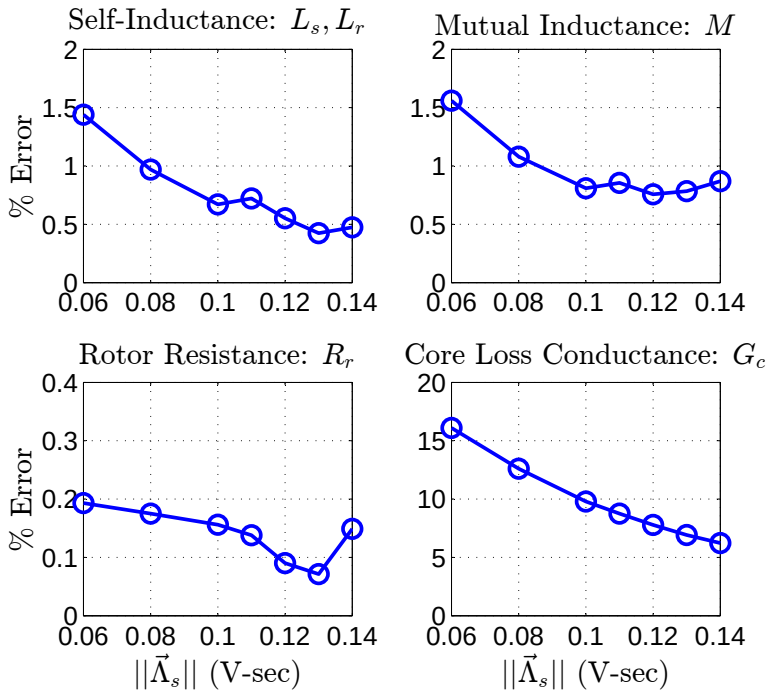

Figure 2.7: Simulated parameter errors in the presence of non-ideal effects.

resistance with high accuracy in the presence of non-ideal effects. Additionally, while the core loss conductance proves to be a more challenging parameter to estimate, the proposed technique provides estimates with reasonable accuracy, and which improve at higher flux linkage magnitudes. This is due to the fact that the dead-time effect, as well as the transistor voltage drops, result in a fixed magnitude voltage error. Their impact on the accuracy of the estimated parameters therefore diminishes as voltage levels increase with higher flux linkage magnitudes, as well as higher speeds.

Nevertheless, this level of accuracy in the estimated core loss conductance is more than sufficient for predicting the impact of core loss on torque regulation. This is verified by plotting the ratio of the "true" (i.e., with core loss) electromagnetic torque to the "commanded" (i.e., without core loss) electromagnetic torque as a function of slip frequency, as shown in Figure 2.8. Inspection of this plot reveals that the impact of even a 20% error in the core loss conductance estimate will have a rather small influence on our ability to capture the impact of core loss on torque regulation performance over the slip frequency range of practical interest (i.e., from the minimum current operating point up to the minimum flux linkage operating point).

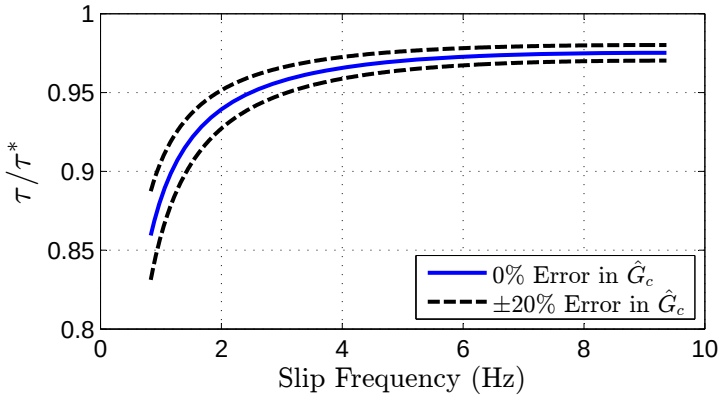

Figure 2.8: Steady-state induction machine torque error (ratio) due to unmodeled core loss as a function of slip. This plot was generated using the following machine parameters: $L_s = L_r = 4.4$ mH, $M = 4.2$ mH, $R_r = 23$ mΩ, $G_c = 30$ mΩ^{-1}, and $\Omega_e = 153.33$ Hz.

2.6 Experimental Results

2.6.1 Experimental Setup

The experimental parameter identification control algorithm is implemented on a Speedgoat real-time target machine using auto-generated code from MATLAB/Simulink. The test motor is a 3-phase, 4,600 rpm (nominal), 43 kW-peak induction machine from Azure Dynamics, driven by an IGBT inverter with a switching frequency of 10 kHz, bus voltage of 300 V, and dead-time of 2 μs. A center-based pulse-width modulation technique is employed to synchronize sampling and switching, thereby

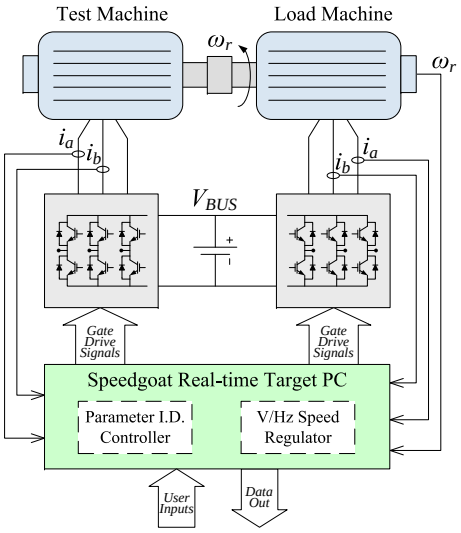

Figure 2.9: Experimental set-up for parameter identification data collection.

avoiding the pickup of electromagnetic interference generated during switching transitions. Thus, the control algorithm for parameter identification is executed at 10 kHz as well, and Space-Vector Modulation (SVM) is used to generate the desired duty-cycles sent to the inverter. An identical induction machine serves as the load for the test machine by regulating the rotor speed (Fig. 2.9).

2.6.2 Experimental Results and Discussion

Steady-state data is recorded for several stator flux linkage magnitudes, ranging from 0.08 V-sec to 0.14 V-sec, at an electrical base frequency of 153.33 Hz. For each flux linkage magnitude, the direct and quadrature currents (in the stator flux linkage reference-frame) are recorded for several different slip frequencies, including zero-slip, roughly up to the current limitations of the machines. The resulting machine parameters, estimated using the proposed technique, are plotted in Figure 2.10 as a function of stator flux linkage magnitude, $||\vec{\Lambda}_s||$.

Inspection of the parameter estimates in Fig. 2.10 reveals that the estimated self and mutual inductance capture the saturation effects in the machine. Additionally, we have plotted the leakage inductances, L_{ls} and L_{lr}, to confirm our expectation that these parameters remain constant. As for the estimated rotor resistance, while there are variations in the estimates, these variations are well within the range expected

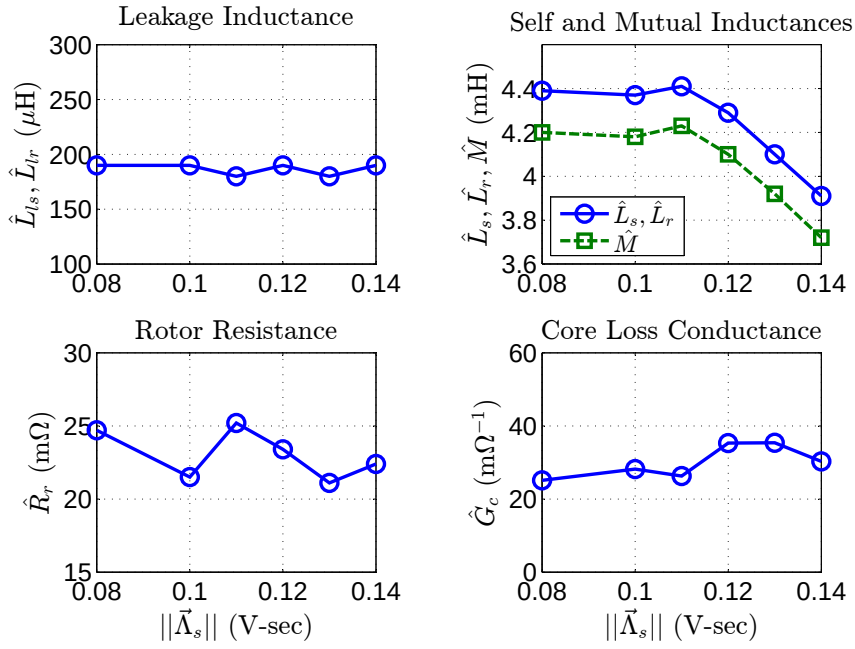

Figure 2.10: Experimental estimated machine parameters as a function of stator flux linkage magnitude.

due to temperature changes. In fact, the lower resistance estimates at 0.1 and 0.13 V-sec correlate with data collected after allowing the machine time to cool. Furthermore, the expected increase in resistance for a 45°C rise in temperature in aluminum conductors [64] is ~ 4.07 mΩ, and supports our suspicion that the variations in rotor resistance observed in Fig. 2.10 are due to temperature changes in the rotor during data collection. Inspection of Fig. 2.10 also reveals that the core loss conductance estimates are reasonably consistent across all of the stator flux linkage magnitudes.

However, since core losses are typically thought of in terms of the power they consume, rather than the equivalent resistance, it is desirable to check the predicted core loss power using the core loss conductance estimates. The estimated power dissipated by the core loss conductance is given by

$$\hat{P}_{core} = \frac{3}{2}\hat{G}_c\Omega_e^2||\vec{\Lambda}_s||^2. \tag{2.37}$$

Thus, using our experimental data, we obtain the plot provided in Figure 2.11. Inspection of Fig. 2.11 reveals the general trend that core losses increase with stator flux linkage magnitude, as expected.

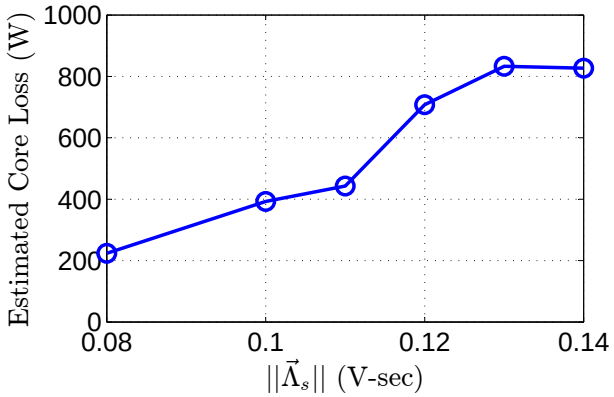

Figure 2.11: Estimated core loss power as a function of stator flux linkage magnitude at a electrical base frequency of 153.33 Hz and switching frequency of 10 kHz.

Finally, the experimental stator current locus plots for several stator flux linkage magnitudes are provided in Figure 2.12. The estimated locus points are computed using the estimated machine parameters along with equations (2.13) and (2.14). Inspection of Fig. 2.12 reveals that there is a good consensus between the experimental and estimated locus points, particularly at high flux linkage magnitudes where the influence of the non-ideal inverter effects and stator flux estimation are less pronounced.

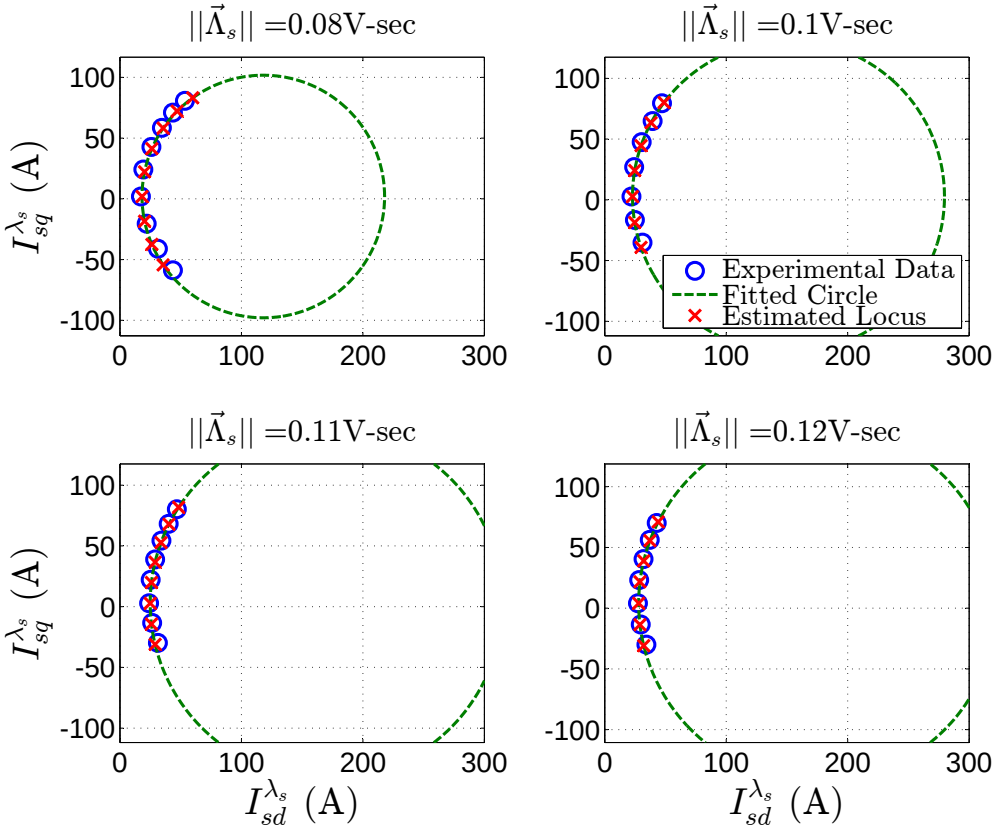

Figure 2.12: Experimental data (blue circles) with fitted current locus circle (green dashed line) and estimated locus points (red X's) for various stator flux linkage magnitudes.

2.7 Conclusion

This chapter presented a new technique for offline identification of induction machine parameters, including core loss conductance, using steady-state measurements. The technique is based on fitting steady-state experimental data to the circular stator current locus in the stator flux linkage reference-frame for various steady-state slip frequencies, providing reliable estimates of the magnetic parameters as well as the rotor resistance and core loss conductance. This approach allows accurate estimation of leakage inductance and rotor resistance while avoiding the practical challenges of implementing a locked-rotor test with a voltage-source inverter. Numerical results verifying the accuracy of estimated parameters in the presence of non-ideal effects were presented, in addition to experimental results for a 43 kW induction machine, which demonstrate the proposed technique's ability to accurately characterize a VSI-driven induction machine over a wide range of operating conditions, including magnetic saturation.

CHAPTER III

Adaptive Excitation Decoupling Approach to Simultaneous Identification and Control of Permanent Magnet Synchronous Machines

3.1 Introduction

In this chapter, we begin our technical discussion of simultaneous identification and control for PMSMs and present the first of three approaches to SIC of PMSMs. As noted in the introduction, parameter identification and output regulation are typically conflicting objectives. Generally, a trade-off must be made between ensuring that inputs to the system under control are persistently exciting and maintaining tight regulation of "performance" (i.e., regulated) outputs. However, in the case of certain overactuated systems there is an opportunity to achieve these objectives simultaneously. For example, field-oriented output torque regulation in Permanent Magnet Synchronous Machines (PMSMs) constitutes an overactuated control problem in that there are two distinct inputs to the system, the direct-axis voltage input and the quadrature-axis voltage input, and one regulated output, torque. The direct-axis voltage is typically used to set magnetic field (flux) levels in the machine by regulating the direct-axis stator current, while the quadrature-axis voltage is used to regulate the electromagnetic torque by regulating the quadrature-axis stator current.

The PMSM is a popular choice in high-performance drives, particularly in transportation applications, thanks to its high torque density and high efficiency. However, temperature changes, skin effect, and magnetic saturation lead to changes in

---

This chapter is based on previously published work:
D. M. Reed, J. Sun, and H. F. Hofmann, "Simultaneous Identification and Torque Regulation of Permanent Magnet Synchronous Machines via Adaptive Excitation Decoupling," in *American Control Conference (ACC), 2015,* pp.3224-3229, 1-3 July 2015.

the machine parameters which in turn detune the drive system, causing performance degradation. The stator winding resistance is primarily impacted by temperature variations, which can lead to increases in resistance by as much as 100% [39]. While the permanent magnet flux magnitude also varies with temperature, the variation can be small for certain types of magnets. For example, in neodymium ($NdFeB$) magnets the variation is around -0.1% per °C [7], which results in a mere 5% error for a rather large 50°C increase in temperature. Finally, while the electrical frequencies needed to see a significant rise in stator resistance due to skin effect are not typically encountered, high-speed applications using motors with a high pole-pair count may see an impact due to skin effect.

Many different approaches to compensating parameter variations in PMSMs have been proposed by researchers. Steady-state machine models have been used to avoid the additional complexity that comes with using dynamic models for parameter estimation [34], [44]. Open-loop [13], as well as closed-loop [77], [27] approaches have been presented which utilize the method of least-squares for PMSM parameter estimation. The gradient method is used in [56] to provide online estimates of the lumped time-varying disturbances caused by parameter variations. While artificial neural networks have been proposed for online adaptation [47], Lyapunov-based adaptive designs provide an attractive alternative, as a stability proof is a byproduct of the design process [48]. However, none of these papers proposes a design which specifically considers Simultaneous Identification and Control (SIC) in their design.

This chapter presents a simultaneous identification and control methodology for PMSMs by exploiting the overactuated nature of the machine. Specifically, the parameters to be identified are the direct and quadrature-axis self-inductances, L_d and L_q, as well as the stator winding resistance, R. And the output to be controlled is the electromagnetic torque, τ. An indirect adaptive control design using the certainty equivalence principle is proposed in which a disturbance decoupling control law is utilized to prevent the input selected for excitation from perturbing the regulated output. The machine parameters used in this excitation decoupling control law are updated via a normalized gradient estimator. Simulation results for a torque regulating controller for PMSMs confirm the effectiveness of the proposed simultaneous identification and control design methodology. Furthermore, while the focus of the chapter is on the application of the proposed adaptive excitation decoupling control methodology to PMSM torque regulation, the prospects of generalizing this methodology for overactuated systems are promising.

Table 3.1: List of notation for PMSMs.

Symbol	Description
Electrical Variables	
$v_d^r(t)$	Direct-axis Voltage in Rotor Ref. Frame
$v_q^r(t)$	Quadrature-axis Voltage in Rotor Ref. Frame
$i_d^r(t)$	Direct-axis Current in Rotor Ref. Frame
$i_q^r(t)$	Quadrature-axis Current in Rotor Ref. Frame
R	Stator Winding Resistance
L_d	Direct-axis Stator Self-Inductance
L_q	Quadrature-axis Stator Self-Inductance
Λ_{PM}	Permanent Magnet Flux Linkage
Mechanical Variables	
τ	Three-Phase Electromagnetic Torque
ω_r	Rotor Angular Velocity
$\omega_{re} = \frac{P}{2}\omega_r$	Rotor Electrical Angular Velocity
P	Number of Poles

3.2 Dynamic Model of PMSMs

The proposed control algorithm is designed around the standard two-phase equivalent model for permanent-magnet synchronous machines [39], the physical cross-section of which is depicted in Figure 3.1. This model, and the subsequent control design, are derived under the following assumptions:

A1. The machine to be controlled has a smooth airgap (i.e., slotting effects are neglected), is fed by an ideal voltage source inverter (VSI), and is balanced in its construction such that it can be accurately represented by its 2-phase equivalent;

A2. A linear magnetics model is assumed (i.e., magnetic saturation effects are neglected) and core losses are neglected;

A3. The rotor and mechanical load have enough inertia that a significant time-scale separation exists between electrical and mechanical dynamics;

A4. The sampling frequency of the digital implementation is high enough that a continuous-time control design can be sufficiently approximated;

A5. The only uncertain parameters are resistance, R, permanent magnet flux linkage, Λ_{PM}, and the direct and quadrature inductance, L_d and L_q, respectively.

These assumptions are typical and valid under normal operation.

The first three assumptions (**A1** - **A3**) simplify the model by reducing its order and maintaining linearity. In particular, given that the mechanical dynamics associated with the rotor velocity are significantly slower than the electrical dynamics and that measurements of rotor velocity are readily available, ω_{re} may be treated as a known constant (**A3**). This simplification allows us to represent the machine as having linear time-invariant dynamics. The last two assumptions (**A4** and **A5**) pertain to the control design and methodology.

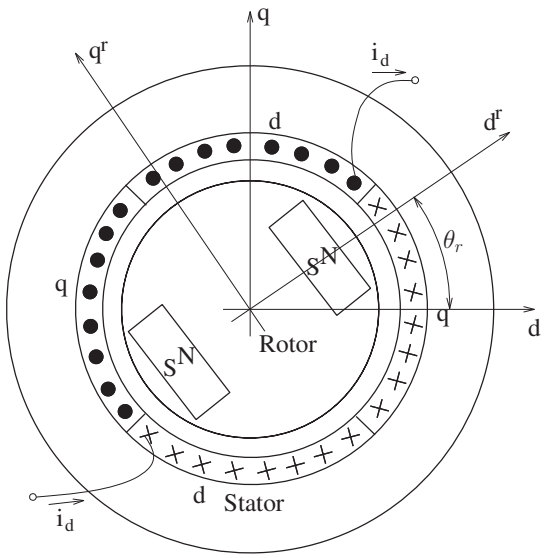

Figure 3.1: Cross-section of the two-phase equivalent, two-pole smooth airgap interior-permanent-magnet PMSM machine.

The dynamic model of a PMSM in the rotor reference frame (denoted by the superscript r), in which the direct-axis is aligned with the rotor permanent magnet flux, is given by,

$$L_d \frac{di_d^r}{dt} = -Ri_d^r + \omega_{re} L_q i_q^r + v_d^r, \tag{3.1}$$

$$L_q \frac{di_q^r}{dt} = -\omega_{re} L_d i_d^r - Ri_q^r + v_q^r - \omega_{re}\Lambda_{PM}, \tag{3.2}$$

with the unmeasured nonlinear torque output mapping,

$$\tau = \frac{3P}{4}\left[(L_d - L_q)\, i_d^r + \Lambda_{PM}\right] i_q^r. \tag{3.3}$$

Finally, the mechanical dynamics are given by

$$\frac{d}{dt}\omega_r = \frac{1}{H}\left[(\tau - \tau_l) - B\omega_r\right], \tag{3.4}$$

where H is the combined moment of inertia of the rotor and load, B is the mechanical damping, and τ_l is the load torque. However, because the separation between the (dominant) electrical and mechanical time constants ($T_{elec} = -\frac{R}{L_q}$ and $T_{mech} = -\frac{B}{H}$, respectively) is roughly a factor of 150 for the experimental machine considered in this work, we will neglect the mechanical dynamics in our design and analysis. We therefore treat the rotor speed as a known constant with respect to the electrical dynamics (3.1)-(3.2), as there exists a significant time-scale separation between the electrical and mechanical dynamics to justify **A3**.

3.3 Adaptive Disturbance Decoupling Approach

The SIC approach presented in this paper is based upon a certainty equivalence design in which an *excitation input decoupling* control law is used to prevent the excitation input signal from perturbing the regulated output. This excitation decoupling control law is derived by reformulating the problem as a *disturbance decoupling* problem [29].

3.3.1 Statement of the Control Objective

The control inputs to the PMSM are the direct and quadrature-axis voltages, u_d^r and u_q^r, and the (unmeasured) regulated output is electromagnetic torque, τ. Thus, the PMSM constitutes an overactuated system. Our control objective is to simultaneously achieve parameter identification and asymptotic output regulation in an overactuated system, namely the PMSM. This is accomplished by using an adaptive excitation (disturbance) decoupling control design in which one input of the overactuated system is designated as the *excitation input* used to ensure that the PMSM dynamics are persistently excited for parameter convergence, and the other input is used for torque output regulation. The excitation decoupling control law ensures that the perturbations in the regulated output go to zero asymptotically as the machine

parameters converge to their true values. Once identified, the presence of the excitation signal ensures that the parameter estimator will track any changes in the parameters.

3.3.2 Review of Disturbance Decoupling

To apply this solution to the simultaneous identification and control problem, we treat the excitation input as a measured disturbance, and derive a state-feedback controller which decouples the excitation input from the regulated output, provided that the system parameters are well known. For convenience, we will first review the general solution for a class of nonlinear systems [29] before applying the result to the PMSM torque regulation problem.

Consider a nonlinear system of the form

$$\Sigma : \begin{cases} \dot{x} = f(x) + g(x)u + p(x)w, \\ y = h(x), \end{cases} \tag{3.5}$$

where $x \in \mathbb{R}^n$ is the state vector, $y \in \mathbb{R}$ is the regulated (or "performance") output, $u \in \mathbb{R}$ is the input and $w \in \mathbb{R}$ is the disturbance input which is to be decoupled.

Given measurements of the full state vector, x, as well as the disturbance, w, it is possible to decouple the disturbance from the output, y, using a state-feedback law of the form $u = \alpha(x) + \beta(x)\psi + \gamma(x)w$, where ψ is a control input which will be designed to yield stable linear closed-loop dynamics provided that,

$$L_p L_f^i h(x) = 0 \quad \text{for all} \quad 0 \leq i \leq \rho - 2, \tag{3.6}$$

$$L_p L_f^{\rho-1} h(x) = -L_g L_f^{\rho-1} h(x)\gamma(x), \tag{3.7}$$

for all x in the neighborhood of the equilibrium, x^o, where $L_f^i h(x)$ denotes the i^{th} Lie derivative of $h(x)$ projected along $f(x)$ and ρ is the *relative degree* of the system, Σ. Note that the second condition is easily satisfied by solving for $\gamma(x)$ and including the term in the feedback law. If these conditions are satisfied for a given plant, a feedback law which achieves disturbance decoupling, is given by:

$$u = -\frac{L_f^\rho h(x)}{L_g L_f^{\rho-1} h(x)} - \frac{L_p L_f^{\rho-1} h(x)}{L_g L_f^{\rho-1} h(x)} w + \frac{\psi}{L_g L_f^{\rho-1} h(x)}. \tag{3.8}$$

The design of ψ is best understood by considering the system in the "normal

form" [29], which is obtained by defining new coordinates such that,

$$\begin{aligned}
\dot{z}_1 &= z_2 \\
&\vdots \\
\dot{z}_{\rho-1} &= z_\rho \\
\dot{z}_\rho &= b(\xi,\eta) + a(\xi,\eta)u + d(\xi,\eta)w \\
\dot{\eta} &= q(\xi,\eta) + k(\xi,\eta)w \\
y &= z_1
\end{aligned}$$

where $\xi = [z_1 \cdots z_\rho]^\top$ and $\eta = [z_{\rho+1} \cdots z_n]^\top$. Note that the term $\dot{\eta} = q(0,\eta)$ represents the *zero dynamics* of the system, which must be stable (i.e., minimum phase) to ensure that the closed-loop design is internally stable. In the new coordinate system (i.e., normal form) the state-feedback law (3.8) takes the form,

$$u = -\frac{b(\xi,\eta)}{a(\xi,\eta)} - \frac{d(\xi,\eta)}{a(\xi,\eta)}w + \frac{\psi}{a(\xi,\eta)},$$

and the closed-loop system takes on the structure depicted in Figure 3.2, effectively isolating the output, y, from the disturbance input, w.

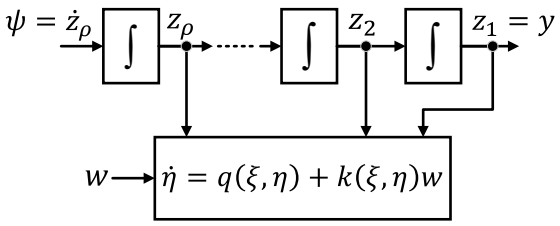

Figure 3.2: Block diagram of closed-loop system after disturbance decoupling (adapted from [29]).

With Figure 3.2 in mind, our choice of the control, $\bar{v}$, is rather intuitive:

$$\begin{aligned}
\psi &= -\left(c_0 z_1 + \cdots + c_{\rho-1} z_\rho\right) + \tilde{y} \\
&= -\left(c_0 h(x) + \cdots + c_{\rho-1} L_f^{\rho-1} h(x)\right) + \tilde{y},
\end{aligned} \tag{3.9}$$

where $\tilde{y}$ is the reference input (i.e., desired output value) and the coefficients $c_0, \cdots, c_{\rho-1}$ are selected to yield the desired linear dynamics with characteristic equation,

$$s^\rho + c_{\rho-1} s^{\rho-1} + \cdots + c_1 s + c_0 = 0. \tag{3.10}$$

It should be noted that, in general, the solution to the disturbance decoupling problem presented here, and its asymptotic stability properties, are *local* results (i.e., they hold only for a neighborhood of the equilibrium point, x^o).

3.3.3 Excitation Decoupling for PMSMs

The dynamic model of the PMSM in the rotor reference frame, (3.1) and (3.2), may be rewritten in the following form,

$$\frac{d}{dt}\begin{bmatrix} i_d^r \\ i_q^r \end{bmatrix} = \underbrace{\begin{bmatrix} -\frac{R}{L_d} & \omega_{re}\frac{L_q}{L_d} \\ -\omega_{re}\frac{L_d}{L_q} & -\frac{R}{L_q} \end{bmatrix}\begin{bmatrix} i_d^r \\ i_q^r \end{bmatrix}}_{\triangleq f(x)} + \underbrace{\begin{bmatrix} 0 \\ \frac{1}{L_q} \end{bmatrix}}_{\triangleq g(x)} u_q^r + \underbrace{\begin{bmatrix} \frac{1}{L_d} \\ 0 \end{bmatrix}}_{\triangleq p(x)} u_d^r, \tag{3.11}$$

with the nonlinear torque output mapping (3.3), repeated for convenience,

$$\tau = \underbrace{\frac{3P}{4}\left[(L_d - L_q)\, i_d^r + \Lambda_{PM}\right] i_q^r}_{\triangleq h(x)}, \tag{3.12}$$

where the direct and quadrature currents are the states (i.e., $x = [i_d^r \;\; i_q^r]^\top$) of the system and the direct and quadrature voltage inputs to the system are assumed to include a EMF cancellation term, i.e., $v_q^r = u_q^r + \Lambda_{PM}\omega_{re}$, and $v_d^r = u_d^r$ for consistency.

To apply the disturbance decoupling solution to our problem, we first need to decide which plant inputs will be used for control and which will be used for excitation (i.e., the "disturbance" to be decoupled). While this can be challenging for general plant models, many applications lend intuition which may be leveraged to make this decision. As it concerns our application, we note that the coupling between the direct and quadrature-axis dynamics is only strong at high speeds (3.11), going to zero at zero speed (i.e., the system matrix is diagonal at zero speed). Additionally, inspection of the torque output mapping (3.12) reveals that, because $(L_d - L_q)$ tends to be much smaller than Λ_{PM}, the quadrature-axis current, i_q^r, and thus, the quadrature-axis voltage input, u_q^r, has the most authority over the torque output. Therefore, we take the quadrature-axis voltage, u_q^r, as the *control input* and the direct-axis voltage, u_d^r, as the *disturbance input* (for excitation) to be decoupled. Thus, the PMSM is treated as a SISO system with control input, u_d^r, regulated output τ, and measured disturbance input, u_d^r. While we have selected our control input based on its authority over the regulated output, for other applications, this decision could also be dictated by which input provides more excitation for identification.

The relative degree of the PMSM system (3.11)-(3.12) from either input (u_d^r or u_q^r) to the output, τ, is one (i.e., $\rho = 1$ for the PMSM), which is easily verified by differentiating the output (3.12) with respect to time. Therefore, we need only include the following feed-forward term

$$\gamma(x) = \frac{L_q}{L_d} \frac{(L_d - L_q) i_q^r}{(L_d - L_q) i_d^r + \Lambda_{PM}}$$

in the excitation decoupling control law to ensure that the conditions (3.6)-(3.7) are satisfied. Furthermore, since the PMSM dynamics (3.11)-(3.12) are minimum phase, we may apply the disturbance decoupling results from the previous section.

While our focus is on the design of the control input, u_q^r, in practice it is beneficial to cancel the cross coupling term in the direct-axis dynamics as it will lead to resonant behavior, as well as a large steady-state direct-axis current, at high rotor velocities. Therefore, we include the following feedback term for the direct-axis,

$$u_d^r = -\omega_{re} \hat{L}_q i_q^r + \hat{R} u_e, \tag{3.13}$$

where u_e is the excitation input which is scaled by the estimated resistance so that it corresponds to the magnitude of the steady-state direct-axis current generated by the direct-axis command voltage. Computing the necessary Lie derivatives specified in (3.8), we obtain the excitation decoupling control law for PMSMs:

$$u_q^r = \hat{R} i_q^r + \omega_{re} \hat{L}_d i_d^r - \frac{\hat{R}}{\hat{L}_d} \frac{\hat{L}_q \hat{\Delta}_L i_q^r}{\hat{\Delta}_L i_d^r + \Lambda_{PM}} (u_e^r - i_d^r) + \frac{4 \hat{L}_q}{3P \left(\hat{\Delta}_L i_d^r + \Lambda_{PM} \right)} \psi, \tag{3.14}$$

where the "hat" ($\hat{\cdot}$) designates parameters which will be adaptively estimated, and $\hat{\Delta}_L = \hat{L}_d - \hat{L}_q$ (for compactness).

Finally, we design the control input, v, in (3.14) as follows:

$$\psi = -\lambda h(x) + \lambda \tilde{\tau}, \tag{3.15}$$

which yields the following first-order (input-output) closed-loop dynamics,

$$\Sigma_{cl} : \begin{cases} \dot{z} = -\lambda z + \lambda \tilde{\tau} \\ \tau = z = h(x) \end{cases} \tag{3.16}$$

where $\lambda > 0$ is a control gain which sets the closed-loop bandwidth, and $h(x)$ is

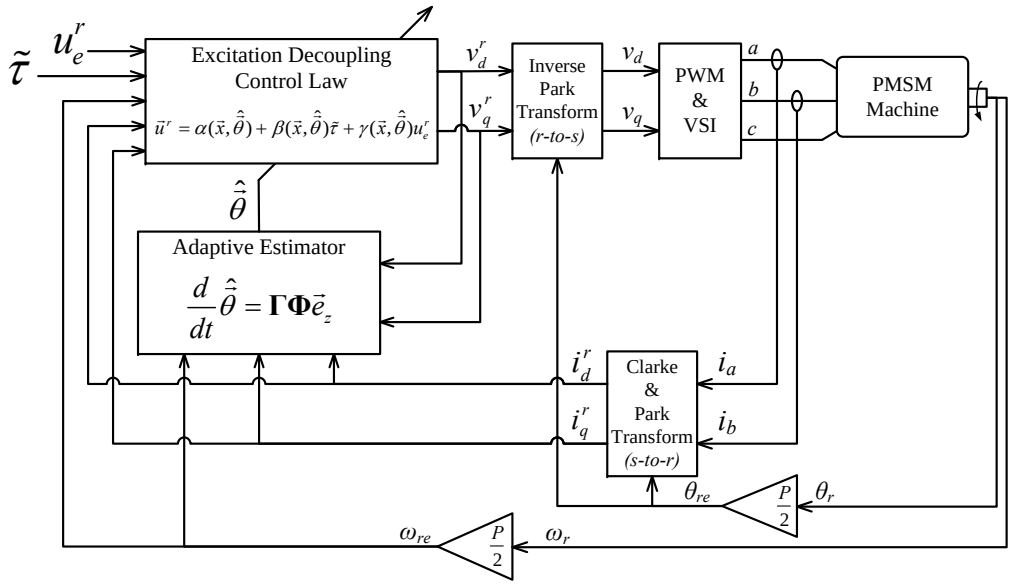

Figure 3.3: Block diagram of the closed-loop system with proposed adaptive excitation decoupling controller.

defined by (3.12). Thus, the disturbance and its associated dynamics are decoupled from the output, z. Finally, we compute the value for λ based on our desired rise-time of 2 milliseconds and the following relationship for first-order systems [18],

$$\lambda = \frac{1.8}{t_r},$$

where t_r is our desired rise time (i.e., $t_r = 2$ msec).

Remark: A comprehensive stability analysis of the adaptive excitation decoupling control will not be pursued in this dissertation. However, once parameter convergence is obtained, which is guaranteed by the algorithm proposed in the next section, stability of the closed-loop system will follow from the non-adaptive disturbance decoupling control. Therefore, for the adaptive control problem, stability can be assured if there is no finite escape time.

Estimates of the machine parameters used in the excitation decoupling control law (3.14) are provided by a normalized gradient-based algorithm. The resistance, as well as the direct and quadrature inductances, are directly estimated by the algorithm. A block diagram of the overall adaptive control system is provided in Figure 3.3.

3.3.4 Gradient-based Parameter Estimation

To formulate the parameter estimator, we first construct a linear parameterization for the system model (3.11),

$$\vec{z} = \mathbf{\Phi}^\top \vec{\theta}, \tag{3.17}$$

where $\vec{z} = [u_d^r \;\; u_q^r]^\top$ is the observation vector, $\vec{\theta} = [R \;\; L_d \;\; L_q]^\top$ is the parameter vector, and the regressor matrix is given by

$$\mathbf{\Phi}^\top = \begin{bmatrix} \vec{\phi}_d^\top \\ \vec{\phi}_q^\top \end{bmatrix} = \begin{bmatrix} i_d^r & \frac{d}{dt} i_d^r & -\omega_{re} i_q^r \\ i_q^r & \omega_{re} i_d^r & \frac{d}{dt} i_q^r \end{bmatrix}. \tag{3.18}$$

In order to avoid direct computation of derivatives in the regressor matrix, we filter each side of (3.17) by a stable first-order filter [28], i.e.,

$$\{M(s)\}\, \vec{z} = \{M(s)\}\, \mathbf{\Phi}^\top \vec{\theta},$$

where

$$\{M(s)\} = \left\{ \frac{K_f}{s + K_f} \right\}$$

is the transfer function representation of a stable first-order filter (i.e., $K_f > 0$) which operates on the individual elements of $\vec{z}$ and $\mathbf{\Phi}$.

The parameter estimates are obtained by integrating the following expression,

$$\begin{aligned} \dot{\hat{\vec{\theta}}} &= \mathbf{\Gamma} \mathbf{\Phi} \vec{e}_z \\ &= \mathbf{\Gamma} \begin{bmatrix} \vec{\phi}_d & \vec{\phi}_q \end{bmatrix} \begin{bmatrix} e_{zd} \\ e_{zq} \end{bmatrix} \\ &= \mathbf{\Gamma} \left(\vec{\phi}_d e_{zd} + \vec{\phi}_q e_{zq} \right) \end{aligned} \tag{3.19}$$

where $\mathbf{\Gamma} = \mathbf{\Gamma}^\top > 0$ is the adaptation gain matrix and $\vec{e}_z = [e_{zd} \;\; e_{zq}]^\top$ is the normalized estimator error vector, whose entries are given by,

$$e_{zd} = \frac{u_d^r - \vec{\phi}_d^\top \hat{\vec{\theta}}}{1 + \vec{\phi}_d^\top \vec{\phi}_d}, \tag{3.20}$$

$$e_{zq} = \frac{u_q^r - \vec{\phi}_q^\top \hat{\vec{\theta}}}{1 + \vec{\phi}_q^\top \vec{\phi}_q}. \tag{3.21}$$

Finally, we note that the rows of the regressor matrix, $\mathbf{\Phi}$, are scaled such that

the nominal signal amplitudes are around unity to ensure that the identification problem is well-conditioned. This is important as the large differences in the order-of-magnitude between resistances and inductances will lead to a numerically poorly-conditioned identification problem if left unscaled.

3.4 Selection of Persistently Exciting Inputs

A disadvantage of the design approach presented in this chapter is that it significantly complicates the analysis of the resulting closed-loop adaptive controller. However, by making some reasonable simplifying assumptions, we are able to gain some intuition to guide the design of persistently exciting inputs.

In the following analysis, we will assume that we have accurate knowledge of the machine parameters, as this represents something of a worst-case scenario since any error in the estimated parameters is expected to provide additional "information" for identification. This is because the excitation signal is only perfectly decoupled from the output when the plant parameters are accurately known. Thus, when there is parameter uncertainty, the excitation signal will excite additional dynamics in the plant as compared to when we have accurate parameter knowledge.

To analyze the influence of the reference torque, $\tilde{\tau}$, and the excitation input, u_e^r, on the conditioning of the regressor matrix (3.18), we need to relate these inputs to the direct and quadrature-axis currents, i_d^r and i_q^r. Under the assumption of accurate parameter knowledge, the closed-loop direct-axis current dynamics are given by

$$\frac{d}{dt} i_d^r = -\frac{R}{L_d} i_d^r + \frac{R}{L_d} u_e^r. \tag{3.22}$$

Additionally, recalling the closed-loop torque regulation dynamics (3.16) and noting that $z = \tau$ in (3.16), we get that

$$\frac{d}{dt} \tau = -\lambda \tau + \lambda \tilde{\tau}. \tag{3.23}$$

To simplify our analysis of the regressor, we will assume that that $L_d \approx L_q$. This is a conservative assumption, however, as a significant magnetic saliency, i.e., $L_q >> L_d$, will provide additional excitation via the coupling between the direct and quadrature currents through the torque expression (4.6). Note that for the torque to remain constant in the presence of excitation introduced via the direct-axis dynamics, the quadrature-axis current must vary in an inverse manner. Under this assumption, the

torque expression is simplified as follows:

$$\begin{aligned}\tau &= \frac{3P}{4}\left[\left(L_d - L_q\right) i_d^r + \Lambda_{PM}\right] i_q^r, \\ &\approx \frac{3P}{4}\Lambda_{PM} i_q^r, \\ &= K_\Lambda i_q^r.\end{aligned} \tag{3.24}$$

Next, we relate the reference torque, $\tilde{\tau}$, to the quadrature-axis current, i_q^r, by substituting the relationship in (3.24) into (3.23), to get that

$$\frac{d}{dt} i_q^r = -\lambda i_q^r + \frac{\lambda}{K_\Lambda}\tilde{\tau}. \tag{3.25}$$

To determine sufficient conditions for persistent excitation on the reference torque, $\tilde{\tau}$, and the excitation input, u_e^r, we will use the definition of persistent excitation. Noting that (from (3.18)),

$$\frac{1}{T}\int_t^{t+T} \mathbf{\Phi}(\sigma)\mathbf{\Phi}^\top(\sigma)d\sigma = \frac{1}{T}\int_t^{t+T} \vec{\phi}_d(\sigma)\vec{\phi}_d^\top(\sigma)d\sigma + \frac{1}{T}\int_t^{t+T} \vec{\phi}_q(\sigma)\vec{\phi}_q^\top(\sigma)d\sigma, \tag{3.26}$$

it follows that a sufficient condition for $\mathbf{\Phi}$ to be persistently exciting is that either $\vec{\phi}_d$ or $\vec{\phi}_q$ (or both) be persistently exciting. Assuming the excitation input is sinusoidal, i.e., $u_e^r = \sin(\omega t)$, it follows that the (sinusoidal) steady-state solution to (3.22) is of the form

$$i_d^r = a\sin(\omega t + b).$$

Additionally, we will assume that the torque reference input is constant. It follows that the steady-state solution to (3.25) is given by

$$i_q^r = \frac{\tilde{\tau}}{K_\Lambda}.$$

Under these assumptions, the direct-axis regressor vector is given by

$$\vec{\phi}_d(t) = \begin{bmatrix} i_d^r \\ \frac{d}{dt} i_d^r \\ -\omega_{re} i_q^r \end{bmatrix} = \begin{bmatrix} a\sin(\omega t + b) \\ a\omega\cos(\omega t + b) \\ -\omega_{re}\frac{\tilde{\tau}}{K_\Lambda} \end{bmatrix}. \tag{3.27}$$

Finally, using the definition of persistent excitation, and taking the time interval to

be $[0, \frac{2\pi}{\omega}]$, it can be shown that

$$\det\left(\frac{\omega}{2\pi}\int_0^{\frac{2\pi}{\omega}} \vec{\phi}_d(\sigma)\vec{\phi}_d^{\top}(\sigma)d\sigma\right) = \frac{\tilde{\tau}^2 a^4 \omega^2 \omega_{re}^2}{4K_\Lambda^2}. \tag{3.28}$$

We conclude that, if $\tilde{\tau}, a, \omega$, and $\omega_{re} \neq 0$, then $\mathbf{\Phi}$ is persistently exciting.

In the next section, we will investigate parameter convergence properties when the reference torque is equal to zero, i.e., $\tilde{\tau} = 0$, and when the excitation input is zero, i.e., $a = 0$, using numerical simulations. Intuitively, we expect these conditions to cause problems with parameter convergence since $\tilde{\tau} = 0$ and $a = 0$ (i.e., $i_d^r = 0$) lead to a row of zeros in the regressor (3.18). Additionally, it will be verified that, by leveraging the excitation input, we can ensure complete parameter convergence.

3.5 Simulation Results

We have validated the proposed adaptive excitation decoupling control methodology for SIC in Matlab/Simulink simulations using a dynamic model of the PMSM and the *ode4* Fixed-step Runge-Kutta solver with a step size of 10 μ-sec. Parameters provided in Table 3.2 were used in all simulations except where noted otherwise.

Table 3.2: Simulation parameters.

Description	**Value**
Electrical Machine Parameters:	
R	102.8 $m\Omega$
L_d	212.3 μH
L_q	424.6 μH
Λ_{PM}	12.644 mV-s
P	10
Control Design Parameters:	
λ	900
$\mathbf{\Gamma}$	diag([16 80 40])
K_f	1000
ω_{pe}	363 rad/sec

3.5.1 On Conditions for Parameter Convergence

Due to the overactuated nature of the PMSM, we are able to ensure that the machine dynamics are persistently excited while minimizing perturbations to the regulated (i.e., torque) output, by utilizing the excitation input. Our only requirement on the torque reference input to ensure full parameter convergence, is that the torque command be nonzero, as the analysis in the preceding section suggested. To investigate parameter convergence properties in the closed-loop system, Simulink simulations are run which examine scenarios when the excitation input is set to zero, and in which the torque (control) command is set to zero.

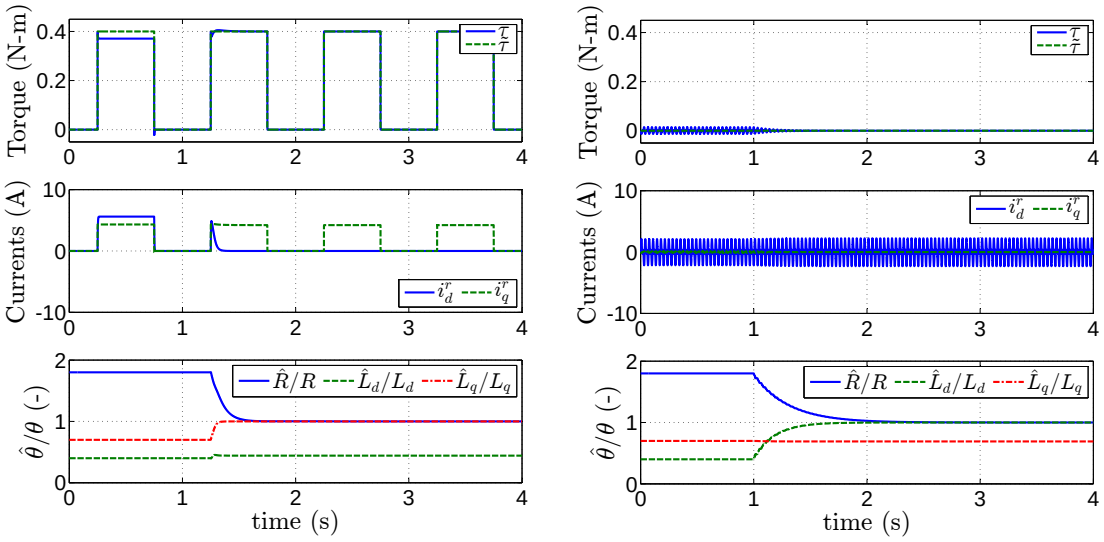

Figure 3.4: Simulations of the closed-loop adaptive system (adaptation turned "on" at t = 1 sec): (a) without persistently exciting input (i.e., $u_e^r = 0$), leading to partial convergence; and, (b) with zero torque command input (i.e., $\tilde{\tau} = 0$), again leading to partial convergence.

In Figure 3.4(a) we see that, without the additional information provided by the excitation input, i.e. $u_e = 0$, the estimate of the direct-axis inductance, $\hat{L}_d$, settles to an incorrect value. This scenario serves as our baseline adaptive control design in which the overactuation in the system *is not* exploited. This essentially gives us the feedback linearization portion of the controller and a fair basis with which to compare. Despite the rich harmonic content of the square wave torque command, the estimated parameters do not fully converge to their true values. However, in Figure 3.4(b) we see that, when the torque command is set to zero, the estimated machine parameters again fail to converge fully to their true values, despite the presence of

a persistently exciting excitation input, $u_e = 1.5\,(\sin(\omega_{pe}t) + \sin(0.5 \cdot \omega_{pe}t))$. The zero torque command results in a lack of sufficient richness for the quadrature-axis inductance estimate, $\hat{L}_q$, to converge to its true value.

3.5.2 Closed-loop Performance

The main objective in this work is to demonstrate an adaptive control methodology for overactuated systems which is capable of achieving simultaneous identification of parameters and control of a regulated output. This is achieved by exploiting the overactuated nature of a PMSM by designating one input as an excitation input, which is designed to ensure that the system is persistently excited for parameter identification, and the other input as the control input used for torque regulation.

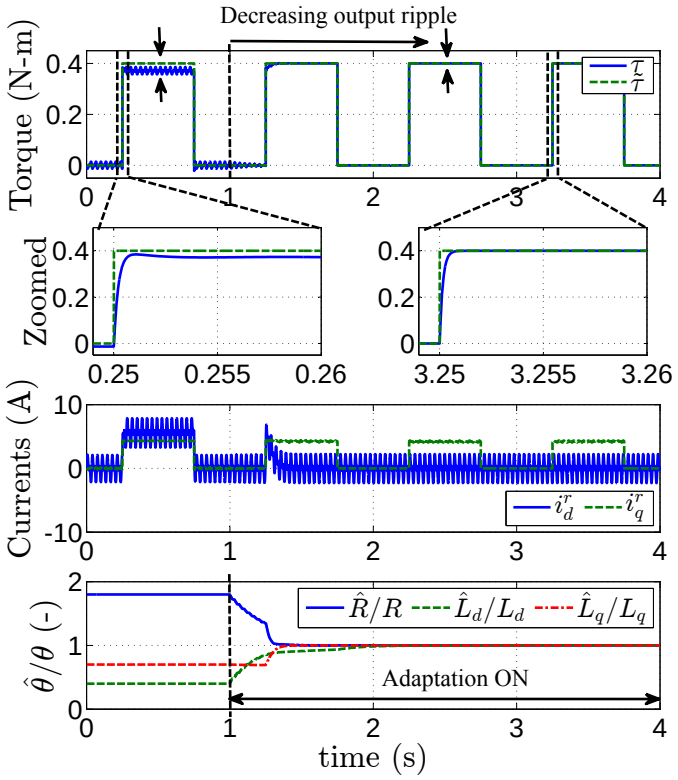

Figure 3.5: Simulation of closed-loop adaptive system at a fixed rotor velocity of 2000 rpm with excitation input (adaptation turned "on" at t = 1 sec).

In Figure 3.4(a) we see that, without leveraging the extra degree of freedom resulting from overactuation (i.e., utilizing the excitation input) the estimated parameters converge to a set where, despite the fact that the control error goes to zero, the estimate of L_d stagnates at an incorrect value. This is the typical scenario for adaptive control in which the adaptation drives the control error to zero, but due to a lack of

persistent excitation, the parameters fail to completely converge to their true values. However, when we use the overactuated nature of the PMSM to our advantage, we are able to ensure that the system is persistently excited and so all of the parameters converge to their true values. This is accomplished by using a disturbance decoupling control law to fix the control allocation such that, given accurate parameter knowledge, the excitation input is decoupled from the regulated output, allowing us to introduce excitation for parameter identification while minimizing the impact on output regulation. Machine parameters used in the control law are then updated by the online identification, ensuring that any perturbations to the torque output vanish as the estimated parameters converge to their true values. Inspection of the results in Figure 3.5 confirm that the closed-loop system performs very well, with torque perturbations due to the excitation input vanishing as the estimated parameters converge to their true values.

Finally, to demonstrate that the closed-loop adaptive excitation decoupling controller does exhibit robustness to uncertainty as well, simulations are run which include zero-mean Gaussian noise on the stator current measurements. Inspection of these results, presented in Figure 3.6, indicate that, despite the presence of measurement noise, the parameters converge to their true values. It should be noted that, in practice, limiting the bandwidth of the adaptive estimator will improve performance

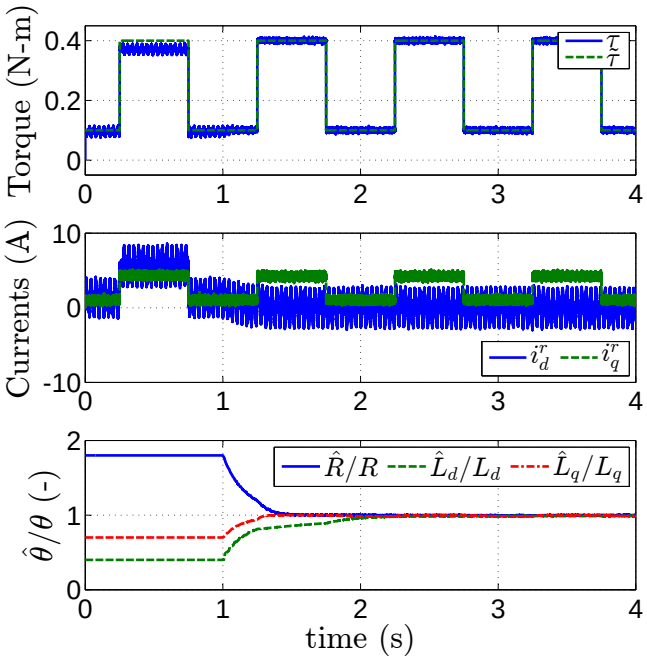

Figure 3.6: Simulation of closed-loop adaptive system at a fixed rotor velocity of 2000 rpm with zero-mean Gaussian noise added to the current measurements.

in presence of measurement noise. Additionally, while the simulations presented here do not include any robustness modification to the adaptive update law (3.19), in an experimental implementation, the addition of a robustness modification such as a switching-sigma or projection is advised [28].

3.6 Conclusion

This chapter presented recent research [67] into the application of disturbance decoupling to the development of a simultaneous identification and control methodology for overactuated systems via a case study with PMSMs. An indirect adaptive control design using the certainty equivalence principle was proposed in which a disturbance decoupling control law, termed *excitation decoupling*, is utilized to prevent the excitation input from perturbing the regulated output. The plant parameters used in the excitation decoupling control law are updated online via a normalized gradient estimator. Simulation results for simultaneous identification and torque regulation in PMSMs confirm the effectiveness of the proposed design methodology. While open issues remain, such as a comprehensive assessment of closed-loop stability, the "adaptive excitation decoupling" approach shows promise for generalization.

CHAPTER IV

Simultaneous Identification and Control of Permanent Magnet Synchronous Machines via Adaptive 2-DOF Lyapunov Design

4.1 Introduction

In the previous chapter, an investigation into the application of disturbance decoupling control theory to the simultaneous identification and control of overactuated systems, dubbed "adaptive excitation decoupling", was presented. The advantage of this approach is that it is based upon well established theory and provides a relatively straightforward design procedure. However, even if the resulting closed-loop adaptive system is globally asymptotically stable, it will be very challenging to demonstrate this analytically. Likely, the best that can be argued is that if the closed-loop system does not posses a finite-escape time, and the system is persistently excited such that the estimated parameters are converging to their true values, then local stability is assured by the disturbance decoupling control law.

This chapter presents a Lyapunov-based simultaneous identification and control design methodology for overactuated systems which is demonstrated on PMSMs and whose stability properties can be rigorously established. By constraining the states to a manifold which corresponds to zero regulated-output error, we are able to achieve excitation and output regulation simultaneously. The controller to be presented for PMSMs is derived using Lyapunov's stability theorem, and so the stability of the closed-loop system is demonstrated in the process of deriving the adaptation law. A

This chapter based on work submitted to a journal and is under review:
D. M. Reed, J. Sun, and H. F. Hofmann, "Simultaneous Identification and Robust Adaptive Torque Control of Permanent Magnet Synchronous Machines," *Under review,* 2015.

switching-σ robust modification to the derived adaptive law is used to ensure closed-loop stability in the presence of unmodeled disturbances. The control law, designed using the certainty equivalence principle [28], utilizes a combination of adaptively-tuned feedforward (to achieve zero steady-state error), $d-q$ decoupling (to improve transient response), and proportional feedback (to add robustness to disturbances) terms. Overactuation of the system is exploited to simultaneously achieve parameter convergence and torque regulation. After reviewing the dynamic PMSM machine model, the derivation and stability proof for the proposed adaptive controller is presented. Necessary conditions for parameter convergence are discussed, and simulation results verifying the performance of the control design are presented. Remarks specific to experimental implementation challenges, as well as experimental results, are presented and discussed.

4.2 Two-Phase Equivalent Dynamic Model for PMSMs

For convenience, and continuity with the material to be discussed in this chapter, presentation of the two-phase equivalent PMSM model is repeated here. This model, and the subsequent control design, are derived under the following assumptions:

A1. The machine to be controlled has a smooth airgap (i.e., slotting effects are neglected), is fed by an ideal voltage source inverter (VSI), and is balanced in its construction such that it can be accurately represented by its 2-phase equivalent model;

A2. Linear magnetics is assumed (i.e., magnetic saturation effects are neglected), and core losses are neglected;

A3. The rotor (electrical) velocity, ω_{re}, is a bounded time-varying input which is known (i.e., measured);

A4. The sampling frequency of the digital implementation is high enough that a continuous-time control design can be sufficiently approximated;

A5. The only uncertain parameters are resistance, R, permanent magnet flux linkage, Λ_{PM}, and the direct and quadrature inductances, L_d and L_q, respectively.

Note that these assumptions differ slightly from those in preceding chapter (i.e., Chapter 3) in that the assumption of constant rotor velocity is relaxed, as it is not

required for the theory to be presented. Additionally, we will consider the permanent magnet flux linkage as an unknown parameter to be estimated.

The first three assumptions (**A1** - **A3**) simplify the model and reduce its order, while the last two assumptions (**A4** and **A5**) pertain to the control design and methodology. Under these assumptions, the dynamic model of a PMSM, repeated here for easy reference, is given by:

$$\begin{aligned} L_d \frac{di_d^r}{dt} &= -Ri_d^r + \omega_{re} L_q i_q^r + v_d^r, \\ L_q \frac{di_q^r}{dt} &= -\omega_{re} L_d i_d^r - Ri_q^r + v_q^r - \omega_{re} \Lambda_{PM}, \end{aligned} \tag{4.1}$$

with the *unmeasured* nonlinear torque output mapping

$$\tau = \frac{3P}{4} \left[(L_d - L_q)\, i_d^r + \Lambda_{PM} \right] i_q^r. \tag{4.2}$$

4.3 Simultaneous Identification and Control Objective and Methodology

The SIC design methodology demonstrated in this chapter on torque regulation in PMSMs is based on constraining the states of the system to a set which corresponds to a particular desired (regulated) output value, and then varying the state within that set in order to excite the system dynamics for parameter identification. Specifically, we are interested in regulating the (unmeasured) electromagnetic torque output of PMSMs, for which the regulated output error is defined as follows:

$$\begin{aligned} e_\tau &= \tilde{\tau} - \tau, \\ &= \tilde{\tau} - h(i_d^r, i_q^r), \end{aligned} \tag{4.3}$$

where the "tilde" denotes the reference input and $h(\,\cdot\,) : \mathbb{R}^2 \mapsto \mathbb{R}$ is the nonlinear torque output mapping provided in (4.2). Note that e_τ describes a 1-D manifold in the two dimensional (real) state-space (see Figure 4.1). We define this output (error) zeroing manifold as follows:

$$(i_d^r, i_q^r) \in \mathcal{M} := \{(i_d^r, i_q^r) \,:\, e_\tau = \tilde{\tau} - h(i_d^r, i_q^r) = 0\}. \tag{4.4}$$

Thus, restricting the system state to this manifold ensures that our regulated output objective is achieved, while the non-zero dimension of $\mathcal{M}$ provides space in which

the state may vary for identification purposes. This "wiggle room" for identification is available provided that the output maps the state-space to a lower-dimensional output space.

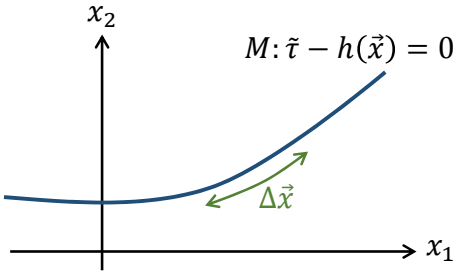

Figure 4.1: Depiction of a 1-D manifold in $\mathbb{R}^2$.

However, while it is possible to drive the state to points in the set $\mathcal{M}$ with a single input, provided that $\mathcal{M}$ is in the controllable subspace, it is generally not possible (with a single input) to vary the state within the set $\mathcal{M}$ without departing for a time, which results in a perturbation of the regulated output. Overactuation provides additional inputs to the system which may be coordinated in such a way that the state not only converges to $\mathcal{M}$, but also varies within the set without departing. The torque regulation problem for PMSMs is overactuated since we have two inputs to the system, v_d^r and v_q^r, but only one *regulated* output, i.e., torque. Thus, for our application, we wish to find an input pair, $(v_d^r, v_q^r)(t)$, such that the states, i_d^r and i_q^r, converge asymptotically to the set $\mathcal{M}$, as defined in (4.4).

Assuming that $(i_d^r, i_q^r)(t_0) \in \mathcal{M}$, the following invariance condition must be satisfied to ensure that $(i_d^r, i_q^r)(t) \in \mathcal{M}$ for all $t \geq t_0$,

$$\begin{aligned}
\dot{e}_\tau &= \dot{\tilde{\tau}} - \dot{\tau}, \\
&= \dot{\tilde{\tau}} - \frac{3P}{4}\left[\Delta_L\left(\frac{d}{dt}i_d^r\right)i_q^r + \left(\Delta_L i_d^r + \Lambda_{PM}\right)\left(\frac{d}{dt}i_q^r\right)\right], \\
&= 0,
\end{aligned} \tag{4.5}$$

where $\Delta_L = L_d - L_q$. At this point, we could substitute the machine dynamics into (4.5) and solve for a state-feedback control law satisfying these output-zeroing and invariance conditions. However, this will result in a highly nonlinear feedback law which may present robustness challenges and make the design and stability proof of the closed-loop adaptive controller difficult. We will instead use (4.4) to generate a reference quadrature stator current, $\tilde{i}_q^r$, given a desired torque output, $\tilde{\tau}$, and direct current, $\tilde{i}_d^r$, which will be treated as our free variable designed to ensure persistent

excitation (i.e., $\tilde{i}_d^r$ is our excitation input). If we can find a control law which ensures that $(i_d^r, i_q^r) \to (\tilde{i}_d^r, \tilde{i}_q^r)$ and $(\frac{d}{dt}i_d^r, \frac{d}{dt}i_q^r) \to (\frac{d}{dt}\tilde{i}_d^r, \frac{d}{dt}\tilde{i}_q^r)$ as $t \to \infty$, then it follows that (4.4) and (4.5) are satisfied asymptotically. Therefore, by designing a stator current regulator capable of *tracking* these reference currents, we will ensure that any perturbation in the torque output due to the excitation input vanishes asymptotically.

Given $\tilde{\tau}$ and $\tilde{i}_d^r$, we solve (4.4) for the reference quadrature current, $\tilde{i}_q^r$, which is the primary torque generating component of the stator currents:

$$\tilde{i}_q^r = \frac{\tilde{\tau}}{\frac{3P}{4}\left(\Delta_L \tilde{i}_d^r + \Lambda_{PM}\right)}. \tag{4.6}$$

The time-derivatives of our reference currents, $\tilde{i}_q^r$ and $\tilde{i}_d^r$, which are needed for tracking, are generated using reference models (i.e., filters), $M(s)$. Next, we seek an adaptive control design which will ensure asymptotic tracking of the reference currents in the presence of parameter uncertainty.

4.4 Adaptive Control Design

We begin our derivation of the adaptive controller by defining the direct and quadrature stator current errors:

$$\begin{aligned} e_{id}^r &= \tilde{i}_d^r - i_d^r, \\ e_{iq}^r &= \tilde{i}_q^r - i_q^r. \end{aligned} \tag{4.7}$$

The following control law,

$$\begin{aligned} v_d^r &= \hat{R}\tilde{i}_d^r + \hat{L}_d \frac{d\tilde{i}_d^r}{dt} - \omega_{re}\hat{L}_q i_q^r + K_{pd} e_{id}^r, \\ v_q^r &= \hat{R}\tilde{i}_q^r + \hat{L}_q \frac{d\tilde{i}_q^r}{dt} + \omega_{re}\hat{L}_d i_d^r + K_{pq} e_{iq}^r + \omega_{re}\hat{\Lambda}_{PM}, \end{aligned} \tag{4.8}$$

where the "hat" ($\hat{}$) is used to denote an estimated value and $K_{pd}, K_{pq} > 0$ are constant proportional control gains, is formulated using a combination of feedforward, feedback, and decoupling terms, designed to yield exponentially stable stator current error dynamics (4.9) under perfect model knowledge (i.e., $\hat{R} = R$, $\hat{L}_d = L_d$, $\hat{L}_q = L_q$, and $\hat{\Lambda}_{PM} = \Lambda_{PM}$):

$$\begin{aligned} \dot{e}_{id}^r &= -\frac{1}{L_d}\left(R + K_{pd}\right) e_{id}^r, \\ \dot{e}_{iq}^r &= -\frac{1}{L_q}\left(R + K_{pq}\right) e_{iq}^r. \end{aligned} \tag{4.9}$$

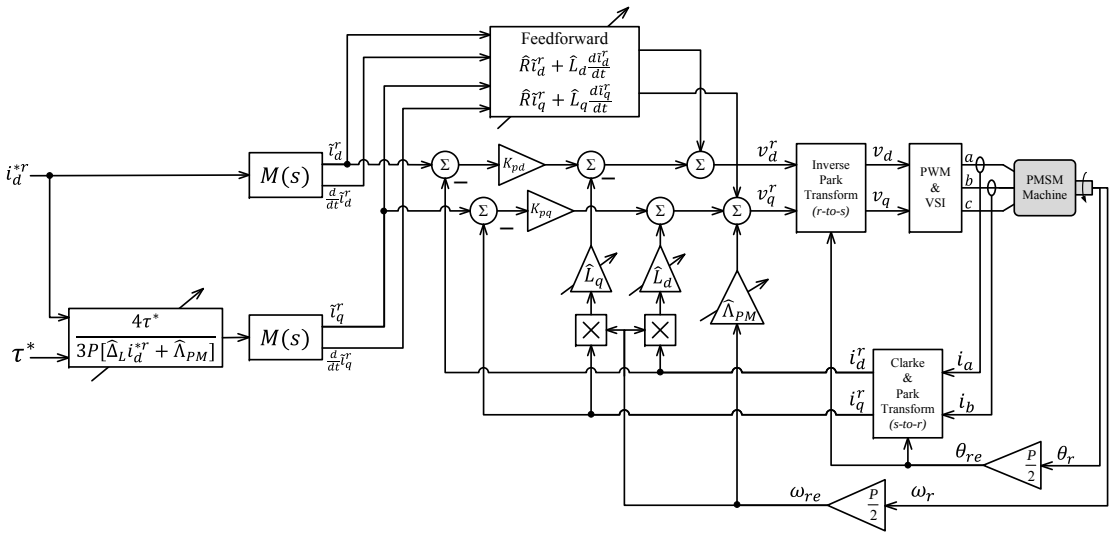

Figure 4.2: Block diagram of the proposed control law.

However, when the parameters R, L_d, L_q, and Λ_{PM} are not well known, one can show that the closed-loop error dynamics are given by:

$$\dot{\vec{e}}_i^r = \mathbf{L}^{-1}\mathbf{\Phi}^T\vec{e}_\theta - (R\mathbf{I} + \mathbf{K}_p)\,\mathbf{L}^{-1}\vec{e}_i^r, \tag{4.10}$$

where $\mathbf{K}_p = \text{diag}\,[K_{pd}, K_{pq}]$ is a diagonal matrix of the proportional control gains, $\mathbf{L} = \text{diag}\,[L_d, L_q]$ is a diagonal matrix of the direct and quadrature axis self-inductance, $\vec{e}_i^r = \begin{bmatrix} e_{id}^r & e_{iq}^r \end{bmatrix}^T$ is the stator current error vector, and $\vec{e}_\theta = \begin{bmatrix} e_R & e_{L_d} & e_{L_q} & e_\Lambda \end{bmatrix}^T$ is the parameter error vector with $e_R = R - \hat{R}$, $e_{L_d} = L_d - \hat{L}_d$, $e_{L_q} = L_q - \hat{L}_q$, and $e_\Lambda = \Lambda_{PM} - \hat{\Lambda}_{PM}$. Finally, the regressor matrix, $\mathbf{\Phi}$, in (4.10) is given by

$$\mathbf{\Phi}^T = \begin{bmatrix} \vec{\phi}_d^T \\ \vec{\phi}_q^T \end{bmatrix} = \begin{bmatrix} \tilde{i}_d^r & \frac{d}{dt}\tilde{i}_d^r & -\omega_{re} i_q^r & 0 \\ \tilde{i}_q^r & \omega_{re} i_d^r & \frac{d}{dt}\tilde{i}_q^r & \omega_{re} \end{bmatrix}. \tag{4.11}$$

To stabilize (4.10) and ensure that our simultaneous identification and control objectives are achieved in the presence of parameter uncertainty, adaptation is required. A block diagram of the proposed controller implementation is given in Figure 4.2, where the crossing arrows behind blocks symbolize portions of the controller which are tuned by the adaptation. Note that, in practice, implementation of the control law (4.8) uses filtered commands, i.e., $\tilde{\vec{i}}^r = \{M(s)\}\,\vec{i}^{*r}$ and $\frac{d}{dt}\tilde{\vec{i}}^r = \{sM(s)\}\,\vec{i}^{*r}$, as depicted in Fig. 4.2, where $M(s)$ is a stable, minimum phase, proper, unity dc gain, first-order transfer function[1], to prevent feeding-forward an unbounded signal during

[1] $\{\cdot\}$ denotes a dynamic operator with transfer function "$\cdot$".

a step-change in references. Furthermore, the use of a derivative term in the feed-forward portion of the control law (4.8) does not amplify noise, as the differentiated reference signals are free of noise.

To derive the adaptive update law, a Lyapunov stability analysis of the closed-loop system is first performed. The adaptive law is then selected such that it makes the Lyapunov function monotonically decreasing, thereby guaranteeing closed-loop stability of the controlled system. The following Lyapunov function candidate forms the basis of the derivation:

$$V(\vec{e}_i^{\,r}, \vec{e}_\theta) = \frac{1}{2}\left(\vec{e}_i^{\,rT}\mathbf{L}\vec{e}_i^{\,r} + \vec{e}_\theta{}^T\mathbf{\Gamma}^{-1}\vec{e}_\theta\right), \tag{4.12}$$

where $\mathbf{\Gamma} = \mathbf{\Gamma}^T > 0$ is the adaptation gain matrix. The first derivative of (4.12) with respect to time is given by

$$\dot{V}(\vec{e}_i^{\,r}, \vec{e}_\theta) = \vec{e}_i^{\,rT}\mathbf{L}\dot{\vec{e}}_i^{\,r} + \vec{e}_\theta{}^T\mathbf{\Gamma}^{-1}\dot{\vec{e}}_\theta. \tag{4.13}$$

Substituting (4.10) into (4.13), with some manipulation, yields:

$$\dot{V} = -\vec{e}_i^{\,rT}\left[R\mathbf{I} + \mathbf{K}_p\right]\vec{e}_i^{\,r} + \vec{e}_\theta^{\,T}\mathbf{\Phi}\vec{e}_i^{\,r} + \vec{e}_\theta^{\,T}\mathbf{\Gamma}^{-1}\dot{\vec{e}}_\theta. \tag{4.14}$$

It is assumed that the actual machine parameters are changing very slowly, i.e.,

$$\dot{\vec{e}}_\theta = \dot{\vec{\theta}} - \dot{\hat{\vec{\theta}}} \approx -\dot{\hat{\vec{\theta}}}, \tag{4.15}$$

where $\hat{\vec{\theta}} = \begin{bmatrix}\hat{R} & \hat{L}_d & \hat{L}_q & \hat{\Lambda}_{PM}\end{bmatrix}^T$. Finally, the adaptive law is selected as,

$$\dot{\hat{\vec{\theta}}} = \mathbf{\Gamma}\mathbf{\Phi}\vec{e}_i^{\,r}, \tag{4.16}$$

and so (4.14) becomes

$$\dot{V}(\vec{e}_i^{\,r}, \vec{e}_\theta) = -\vec{e}_i^{\,rT}\left[R\mathbf{I} + \mathbf{K}_p\right]\vec{e}_i^{\,r} \leq 0. \tag{4.17}$$

Therefore, the closed-loop system (4.1), with control law (4.8) and adaptation (4.16), is stable in the sense of Lyapunov [71].

To establish asymptotic convergence of the stator current error (i.e., $\vec{e}_i^{\,r} \to 0$ as $t \to \infty$), Barbalat's lemma [71] is used to show that $\dot{V}(\vec{e}_i^{\,r}, \vec{e}_\theta) \to 0$ as $t \to \infty$. Note that the preceding Lyapunov stability analysis has established that $V(\vec{e}_i^{\,r}, \vec{e}_\theta)$

is differentiable and has a finite limit as $t \to \infty$. To establish uniform continuity of $\dot{V}(\vec{e}_i^r, \vec{e}_\theta)$ we compute:

$$\ddot{V}(\vec{e}_i^r, \vec{e}_\theta) = -2\vec{e}_i^{rT} \left[R\mathbf{I} + \mathbf{K}_p\right] \dot{\vec{e}}_i^r, \tag{4.18}$$

and note that:

- $\vec{e}_i^r$ and $\vec{e}_\theta$ are bounded from (4.12) and (4.17),
- $\tilde{\vec{i}}^r$ and $\frac{d}{dt}\tilde{\vec{i}}^r$ are bounded by design, and so
- $\vec{i}^r = \tilde{\vec{i}}^r - \vec{e}_i^r$ is bounded,

thus $\dot{\vec{e}}_i^r$ is bounded (from inspection of (4.10)), and so $\ddot{V}(\vec{e}_i^r, \vec{e}_\theta)$ is also bounded. Therefore, from Barbalat's lemma we have that $\dot{V}(\vec{e}_i^r, \vec{e}_\theta) \to 0$ as $t \to \infty$; and so we conclude that the control law (4.8) with adaptive law (4.16) renders the system (4.1) stable in the sense of Lyapunov, with $\vec{e}_i^r \to 0$ as $t \to \infty$.

Lastly, we note that in practice our implementation of the adaptive update law (4.16) includes a switching σ-modification [28] for robustness, which acts as a "soft projection", applying a leakage term, σ, to the adaptive law only when a parameter is exceeding an expected limit on its range of variation. A benefit of this modification is that the ideal behavior of the adaptive law is preserved so long as the estimated parameters remain within their acceptable bounds (i.e., $|\hat{\vec{\theta}}_i(t)| < M_{0,i}$).

4.5 Simultaneous Parameter Identification

In the previous section, our analysis established that $\vec{e}_i^r \to 0$ as $t \to \infty$, without requiring parameter convergence. This is typical of adaptive control designs, as the estimated parameter set which yields zero steady-state control error is generally not unique. For the simultaneous identification and control problem, however, parameter identification is part of the design objective. To establish conditions for parameter convergence, we will apply two-time-scale theory. While this approach requires the assumption that the adaptation gain matrix is selected such that the parameter estimates converge at a much slower rate than the control error, it leads to a much more intuitive and cleaner analysis. Furthermore, in practice it is often desirable to limit the size of the adaptation gains in order to reduce sensitivity to noise and unmodelled high-frequency dynamics.

4.5.1 Parameter Convergence using Two-Time-Scale Analysis

With the controller and adaptive laws presented in the previous section, the closed-loop error dynamics (control and parameter) take the form

$$\begin{aligned} \mathbf{L}\dot{\vec{e}}_i^r &= \mathbf{\Phi}^T \vec{e}_\theta - (R\mathbf{I} + \mathbf{K}_p)\, \vec{e}_i^r \\ \dot{\vec{e}}_\theta &= -\mathbf{\Gamma}\mathbf{\Phi}\vec{e}_i^r. \end{aligned} \tag{4.19}$$

Note that $\mathbf{L}$ and $(R\mathbf{I} + \mathbf{K}_p)$ are diagonal matrices, and so their multiplication is therefore commutative. In practice, the inductances of the machine are relatively small numbers and can therefore play the role of the "epsilon scalar" commonly used in singular perturbation analyses to indicate small terms which are to be neglected [36]. Therefore, we may approximate (4.19) as,

$$\begin{aligned} 0 &\approx \mathbf{\Phi}^T \vec{e}_\theta - (R\mathbf{I} + \mathbf{K}_p)\, \vec{e}_i^r \\ \dot{\vec{e}}_\theta &= -\mathbf{\Gamma}\mathbf{\Phi}\vec{e}_i^r. \end{aligned} \tag{4.20}$$

Thus, assuming the *fast* stator current error dynamics have converged to a quasi-steady-state, the *slow* parameter error dynamics are given by,

$$\begin{aligned} \dot{\vec{e}}_\theta &= -\mathbf{\Gamma}\mathbf{\Phi}\left[R\mathbf{I} + \mathbf{K}_p\right]^{-1} \mathbf{\Phi}^T \vec{e}_\theta, \\ &= -\mathbf{\Gamma}\left(\frac{1}{R + K_{pd}}\vec{\phi}_d\vec{\phi}_d^T + \frac{1}{R + K_{pq}}\vec{\phi}_q\vec{\phi}_q^T\right)\vec{e}_\theta, \end{aligned} \tag{4.21}$$

where $\vec{\phi}_d$ and $\vec{\phi}_q$ are functions of time as defined in (4.11). Note that the *slow* parameter error dynamics are of the form

$$\dot{\vec{x}}(t) = \mathbf{A}(t)\vec{x}(t).$$

It follows that, so long as $\vec{\phi}_d$ and/or $\vec{\phi}_q$ is *persistently exciting*, that is

$$\alpha_1\mathbf{I} \geq \frac{1}{T}\int_t^{t+T} \vec{\phi}_{d,q}(\sigma)\vec{\phi}_{d,q}^T(\sigma)d\sigma \geq \alpha_0\mathbf{I}, \;\; \forall\; t \geq 0, \tag{4.22}$$

for some $T, \alpha_0, \alpha_1 > 0$, then $\vec{e}_\theta \to 0$ as $t \to \infty$.

4.5.2 Persistently Exciting Inputs

To determine necessary and sufficient conditions for persistent excitation, and thus, sufficient conditions for parameter convergence, we will take advantage of the connection between persistent excitation and linear independence of the functions which make up the rows of the regressor matrix. The definition for linear independence of vector-valued functions (of time) is similar to that of constant vectors (e.g., in $\mathbb{R}^n$) with the difference being that an interval of interest (i.e., the domain) is specified. The definition for linear independence of vector-valued functions is given here for convenience:

Definition IV.1. (Linear Independence of Functions [9]): *A set of $1 \times p$ real-valued functions, $\vec{f}_i(t)$ where $i = 1, \cdots, n$, is said to be **linearly dependent** on the interval $[t_0, t_1]$ over the field of reals if there exist scalars c_i, not all zero, such that*

$$c_1\vec{f}_1(t) + c_2\vec{f}_2(t) + \cdots + c_n\vec{f}_n(t) = 0$$

*for all $t \in [t_0, t_1]$. Otherwise, they are said to be **linearly independent** on the interval $[t_0, t_1]$.*

Naturally, there are a number of theorems which may be used to check whether or not a set of functions is linearly independence. For example, the Grammian matrix may be used:

Theorem IV.2. *(Grammian [9]): Let $\vec{f}_i(t)$, for $i = 1, 2, \cdots, n$, be $1 \times p$ real-valued continuous functions defined on the interval $[t_1, t_2]$. Let $\mathbf{F}$ be the $n \times p$ matrix with $\vec{f}_i(t)$ as its i^{th} row. Define*

$$\mathbf{W}(t_1, t_2) \triangleq \int_{t_1}^{t_2} \mathbf{F}(t)\mathbf{F}^\top(t)dt$$

*Then $\vec{f}_1(t), \vec{f}_2(t), \cdots, \vec{f}_n(t)$ are **linearly independent** on $[t_1, t_2]$ if, and only if, the $n \times n$ constant Grammian matrix, $\mathbf{W}(t_1, t_2)$, is **positive definite**.*

At this point, the connections between linear independence of the functions which comprise the rows of the regressor matrix, and persistent excitation can be made by noting that the definition of persistent excitation (Definition I.1) is based on the Grammian matrix. For completeness and easy reference, this connection is summarized in the following theorem:

Theorem IV.3. *(Linearly Independent Functions and Persistent Excitation): Consider the matrix function* $\mathbf{\Phi}(t) : \mathbb{R}^+ \mapsto \mathbb{R}^{n\times m}$ *where the elements of* $\mathbf{\Phi}(t)$ *are bounded for all time,* t*. The regressor matrix* $\mathbf{\Phi}(t)$ *is* ***persistently exciting*** *if, and only if, the rows of* $\mathbf{\Phi}(t)$ *are* ***linearly independent*** *on the interval* $[t,\, t+T]$ *for all* $t \geq 0$ *and some* $T > 0$*.*

Proof: Follows from the Grammian matrix and its properties. ⊠

Our regressor matrix (4.11) is a function of the reference signals, $\tilde{i}_d^r$ and $\tilde{i}_q^r$, as well as the states of the system, i_d^r and i_q^r. However, we may rewrite the states in terms of their corresponding reference signals and tracking errors, i.e.,

$$\mathbf{\Phi}^T = \begin{bmatrix} \vec{\phi}_d^T \\ \vec{\phi}_q^T \end{bmatrix} = \begin{bmatrix} \tilde{i}_d^r & \frac{d}{dt}\tilde{i}_d^r & -\omega_{re}(\tilde{i}_q^r - e_{iq}^r) & 0 \\ \tilde{i}_q^r & \omega_{re}(\tilde{i}_d^r - e_{id}^r) & \frac{d}{dt}\tilde{i}_q^r & \omega_{re} \end{bmatrix}. \tag{4.23}$$

Recall that our analysis in Section 4.4 established that the stator current error is bounded (i.e., $\vec{e}_i^r \in \mathcal{L}_\infty$) and goes to zero asymptotically (i.e., $\vec{e}_i^r \to 0$ as $t \to \infty$). From Lemma 4.8.3 in [28], it follows that if $\vec{\tilde{i}}^r$ is persistently exciting and $\vec{\tilde{i}}^r \in \mathcal{L}_\infty$, then $\vec{\tilde{i}}^r - \vec{e}_i^r$ is persistently exciting. Therefore, we need only consider the properties of the reference signals in our analysis of the regressor matrix (i.e., we will take $\vec{e}_i^r = 0$).

To simplify our analysis, will conservatively assume that the command torque and rotor electrical velocity are constant, i.e., $\tilde{\tau} = \tilde{T}_0$ and $\omega_{re} = \Omega_{re}$, as well as $L_d \approx L_q$. These assumptions represent something of a "worst-case" scenario since time-varying torque references and/or rotor electrical velocity, as well as a significant magnetic saliency, i.e., $L_q >> L_d$, will aid in parameter identification by providing additional excitation; either directly, in the case of a varying torque command (and/or rotor velocity), or indirectly, via coupling between the command currents through the torque expression (4.6) in the presence of a significant magnetic saliency. With respect to the latter, note that for the torque to remain constant in the presence of excitation introduced via the direct-axis dynamics, the quadrature-axis current must vary in an inverse manner, introducing additional excitation to the quadrature axis dynamics. Under these assumptions, we can rewrite the regressor matrix (4.11) as follows,

$$\mathbf{\Phi}(t) = \begin{bmatrix} \tilde{i}_d^r(t) & C_\tau \tilde{T}_0 \\ \frac{d}{dt}\tilde{i}_d^r(t) & \Omega_{re}\tilde{i}_d^r(t) \\ -\Omega_{re} C_\tau \tilde{T}_0 & 0 \\ 0 & \Omega_{re} \end{bmatrix}. \tag{4.24}$$

where C_τ is a positive constant scalar, $C_\tau = \frac{4}{3P\Lambda_{PM}} > 0$. Additionally, we will neglect the reference filter $M(s)$ in our analysis as it has no effect on the results[2]. Without loss of generality, we may take $\tilde{i}_d^r = \sin(\omega t)$:

$$\mathbf{\Phi}(t) = \begin{bmatrix} \sin(\omega t) & C_\tau \tilde{T}_0 \\ \omega \cos(\omega t) & \Omega_{re} \sin(\omega t) \\ -\Omega_{re} C_\tau \tilde{T}_0 & 0 \\ 0 & \Omega_{re} \end{bmatrix}. \tag{4.25}$$

From Theorem IV.3, we may establish necessary and sufficient conditions for the regressor matrix (4.25) to be persistently exciting, by establishing conditions under which the rows of $\mathbf{\Phi}(t)$ in (4.25) are linearly independent. To do this, we will use the following theorem for checking linear independence of functions:

Theorem IV.4. *(Derivative Test [9]): Assume that the $1 \times p$ real-valued continuous functions $\vec{f}_1(t), \vec{f}_2(t), \cdots, \vec{f}_n(t)$ have continuous derivatives up to order $(n-1)$ on the interval $[t_1, t_2]$. Let $\mathbf{F}$ be the $n \times p$ matrix with $\vec{f}_i(t)$ as its i^{th} row, and let $\mathbf{F}^{(k)}$ be the k^{th} derivative of $\mathbf{F}$. If there exists some t_0 in (t_1, t_2) such that the $n \times np$ matrix*

$$\left[\mathbf{F}(t_0) \vdots \mathbf{F}^{(1)}(t_0) \vdots \mathbf{F}^{(2)}(t_0) \vdots \cdots \vdots \mathbf{F}^{(n-1)}(t_0) \right]$$

has rank n, then the functions, $\vec{f}_i(t)$, are linearly independent on the interval $[t_1, t_2]$ over the field of reals.

Since we are interested in sinusoidal inputs, we will consider $t_0 \in [0, \frac{2\pi}{\omega}]$. Applying Theorem IV.4 to (4.25), we take $t_0 = \frac{\pi}{2\omega}$ and compute:

$$\det\left(\left[\mathbf{\Phi}(t_0) \;\; \dot{\mathbf{\Phi}}(t_0) \right] \right) = -C_\tau \tilde{T}_0 \omega^2 \Omega_{re}^3. \tag{4.26}$$

We conclude that the rows of $\mathbf{\Phi}(t)$ are linearly independent on $[0, \frac{2\pi}{\omega}]$, and $\mathbf{\Phi}(t)$ is therefore persistently exciting, provided that:

1. the direct-axis command current, $\tilde{i}_d^r$, has at least one sinusoidal component (i.e., $\omega \neq 0$),

2. the command torque is non-zero, $\tilde{T}_0 \neq 0$,

[2]Given a persistently exciting u with $\dot{u}$ bounded, and a stable, minimum phase, proper transfer function $M(s)$, it follows that $y = M(s)u$ is also persistently exciting [28].

3. the rotor (electrical) velocity is non-zero, $\Omega_{re} \neq 0$.

Remark: It should be noted that, in practice, it is important to normalize the rows of the regressor matrix such that the peak values are all around unity. Otherwise, the wide range of machine parameters, which are separated by orders of magnitude, will lead to convergence issues due to poor numerical conditioning. Note that this scales the corresponding parameter estimates as well.

4.6 Simulation Results

4.6.1 Ideal Case

Simulations using Matlab/Simulink are used to validate the proposed SIC design for PMSMs. We present results for the ideal case first, which assume a "continuous-time" controller implementation, no time delay, and noise-free stator current measurements. Additionally, the inverter is assumed to be ideal in that the sinusoidal voltage commands generated by the control algorithm are fed directly into the machine model.

The proposed control methodology is demonstrated in Figure 4.3, specifically constraining the system state (i.e., the stator currents) to manifolds, $\mathcal{M}$, which correspond to a constant torque output (i.e., zero regulated output error). The adaptive controller is initialized with mismatched parameters and a step-change in the com-

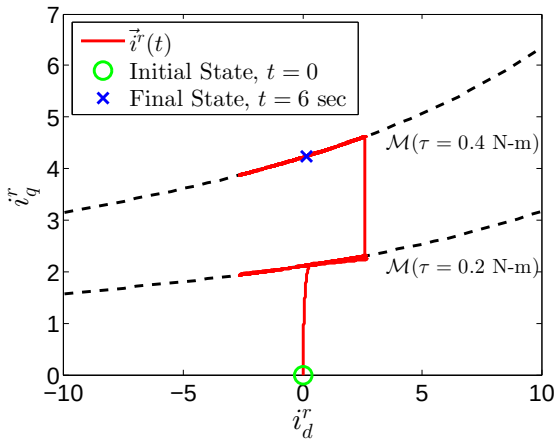

Figure 4.3: Simulation result demonstrating state-trajectory convergence to the desired constant-torque manifolds using the proposed adaptive control design methodology with a step change in the commanded torque from 0.2 N-m to 0.4 N-m at a fixed rotor speed of 2000 RPM.

mand torque occurs 3 seconds into the simulation. Machine parameters which exaggerate the curvature of the manifolds were selected for the purpose of demonstrating the effectiveness of the proposed methodology.

The simulation results presented in Figure 4.4 demonstrate the stagnation of the parameter estimates when there is a lack of persistent excitation ($t \leq 0.75$ sec). Inspection of Fig. 4.4 reveals that, initially, when the direct-axis current and output torque commands are zero, the parameters fail to fully converge, as expected. Additionally, while there is partial convergence at 0.25 seconds due to excitation provided by the step change in command torque, the resistance and direct-axis inductance estimates do not converge quickly and fully until the excitation signal is added at 0.75 seconds. Finally, the black arrows in the "zoomed" plots in Fig. 4.4 point out overshoot in the torque resulting from the lack of parameter convergence.

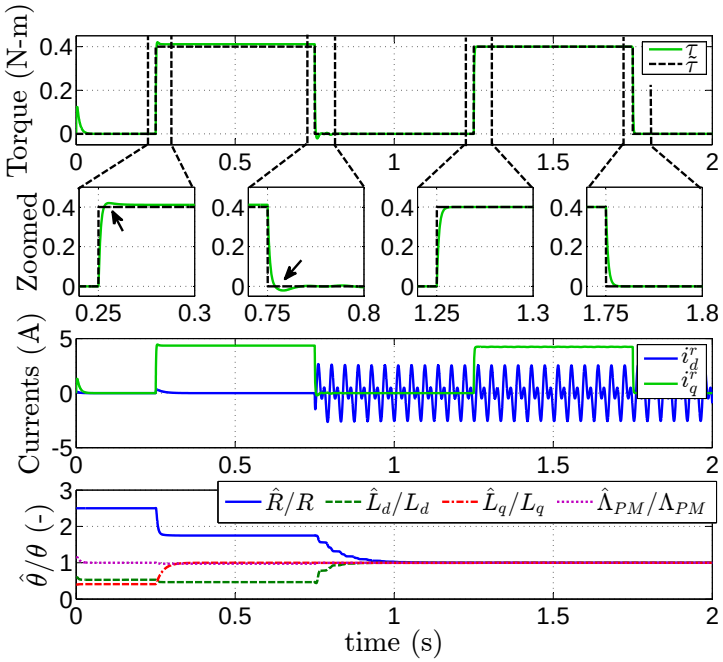

Figure 4.4: Simulation of an ideal implementation of the proposed SIC design for PMSMs demonstrating parameter stagnation due an initial lack of persistent excitation, and the improvement resulting from the introduction of the excitation signal at 0.75 seconds.

4.6.2 Sampled-data Implementation: Time Delay and Compensation

The experimental implementation of the proposed control algorithm must take into account the sampled-data nature of its execution on a microprocessor. In particular, sampling of stator currents and encoder measurements is synchronized with a

center-based pulse-width modulation (PWM) structure to prevent the pickup of electromagnetic interference (EMI) generated by switching transitions during sampling. A consequence of this synchronization is that it leads to a one-switching-period delay between sampling measurements and updating duty cycles, as depicted in Figure 4.5.

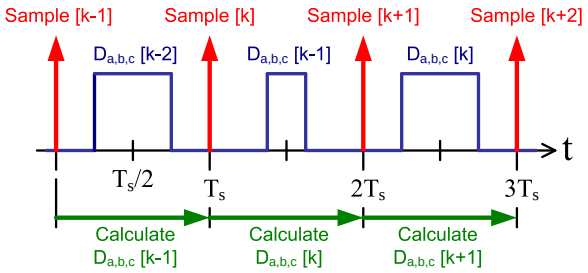

Figure 4.5: Timing sequence of digital controller implementation.

The presence of this time-delay will impose limits on control gains, K_{pd} and K_{pq}. Additionally, the use of reference-frame advancing in the inverse Park transform is required (see Fig. 4.2), as the rotor angular displacement during the delay interval can be significant. This discrepancy between the rotor position at the beginning and at the end of a sample period can lead to instability and parameter drift in the adaptive controller. To compensate for this angular displacement, the rotor position, θ_{re}, at the center of the next sample period is predicted assuming that the rotor velocity, ω_{re}, is constant over the sample period, T_s:

$$\hat{\theta}_{re}[k+1] = \theta_{re}[k] + \frac{3}{2}\omega_{re}[k]T_s, \tag{4.27}$$

where $k = 1, 2, 3...$ represents the discrete time indices. The predicted rotor position (4.27) is then used to compute the inverse Park transform in the discrete-time controller implementation.

To demonstrate the impact that this rotor angle discrepancy has on the parameter estimator, we include the simulation results in Figure 4.6. A "triggered subsystem" is used in Simulink to capture the sampled-data nature of the experimental implementation. The subsystem is triggered by an inverter model which is using center-based PWM at a rate of 8 kHz, like the experimental set-up, and includes a one-time-step delay. The simulation which produced Fig. 4.6 *did not* include reference-frame advancing based on (4.27). The switching-σ modification bounds the parameter estimates. However, inspection of Fig. 4.6 clearly shows that the parameter estimates (particularly resistance and quadrature-axis inductance) are sensitive to this rotor angle error due to the time delay present in the sampled-data implementation.

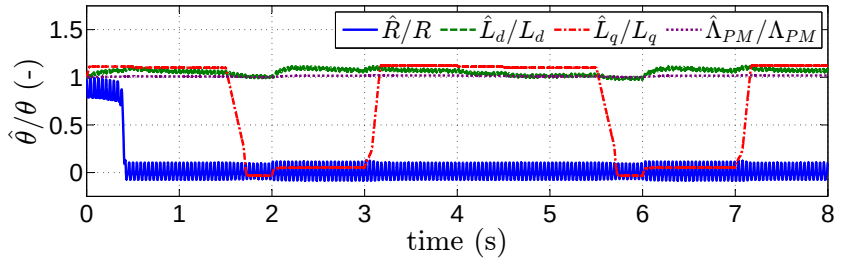

Figure 4.6: Simulation of sampled-data system *without* reference-frame advancing at a speed of 2000 RPM with step changes in command torque (the same as in Fig. 4.7), leading to poor parameter estimator performance.

For comparison (to Fig. 4.6), we include simulation results which include reference-frame advancing based on (4.27) in Figure 4.7. This simulation uses the same Simulink code that was used to generate the experimental code using Real-time Workshop. It should be noted that this simulation did not include dead-time effect [7]. The "nominal" parameters provided in Table 4.1 were used in the PMSM model. Inspection of Fig. 4.7 reveals that the algorithm works as intended under sampled-data conditions, provided that the time delay is compensated via reference-frame advancing.

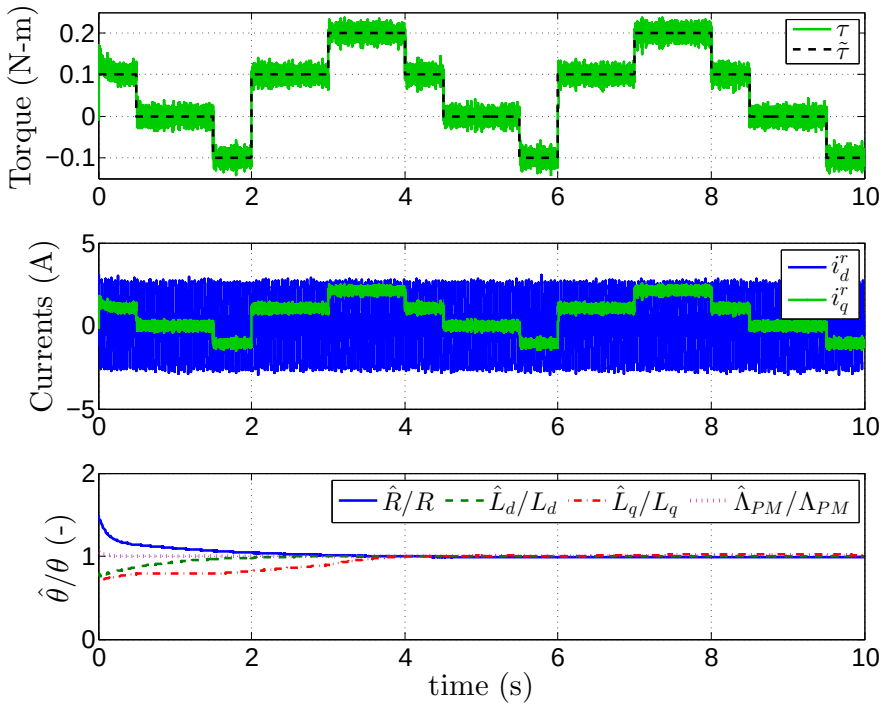

Figure 4.7: Simulation of the proposed adaptive control design in a sampled-data scenario *with* reference-frame advancing based on (4.27) and measurement noise at a rotor speed of 2000 RPM.

4.7 Experimental Validation

4.7.1 Test Machine Parameters

For simulation and comparison purposes, the "nominal" test machine parameters were determined offline using standard techniques. The (DC) stator resistance was measured with a Digital Multi-Meter, inductance with an Agilent E4980A LCR meter, and the permanent magnet flux linkage was identified using an open-circuit test and a linear regression. These nominal parameters, denoted by an overbar, are provided in Table 4.1. We must emphasize that we *do not* expect that the parameter estimates provided by our adaptive controller will converge to these values, since they are not necessarily the *true* physical parameters of the machine. For instance, the resistance measured with a DMM does not account for skin-effect and inverter losses, while the formation of eddy currents in the rotor iron can lead to an error in the measured inductance when using a standard LCR meter.

Table 4.1: "Nominal" test machine parameters.

Parameter	**Value**
Resistance, $\bar{R}$	109 mΩ
Direct-axis self-inductance, $\bar{L}_d$	192 μH
Quadrature-axis self-inductance, $\bar{L}_q$	212 μH
PM Flux Linkage, $\bar{\Lambda}_{PM}$	12.579 mV-s
No. of Poles, P	10

4.7.2 Description of the Experimental Set-up

The proposed robust adaptive control algorithm has been implemented on experimental hardware using a dSPACE DS1104 controller board, and the test machine (Table 4.2) is a 3-phase, 10-pole, 250 watt SMPM machine from MOTORSOLVER with "nominal" parameters (denoted by the over bar) listed in Table 4.1. A 250 watt DC machine from the same manufacturer serves as the load for the SMPM machine.

A power MOSFET inverter is used to drive the motors with a switching frequency of 8 kHz and a bus voltage of 42 VDC. First-harmonic dead-time compensation is used to mitigate the voltage discrepancy resulting from the insertion of dead-time in the gate-drive signals [64]. Duty cycles are calculated using conventional pulse-width-modulation, and the ADC sampling is synchronized with, and offset from, the

center-based PWM signals to avoid sampling during a switching event (as discussed in the previous section).

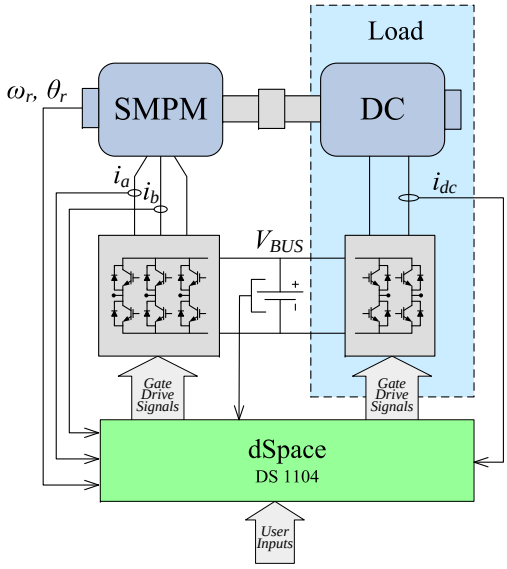

Figure 4.8: Experimental setup.

Table 4.2: Manufacturer machine ratings.

Test Motor	
Type:	PM Brushless
No. Phases:	3
V/I:	42 V/5.7 A
Max. Speed:	4000 RPM
Rated Power:	250 W

Load Motor	
Type:	DC
No. Phases:	N.A.
V/I:	42 V/6 A
Max. Speed:	4000 RPM
Rated Power:	250 W

4.7.3 Experimental Results

Since mechanical torque was not measured during these experiments, the quadrature stator current (in the rotor reference frame) is used to evaluate the transient performance of the proposed torque regulator in addition to the estimated electromagnetic torque (4.28), which can vary with the parameter estimates:

$$\hat{\tau} = \frac{3P}{4}\left[\left(\hat{L}_d - \hat{L}_q\right) i_d^r + \hat{\Lambda}_{PM}\right] i_q^r. \tag{4.28}$$

It should be noted that, since torque is not measured directly, accurate knowledge of the permanent magnet flux linkage, as well as the direct and quadrature self-inductance, is required for accurate torque regulation. Torque steps, used to evaluate

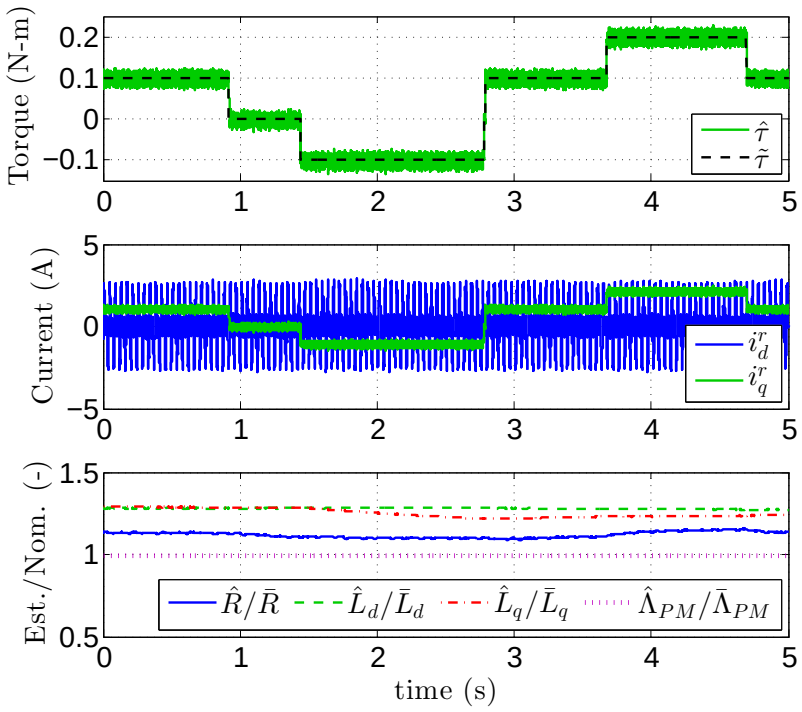

Figure 4.9: Experimental torque steps with adaptation on at 2000 rpm.

the performance of the proposed adaptive torque regulator, are provided in Figures 4.9 and 4.10.

In Fig. 4.9 we see that the estimated torque tracks the commanded value very well without any undesirable jumps or drifting in the parameter estimates. A direct-axis current reference of $\tilde{i}_d^r = 1.5\sin(150t) + 1.5\sin(300t)$ amps provides excitation for parameter estimation. Note that the estimated parameter values have been normalized with respect to their "nominal" values in Table 4.1, which are not necessarily the *true* values (which are unknown), to facilitate plotting on the same axis for comparison.

A feature of the proposed adaptive controller design is that its closed-loop transient response remains consistent across a wide range of operating points. To demonstrate this, torque steps from 0 to 0.4 N-m were performed at 2500, 1200, and 0 RPM[3], and are plotted in Fig. 4.10. Note that the responses overlay, indicating that the controller is performing as expected. Additionally, the "ripple" or "noise" which can be seen in the signals is expected, and is largely due to the non-ideal slotting effects in the machine.

As discussed earlier in this paper, the proposed adaptive control design achieves the simultaneous identification and control objective in that it allows excitation sig-

[3]Voltages begin to saturate due to inverter-created voltage constraints above 2500 RPM.

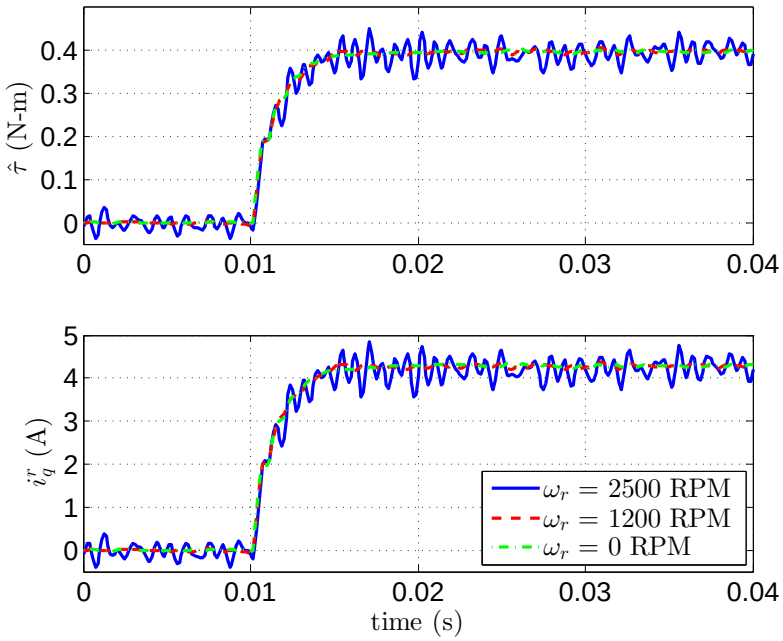

Figure 4.10: Experimental transient responses of estimated torque (*top*) and measured quadrature-axis current (*bottom*) across a wide range of rotor speeds.

nals to be introduced for parameter identification whose impact on the output is minimized (asymptotically, in the case of our design). This property is demonstrated in Figure 4.11, in which the transient response of the experimental adaptive parameter estimator for a constant torque command of 0.2 N-m at a fixed rotor speed of 2000 RPM is plotted. Initially, the parameter values are intentionally mismatched such that the excitation signal disturbs the torque output. Inspection of Fig. 4.11 reveals that, as the estimates converge, the disturbance caused by the excitation signal vanishes, as expected.

To gauge the performance of our parameter identification, we recorded the steady-state values of the estimated parameters over a range of operating points in which the parameters are all identifiable (i.e., non-zero rotor speed and torque command). Inspection of the results in Figure 4.12 indicate that the parameter estimation is working very well overall. The resistance estimate is fairly consistent across rotor speed, but increases slightly with the torque command, potentially due to temperature rise. The estimated direct-axis inductance and permanent magnet flux linkage are very consistent across rotor speed and torque, as expected. The drop in the estimated permanent magnet flux linkage at 500 RPM is likely due to the increasing impact of the dead-time effect at lower speeds (which generally correspond to smaller

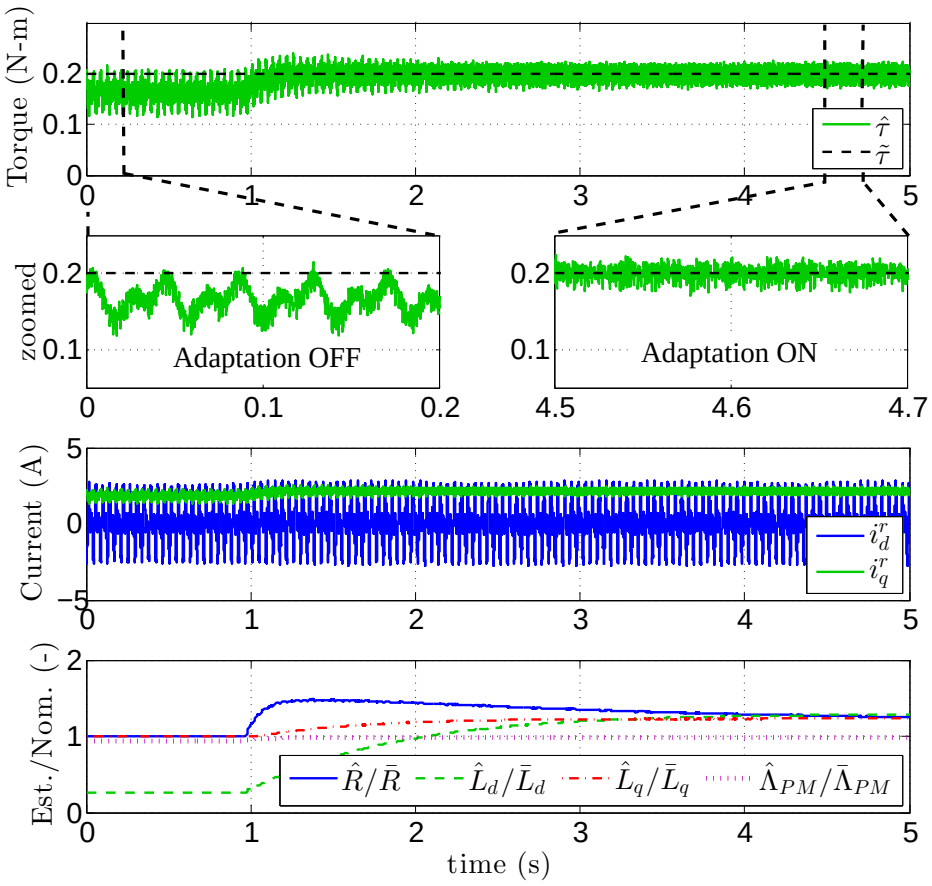

Figure 4.11: Experimental adaptive parameter estimator for a constant torque command of 0.2 N-m at a fixed rotor speed of 2000 RPM demonstrating transient characteristics of the parameter estimator as well as asymptotically vanishing torque perturbation due to the excitation signal.

stator voltages). Finally, the wider variation in the quadrature-axis inductance was anticipated, as this parameter was observed to be particularly sensitive to encoder misalignment while tuning the experimental controller. This behavior was also observed in simulations which introduced a fixed rotor angle offset error. However, we have found that the impact of this variation on the controller performance (i.e., output regulation) is negligible.

Still, it is worth noting that the quadrature-axis inductance estimate seems to improve at higher speeds, yielding a nearly flat trend at 2000 RPM (see Fig. 4.12), and estimates around the same value as the direct-axis inductance. This is to be expected as our test machine was a surface-mount permanent magnet (SMPM) machine which, characteristically, have a negligible magnetic saliency (i.e., it is commonly assumed that $L_d \approx L_q$ for SMPM machines). Recall that under a constant torque command

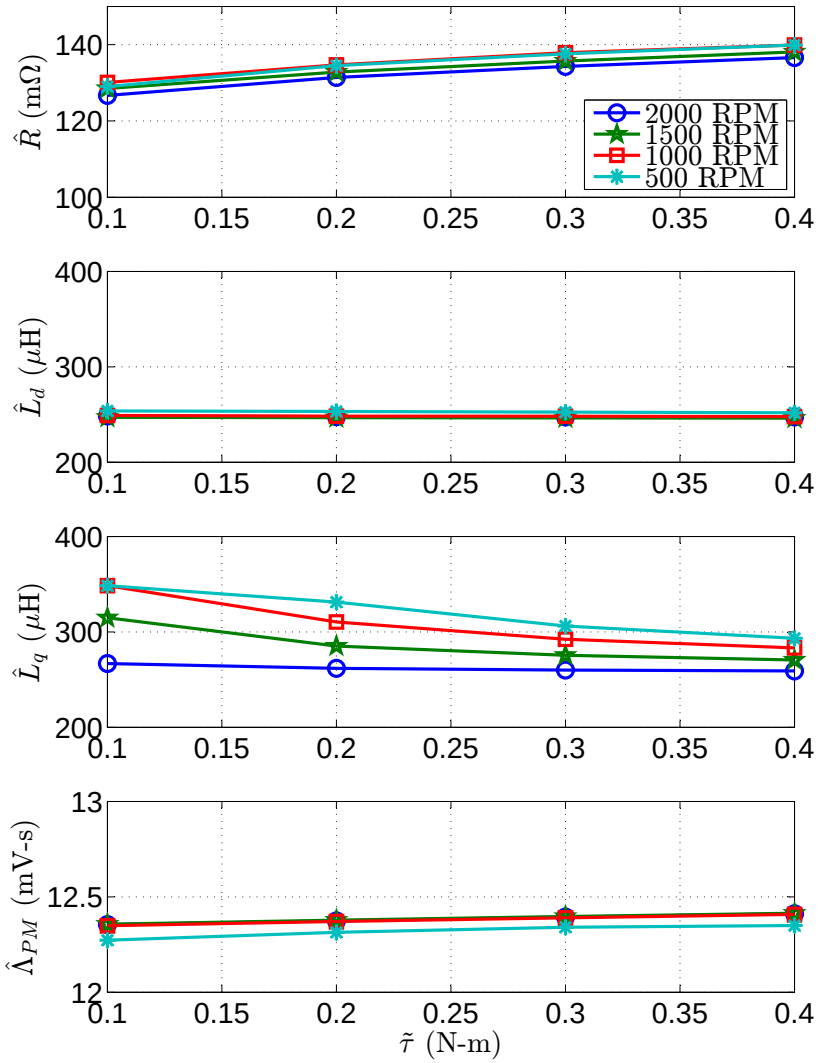

Figure 4.12: Experimental characterization of steady-state parameter estimates over a wide range of rotor speeds and torque commands.

and rotor speed, the third row of the regressor, which relates to the quadrature inductance estimate (see equation (4.25)), is dependent on the following term: $-\Omega_{re}C_{\tau}\tilde{T}_0$. At a minimum, a nonzero torque command, $\tilde{T}_0$, and rotor speed, Ω_{re}, are needed for the regressor to be persistently exciting, otherwise the third row of the regressor will be all zeros and the estimate of quadrature-axis inductance will stagnate. Practically, it is expected that the estimate of the quadrature-axis inductance, L_q, will suffer from drifting in the presence of modeling errors, such as encoder misalignments, at low speeds and/or torque commands. This may explain why the estimate of L_q seems to improve at high speeds, as well as higher torque commands, as observed in Fig. 4.12.

4.8 Chapter Conclusion

This chapter extended results from [66], which presented a new robust adaptive torque regulating controller for SMPM machines that estimates resistance, inductance, and permanent magnet flux linkage online. The adaptive controller for PMSMs presented was derived using Lyapunov's stability theorem, and a robust modification to the derived adaptive law is used to ensure closed-loop stability in the presence of unmodeled disturbances. The control law utilizes a combination of adaptively-tuned feedforward (to achieve zero steady-state error), $d-q$ decoupling (to improve transient response), and proportional feedback (to add robustness to disturbances) terms. Overactuation of the system is exploited to simultaneously achieve parameter convergence and torque regulation. Necessary conditions for persistent excitation were discussed, and simulation results verifying the performance of the control design were presented. Finally, remarks specific to experimental implementation challenges, and experimental results validating the performance of the proposed design, were discussed.

CHAPTER V

Receding Horizon Control Allocation for Simultaneous Identification and Control of PMSMs

5.1 Introduction

Chapters 3 and 4 explored more traditional control designs for achieving SIC in PMSMs with emphasis on exploiting overactuation. In this chapter, we present an optimization-based simultaneous identification and control methodology for achieving the same objective. A receding horizon control allocation (RHCA) is used which includes a metric for maximizing the excitation characteristics of the generated reference current trajectories. The reference currents produced by the RHCA are fed to the lower-level adaptive current regulator, presented in Chapter 4, which ensures asymptotic tracking of a reference model. We begin by discussing the proposed control architecture and introduce the (static) control allocation problem for PMSM torque regulation. Metrics for optimizing the conditioning of the Fisher information matrix and their application to generating persistently exciting inputs are then discussed; as well as the necessary modifications to the control allocation problem, needed for excitation maximization, which lead to the RHCA formulation. Finally, the crucial role of past input and state data in the RHCA-SIC algorithm is discussed, and simulation results demonstrating the effectiveness of the methodology, as well as the need for past data, are presented.

This chapter based on work submitted to a conference and is under review:
D. M. Reed, J. Sun, and H. F. Hofmann, "A Receding Horizon Approach to Simultaneous Identification and Torque Control of Permanent Magnet Synchronous Machines," *Under review,* 2015.

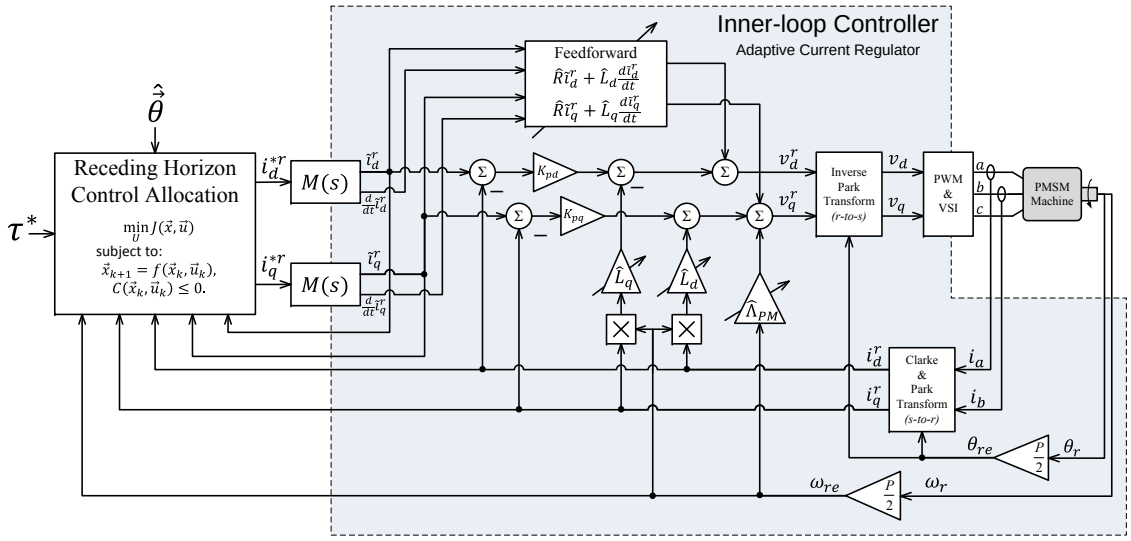

Figure 5.1: Block diagram of the proposed RHCA-SIC methodology for PMSM torque regulation.

5.2 Proposed Control Architecture

The proposed RHCA-SIC design utilizes a two-level structure with reference signals generated by the RHCA being fed to the inner-loop adaptive current regulator, as depicted in Figure 5.1. The adaptive current regulator ensures fast, accurate tracking of the filtered[1] reference current trajectories, while the "outer-loop" RHCA exploits the over-actuated nature of the PMSM to generate reference currents which are both persistently exciting and produce the desired torque. For convenience, we briefly review the inner-loop adaptive current regulator presented in Chapter 4.

5.2.1 Inner-loop Controller

The inner-loop controller is a Lyapunov-based adaptive current regulator [66] which has been extended to include PMSMs (i.e., magnetic saliency is considered). The adaptive current regulator ensures that the 2-phase equivalent stator currents asymptotically converge to track the trajectories produced by the reference models. We define the direct and quadrature stator current errors as follows:

$$\begin{aligned} e_{id}^r &= \tilde{i}_d^r - i_d^r, \\ e_{iq}^r &= \tilde{i}_q^r - i_q^r, \end{aligned} \tag{5.1}$$

[1] By the reference models, $M(s) = \frac{\lambda}{s+\lambda}$.

where the "tilde" ($\tilde{\cdot}$) denotes filtered reference signals, i.e., the output of $M(s)$.

The control law for our adaptive current regulator uses a mix of feedforward, feedback decoupling, and proportional feedback terms, and is given by

$$\begin{aligned} v_d^r &= \hat{R}\tilde{i}_d^r + \hat{L}_d \frac{d\tilde{i}_d^r}{dt} - \omega_{re}\hat{L}_q i_q^r + K_{pd} e_{id}^r, \\ v_q^r &= \hat{R}\tilde{i}_q^r + \hat{L}_q \frac{d\tilde{i}_q^r}{dt} + \omega_{re}\hat{L}_d i_d^r + K_{pq} e_{iq}^r + \omega_{re}\hat{\Lambda}_{PM}, \end{aligned} \tag{5.2}$$

where the "hat" ($\hat{\cdot}$) denotes estimated parameters, K_{pd} and K_{pq} are the respective direct and quadrature-axis proportional gains, and the derivative terms are produced by the reference model (i.e., $\vec{\tilde{i}}^r = \{M(s)\}\,\vec{i}^{*r}$ and $\frac{d}{dt}\vec{\tilde{i}}^r = \{sM(s)\}\,\vec{i}^{*r}$, where $M(s)$ is a a stable, minimum phase, proper, unity dc gain, first-order transfer function[2]).

The estimated parameters in (5.2) are updated via the following adaptive parameter update law

$$\dot{\hat{\vec{\theta}}} = \mathbf{\Gamma}\mathbf{\Phi}\vec{e}_i^r, \tag{5.3}$$

where $\mathbf{\Gamma} = \mathbf{\Gamma}^T > 0$ is the adaptation gain matrix, $\vec{e}_i^r = \begin{bmatrix} e_{id}^r & e_{iq}^r \end{bmatrix}^T$ is the stator current error vector, and the regressor matrix, $\mathbf{\Phi}$, is given by

$$\mathbf{\Phi} = \begin{bmatrix} \tilde{i}_d^r & \tilde{i}_q^r \\ \frac{d}{dt}\tilde{i}_d^r & \omega_{re} i_d^r \\ -\omega_{re} i_q^r & \frac{d}{dt}\tilde{i}_q^r \\ 0 & \omega_{re} \end{bmatrix}. \tag{5.4}$$

It can be shown, using Barbalat's lemma [71] and the following Lyapunov function

$$V(\vec{e}_i^r, \vec{e}_\theta) = \frac{1}{2}\left(\vec{e}_i^{rT}\mathbf{L}\vec{e}_i^r + \vec{e}_\theta{}^T\mathbf{\Gamma}^{-1}\vec{e}_\theta\right), \tag{5.5}$$

that the control law (5.2) with adaptive update (5.3) renders the PMSM dynamics (4.1) stable in the sense of Lyapunov with $\vec{e}_i^r \to 0$ as $t \to \infty$, where $\mathbf{L} = \text{diag}\,[L_d, L_q]$ is a diagonal matrix of the direct and quadrature axis self-inductances, and $\vec{e}_\theta^T = [R \;\; L_d \;\; L_q \;\; \Lambda_{PM}] - \begin{bmatrix} \hat{R} & \hat{L}_d & \hat{L}_q & \hat{\Lambda}_{PM} \end{bmatrix}$ is the parameter error vector. Convergence of the parameter error follows when the regressor matrix (5.4) is persistently exciting. Lastly, we note that a "switching σ-modification" [28] is used on (5.3) for robustness.

[2] $\{\cdot\}$ denotes a dynamic operator with transfer function "$\cdot$".

5.2.2 Control Allocation

The primary objective in any control allocation problem is to find the "best" distribution of control effort among multiple actuators to achieve a desired effect (e.g., generate a "virtual" control input which achieves the desired output). Additionally, by solving the problem online, the effects of actuator saturation and failures can be taken into account. Control allocation is particularly well suited to over-actuated problems which permit the inclusion of secondary objectives, such as control effort minimization.

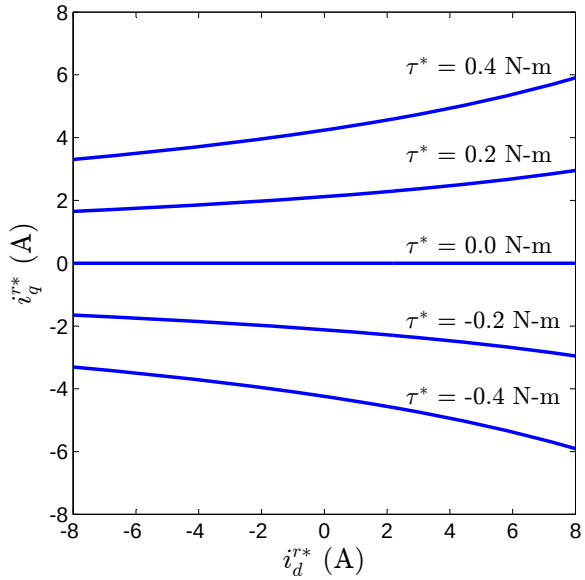

Figure 5.2: Sets of current pairs, (i_d^{*r}, i_q^{*r}), which yield various torques for a machine with large saliency (to magnify nonlinearity).

Typically, the control allocation problem is treated as a static optimization problem, assuming that the "actuator" response is instantaneous [6, 31]. As it concerns torque control for the (over-actuated) PMSM, the control allocation problem consists of finding a reference current pair, (i_d^{*r}, i_q^{*r}), which produce a desired torque, τ^*. The inner-loop controller, discussed in the previous subsection, is then tasked with producing the voltage pair, (v_d^r, v_q^r), which generates these reference currents. Since the problem is over-actuated, there exists an infinite number of reference currents which yield a given torque. The reference current solution set for some τ^* is described by all pairs $(i_d^{*r}, i_q^{*r}) \in \mathcal{M} := \{(i_d^{*r}, i_q^{*r}) \,:\, |\tau^* - h(\vec{i}^{*r}, \vec{\theta})| = 0\}$, and are depicted in Figure 5.2. In discrete-time, the static control allocation problem for a torque-regulated PMSM

can be stated as

$$\begin{aligned} \min_{\vec{i}_k^{*r}} \quad & \vec{i}_k^{*r\,T}\mathbf{R}\vec{i}_k^{*r} \\ \text{s.t.} \quad & |\vec{i}_k^{*r}| \leq I_{max}, \\ & |\tau_k^* - h(\vec{i}_k^{*r}, \hat{\vec{\theta}}_k)| = 0, \end{aligned} \tag{5.6}$$

where our secondary objective is the standard weighted quadratic function of the reference input with $\mathbf{R} > 0$, which minimizes the control effort and, therefore, the ohmic losses as well. While this problem formulation is sufficient for torque regulation, it doesn't ensure persistently exciting reference currents without varying the commanded torque. In the next section, we discuss metrics for persistent excitation and their inclusion in the control allocation problem.

5.3 Receding Horizon Control Allocation for Simultaneous Identification and Control

To ensure that the reference currents generated by the control allocation are persistently exciting, we seek a metric which will provide a measure of how persistently exciting the regressor matrix (5.4) is over some time interval. Such a metric will then be included in the objective (or cost) function of the control allocation problem to encourage the generation of reference signals which are persistently exciting.

5.3.1 The Fisher Information Matrix and Persistent Excitation

The identification of parametric models is of interest to a wide variety of disciplines, well beyond that of the control community. In statistics, as well as other fields, the conditioning of the *Fisher information matrix* is used to judge how *informative* an experiment (i.e., its data) is with respect to the identification of a given parametric model. Mathematically, given N discrete observations (i.e., measurements) of a single output[3], $y(t_k)$, at time t_k with $k \in [1 \cdots N]$, of some process described by

$$y(t_k) = \mathcal{H}(t, \vec{\theta}), \tag{5.7}$$

the Fisher information matrix is defined as

$$\mathbf{F} = \sum_{k=1}^{N} \left(\frac{\partial y(t_k)}{\partial \vec{\theta}} \right)^T \left(\frac{\partial y(t_k)}{\partial \vec{\theta}} \right), \tag{5.8}$$

[3]The extension to multiple outputs is trivial.

where $\vec{\theta}$ is the parameter vector we are interested in identifying. Note that $\mathbf{F}$ is a symmetric positive-semidefinite matrix. When Gaussian noise is considered in the estimation problem formulation, $\mathbf{F}^{-1}$ gives the *Cramer-Rao lower bound* on the achievable covariance of an unbiased estimator. Clearly, if the experiments are not informative, the Fisher information matrix (5.8) will be poorly conditioned, leading to high uncertainty in the parameter estimates.

For processes described by a linear parameterization, e.g.,

$$y(t_k) = \vec{\phi}^T(t)\vec{\theta}, \tag{5.9}$$

the Fisher information matrix (5.8) simplifies to the familiar form used when defining persistent excitation

$$\mathbf{F} = \sum_{k=1}^{N} \vec{\phi}(t_k)\vec{\phi}^T(t_k), \tag{5.10}$$

where $\vec{\phi}(t_k)$ is the *regressor* vector. In discrete-time, a bounded vector signal $\vec{\phi}(t_k)$ is said to be *persistently exciting* (PE) if there exists $N > 0$ and $\alpha_0 > 0$ such that

$$\mathbf{F} = \sum_{k=1}^{N} \vec{\phi}(t_k)\vec{\phi}^T(t_k) \geq \alpha_0 \mathbf{I} \tag{5.11}$$

for all $t_k \geq t_0$ [74].

Finally, we will use the log-determinant of $\mathbf{F}$ as our measure of the conditioning of the Fisher information matrix, i.e.,

$$J_D = \log\left(\det\left(\mathbf{F}\right)\right), \tag{5.12}$$

which is often used for the purpose of "optimal experiment design" (sometimes referred to as "D-optimality") [49, 53].

5.3.2 Receding Horizon Control Allocation for Simultaneous Identification and Control

Since the Fisher information matrix (5.8) becomes singular when evaluated at any given time instant, the addition of a metric for persistent excitation requires modifying the control allocation problem (5.6) to consider a finite time horizon in the optimization, making a receding horizon (or MPC) framework a natural choice. In the past, researchers have proposed receding horizon control allocation (or MPCA)

approaches to account for actuator dynamics, e.g., [51, 78]. In this work, we will utilize the receding horizon control allocation (RHCA) framework to accommodate the addition of the persistent excitation metric (5.12).

Implementation of a RHCA requires a dynamic model of the inner-loop system to predict future state trajectories and evaluate the regressor matrix for optimization. The prediction model is formulated using the certainty equivalence principle; that is, assuming that the estimated parameters are equal to their true values. This turns out to be a minor assumption, however, because we are assured that, as long as the system is persistently excited, the estimated parameters will converge to their true values. Augmenting the reference filter states, $\tilde{\vec{i}}^r$, with the PMSM states, $\vec{i}^r$, the inner-loop dynamics for prediction are therefore given by

$$\begin{aligned} \dot{\vec{x}} &= \bar{\mathbf{A}}(\hat{\vec{\theta}})\vec{x} + \bar{\mathbf{B}}\vec{i}^{*r}, \\ \vec{z} &= \bar{\mathbf{C}}\vec{x} + \bar{\mathbf{D}}\vec{i}^{*r}, \end{aligned} \tag{5.13}$$

with,

$$\bar{\mathbf{A}}(\hat{\vec{\theta}}) = \begin{bmatrix} -\left(\hat{R}\mathbf{I} + \mathbf{K}_p\right)\hat{\mathbf{L}}^{-1} & \left(\hat{R}\mathbf{I} + \mathbf{K}_p\right)\hat{\mathbf{L}}^{-1} - \lambda\mathbf{I} \\ \mathbf{0} & -\lambda\mathbf{I} \end{bmatrix},$$

$$\bar{\mathbf{B}} = \lambda \begin{bmatrix} \mathbf{I} \\ \mathbf{I} \end{bmatrix}, \bar{\mathbf{C}} = -\lambda \begin{bmatrix} \mathbf{0} & \mathbf{I} \end{bmatrix}, \bar{\mathbf{D}} = \lambda\mathbf{I},$$

where $\vec{x}^\top = [\vec{i}^r \ \tilde{\vec{i}}^r]$ is the augmented state vector, $\vec{z} = \frac{d}{dt}\tilde{\vec{i}}^r$ is needed to evaluate the regressor matrix, and so we treat it as an output of the prediction model, and $\lambda > 0$ sets the bandwidth of the (first-order) reference model filters. For the discrete-time implementation, the prediction model (5.13) is discretized using a zero-order hold.

Since the reference currents, $\vec{i}^{*r}$, have no effect on the estimation of the permanent magnet flux linkage[4], Λ_{PM}, we do not include the bottom row of the regressor matrix (5.4), which corresponds to the Λ_{PM} term, in our optimization. We define the truncated regressor matrix, used in the optimization, as follows:

$$\bar{\mathbf{\Phi}}(\vec{x}, \vec{z}) = \begin{bmatrix} \tilde{i}_d^r & \tilde{i}_q^r \\ \frac{d}{dt}\tilde{i}_d^r & \omega_{re} i_d^r \\ -\omega_{re} i_q^r & \frac{d}{dt}\tilde{i}_q^r \end{bmatrix}. \tag{5.14}$$

Assuming the estimated parameters, $\hat{\vec{\theta}}_k$, torque reference, τ_k^*, and rotor electrical

[4]It can be shown that identification of Λ_{PM} only requires a non-zero rotor velocity, i.e., $\omega_{re} \neq 0$.

velocity, $\omega_{re,k}$, to all be constant over the prediction horizon, the extension of (5.6) to include a metric (5.12) for persistent excitation is given by

$$\begin{aligned}
\min_{\vec{i}_j^{*r}} \quad & \sum_{j=k}^{k+N-1} \vec{i}_j^{*r\,T}\mathbf{R}\vec{i}_j^{*r} - \rho \log\det\left(\mathbf{F}(\vec{x},\vec{z})\right) \\
\text{s.t.} \quad & \vec{x}_{j+1} = \bar{\mathbf{A}}(\hat{\vec{\theta}}_k)\vec{x}_j + \bar{\mathbf{B}}\vec{i}_j^{*r}, \\
& \vec{z}_j = \bar{\mathbf{C}}\vec{x}_j + \bar{\mathbf{D}}\vec{i}_j^{*r}, \\
& \mathbf{F}(\vec{x},\vec{z}) = \sum_{j=k}^{k+N-1} \bar{\mathbf{\Phi}}(\vec{x}_j,\vec{z}_j)\bar{\mathbf{\Phi}}^T(\vec{x}_j,\vec{z}_j), \\
& |\vec{i}_j^{*r}| \le I_{max},\ \forall\, j \in [k \cdots k+N-1], \\
& |\tau_k^* - h(\vec{i}_j^{*r}, \hat{\vec{\theta}}_k)| \le \epsilon,\ \forall\, j \in [k \cdots k+N-1],
\end{aligned} \tag{5.15}$$

where $\mathbf{R} \ge 0$ is the input weighting matrix, $\rho \ge 0$ is the PE metric weighting, and $\epsilon > 0$ determines the maximum allowable perturbation in the regulated torque output. While the constraint on the regulated output error could be included in the objective function and penalized[5], the over-actuated nature of our problem permits the use of it as a constraint[6]. We do, however, include it here as a "relaxed" (i.e., inequality) constraint to speed up the numerical optimization, help ensure that a feasible solution exists, and allow for small perturbations in regulated output if it will aid the parameter identification.

5.3.3 The Crucial Role of Past Input and State Data

The standard RHCA formulation defined by (5.15), where only future inputs are considered in calculating the Fisher information matrix, $\mathbf{F}(\vec{x},\vec{z})$, turns out to be problematic in that it fails to generate persistently exciting trajectories. This is due to the fact that (1) the effects of past data are not included in evaluating the Fisher information matrix, and (2) RHCA only implements the first element of the optimizing sequence.

To highlight the importance of incorporating recent past input and state data in the calculation of the Fisher information matrix for maximizing excitation in the receding horizon framework, imagine conditions are such that the optimal predicted

[5]This approach was briefly investigated in numerical simulations, but was found to require very large penalties to achieve reasonable tracking performance which could lead to numerical conditioning issues.

[6]Since we know that, under normal operating conditions, solutions satisfying $|\tau_k^* - h(\vec{i}_{k+i}^{*r}, \hat{\vec{\theta}}_k)| \le \epsilon$ exist.

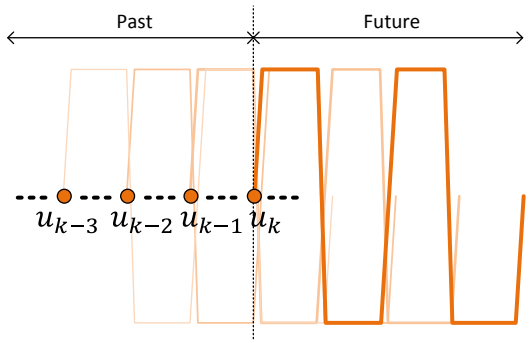

Figure 5.3: Disregard for past input (and state) data leading to a lack of persistent excitation.

input trajectory is the same at every subsequent time step. In the receding horizon (or MPC) framework, only the first step of the optimal sequence is applied at any given time step. So while the optimal predicted sequence may be persistently exciting, the actual sequence applied to the system is very much not persistently exciting. This is depicted graphically in Figure 5.3. When past data is considered, it is clear that the first time step in each subsequent optimal sequence, which will be applied to the system, must differ from the previous to ensure that persistently exciting inputs are indeed generated.

With this issue in mind, we modify the RHCA problem proposed in (5.15) to include N_p points of recent (past) data (i.e., the last N_p values of the states and inputs) in addition to the usual prediction horizon, N_f, in evaluating the Fisher matrix, $\mathbf{F}(\vec{x}, \vec{z})$:

$$
\begin{aligned}
\min_{\vec{i}_j^{*r}} \quad & \sum_{j=k}^{k+N_f-1} \vec{i}_j^{*r\,T} \mathbf{R} \vec{i}_j^{*r} - \rho \log\det\left(\mathbf{F}(\vec{x}, \vec{z})\right) \\
\text{s.t.} \quad & \vec{x}_{j+1} = \bar{\mathbf{A}}(\hat{\vec{\theta}}_k)\vec{x}_j + \bar{\mathbf{B}}\vec{i}_j^{*r}, \\
& \vec{z}_j = \bar{\mathbf{C}}\vec{x}_j + \bar{\mathbf{D}}\vec{i}_j^{*r}, \\
& \mathbf{F}(\vec{x}, \vec{z}) = \sum_{j=k-N_p}^{k+N_f-1} \bar{\mathbf{\Phi}}(\vec{x}_j, \vec{z}_j)\bar{\mathbf{\Phi}}^T(\vec{x}_j, \vec{z}_j), \\
& |\vec{i}_j^{*r}| \leq I_{max},\ \forall\, j \in [k \cdots k+N_f-1], \\
& |\tau_k^* - h(\vec{i}_j^{*r}, \hat{\vec{\theta}}_k)| \leq \epsilon,\ \forall\, j \in [k \cdots k+N_f-1].
\end{aligned}
\tag{5.16}
$$

The change is subtle, but the effects are profound, as will be demonstrated in the simulation results to follow.

Finally, to reduce the dimension of the numerical optimization problem, a linear B-spline is used to approximate the control input [37]. For the purpose of trajectory optimization, the reference currents on the time interval $t_k \in [0, T]$ are given by

$$i_{d,q}^{*r}(t_k) = \sum_{j=0}^{J} \alpha_j \mathcal{B}\left(\bar{t}_k\right), \tag{5.17}$$

where $\bar{t}_k$ is the normalized time sequence, given by

$$\bar{t}_k = \frac{t_k}{T}\frac{J-1}{2} - \frac{j-1}{2},$$

and $\mathcal{B}(\bar{t}_k)$ are the triangular basis functions,

$$\mathcal{B}(\bar{t}_k) = \begin{cases} 1 - 2|\bar{t}_k| & \text{for } |\bar{t}_k| \leq 0.5, \\ 0 & \text{otherwise,} \end{cases}$$

which are precomputed and stored in memory. Thus, we optimize over a vector of the weighting coefficients, α_j, rather than the full resolution time sequence.

Note that a sufficient number of "knot" points (i.e., sufficiently large J) must be used with respect to the length of the time interval, T, to ensure that signals are approximated with sufficient fidelity. The advantages of using a linear spline are that constraints can be enforced simply by looking at the weighting coefficients, α_j, which give the signal value at the knot points[7] and a reduction in the dimension of the optimization problem, speeding up the numerical optimization.

5.4 Simulation Results

Numerical simulations using Matlab/Simulink are used to verify the effectiveness of the proposed receding horizon control allocation methodology for SIC of PMSMs. The simulations capture the sampled-data nature of a practical implementation by implementing the controller in a triggered subsystem which runs at 8 kHz for the inner-loop (high-bandwidth) adaptive current regulator and a quarter of that (i.e., 2 kHz) for the RHCA, while the machine dynamics are solved using *ode45*. An ideal "average-value" inverter model is assumed, that is, the voltage commands generated by the controller are fed directly into the PMSM model. The optimization problem is solved using the active-set algorithm in *fmincon*, and the simulation parameters in

[7]Higher-order polynomial basis functions can lead to "peaking" and constraint violation.

Table 5.1: Simulation parameters.

Description	Value
Electrical Machine Parameters:	
R	109 $m\Omega$
L_d	192 μH
L_q	212 μH
Λ_{PM}	12.579 mV-s
P	10
Control Design Parameters:	
K_{pd}, K_{pq}	0.2
$\mathbf{\Gamma}$	diag([30 30 30 30])
λ	225
$\mathbf{R}$	$0.1 \cdot \mathbf{I}$
ρ	10
Prediction Horizon, N_f	25
No. of Recent Data Points, N_p	25
Simulation Settings:	
Solver	ode45
Max Step Size	25 μ-sec

Table 5.1 were used in all simulations except where otherwise noted.

5.4.1 Static Control Allocation

For completeness, simulation results for the static control allocation problem (5.6) are provided in Figure 5.4. Inspection of the results in Fig. 5.4 reveals that, without a metric for excitation, the control allocation algorithm is simply trying to track the desired torque command using a minimal amount of control effort. Thus, the commanded direct-axis current is essentially zero for the entirety of the simulation, corresponding to a minimal current magnitude operating point. The lack of excitation leads to slow parameter convergence, since excitation is only provided by the step changes in torque. Additionally, the lack of accurate parameter knowledge leads to a small but undesirable overshoot in the transient torque responses (see "zoomed" plots

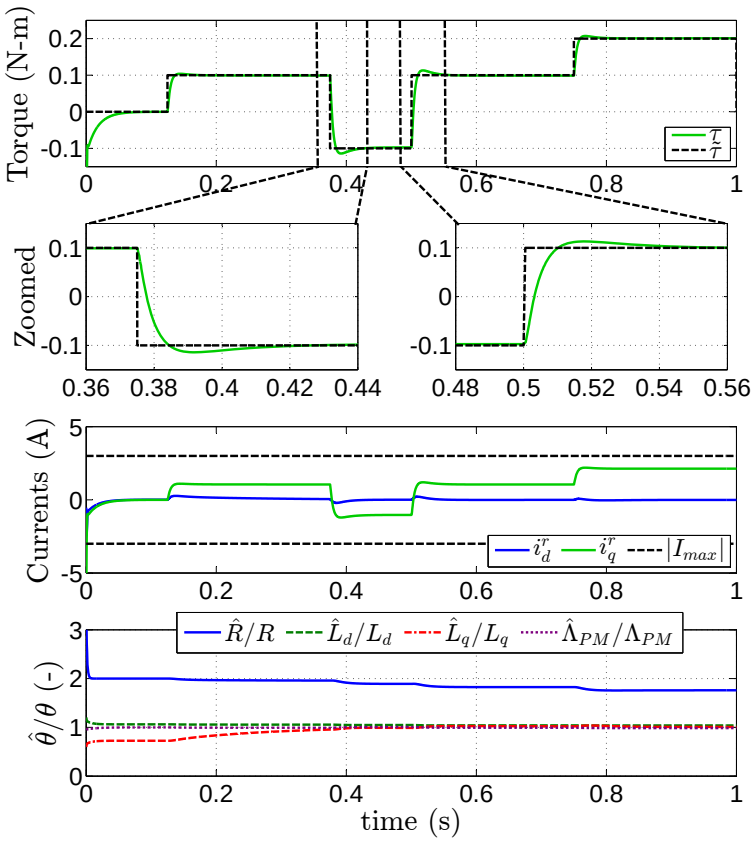

Figure 5.4: Simulation of the static control allocation (5.6) without PE maximization.

in Fig. 5.4). Finally, the steady-state tracking is expected given that the magnetic parameters more or less converge to their true values, and the inner-loop controller is designed to guarantee asymptotic convergence of the stator current error regardless of the accuracy of the parameter estimates.

5.4.2 RHCA-SIC without Past Input and State Data

Again, for completeness, simulation results for the standard RHCA-SIC problem formulation when past input and state data is not considered (5.15) are provided in Figure 5.5. Inspection of the results in Fig. 5.5 reveals that, while the controller does do a good job of tracking the desired torque, the RHCA algorithm fails to generate persistently exciting signals. The lack of persistently exciting inputs once again leads to parameter stagnation.

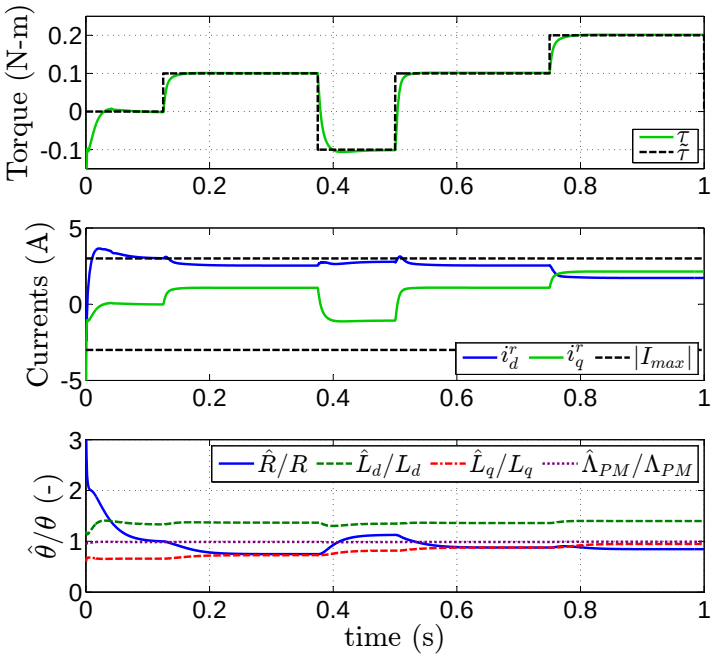

Figure 5.5: Simulation of the RHCA with PE maximization and *without* past input and state data (5.15).

5.4.3 RHCA-SIC with Past Input and State Data

When past input and state data are included in the RHCA (5.16), we see that all of the parameters converge to their true values, as the simulation results in Figure 5.6 demonstrate. Inspection of the results in Fig. 5.6 reveals that, not only does the PE metric with past data generate persistently exciting reference currents, but the overall RHCA-SIC strategy takes advantage of the over-actuated nature of the plant by utilizing the direct-axis current, which has a small impact on the torque production, for the majority of the excitation. Meanwhile, the quadrature-axis current is primarily used to satisfy the torque regulation (i.e., control) objective, agreeing with our intuition about the SIC problem for PMSMs [66, 67].

Note that, while the torque output is initially perturbed by the additional excitation introduced for parameter identification, this perturbation vanishes asymptotically as the parameter estimates converge to their true values. This happens because accurate parameter knowledge is needed in order to accurately define the set $\mathcal{M}$ in which the states may vary without perturbing the regulated output. In addition to the initial perturbations in the regulated output, another trade-off of practical interest is between the losses incurred due to the excitation, and the identification objective which favors large signals (which results in faster convergence). This trade-

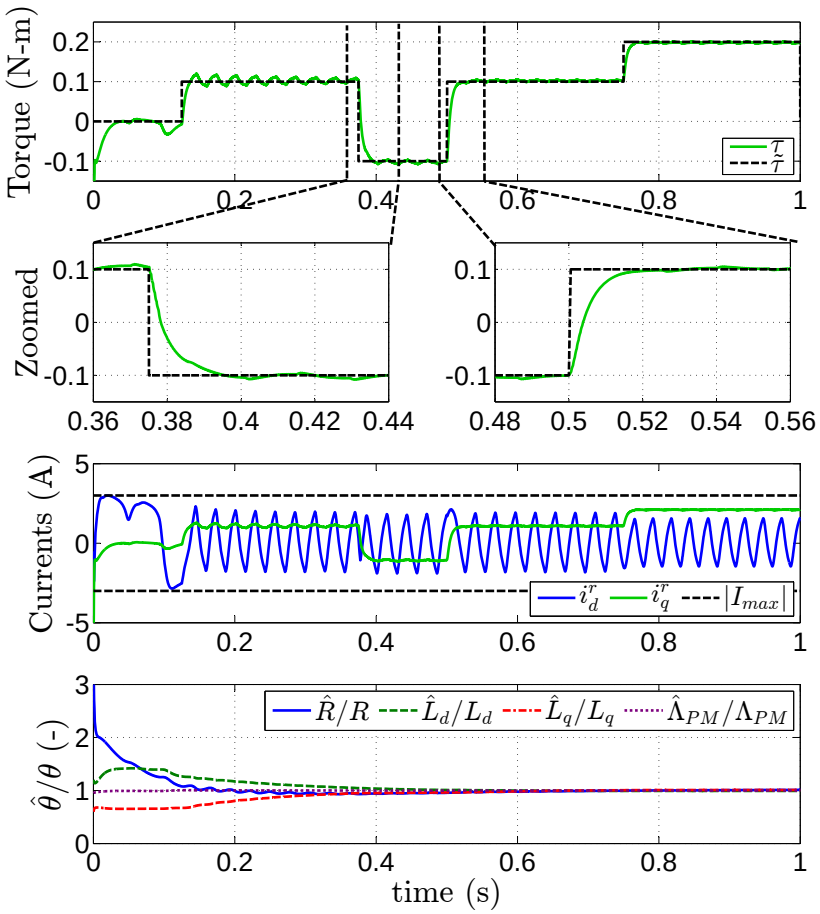

Figure 5.6: Simulation of the proposed RHCA-SIC methodology for over-actuated systems with PE maximization and past data (5.16).

off is managed by adjusting the penalty, $\mathbf{R}$, and the generation of exciting signals can be "turned off" (e.g., after an initial commissioning phase) by setting $\mathbf{R}$ to be the zero matrix. Lastly, while intuition can sometimes be leveraged to decide how the excitation and control efforts should be allocated (e.g., using the direct-axis for excitation and the quadrature-axis for control), as was the case in Chapters 3 and 4, a distinct advantage of the proposed optimization-based RHCA-SIC methodology is that it automatically determines the optimal allocation strategy for SIC in systems where intuition is lacking.

5.5 Conclusion

In this chapter we presented an optimization-based simultaneous identification and control methodology for PMSMs which exploits the overactuated nature of the machine. A receding horizon control allocation (RHCA) framework is used which includes a metric for maximizing the excitation characteristics of the generated reference current trajectories. The RHCA feeds the computed reference currents to a lower-level adaptive current regulator which ensures asymptotic tracking of a reference model. The importance of including past input and state data in the RHCA-SIC algorithm is discussed, and simulation results demonstrating the effectiveness of the proposed RHCA-SIC methodology with past input and state data are presented, as well as scenarios without PE maximization and which disregard past data. Finally, it is worth noting that the optimization problem as posed in this chapter, could lack a feasible solution in the event that either a exceedingly large torque is commanded; or if an exceedingly large load torque is preset, requiring stator current magnitudes beyond the limits of the machine. In this scenario, there is no feasible solution which satisfies both the current limits and output (i.e., torque) error objective. However, by introducing a slack variable (or "soft constraint") [52] on the output error, we can ensure that feasible solutions exist, at the expense of tracking error performance.

CHAPTER VI

Conclusions and Future Work

6.1 Conclusions

6.1.1 Offline Identification of Induction Machine Parameters

In Chapter 2, a new technique for offline identification of induction machine parameters using steady-state data was presented. This work addresses the need for an alternative to the IEEE standard, and one which is well suited to modern VSI drives and the characterization of machines over their full range of operation. The proposed technique is based on fitting experimental data to the circular stator current locus in the stator flux linkage reference-frame for varying steady-state slip frequencies, and provides accurate estimates of the magnetic parameters, as well as the rotor resistance and core loss conductance. Implementation issues related to the sampled-data nature of experimental implementations are considered in the design of the stator flux linkage estimators, as well the compensation of the dead-time effect. Numerical simulations evaluating the accuracy of the estimated parameters in the presence of nonideal effects were presented, and experimental results for a 43 kW induction machine demonstrate the utility of the proposed technique by characterizing the machine over a wide range of flux levels, including magnetic saturation.

6.1.2 Simultaneous Identification and Adaptive Control of PMSMs

In Chapter 3, an adaptive excitation decoupling approach to achieving simultaneous identification and control was explored via a case study with PMSMs. The input(s) which have the most authority over the regulated output are designated the *control input(s)*, while the remaining plant inputs serve as the *excitation input(s)*. A disturbance decoupling control law is then utilized to prevent the excitation input from perturbing the regulated output. The machine parameters used in this excitation

decoupling control law are updated via an online parameter estimator (normalized gradient estimator in this work). Simulation results for a torque regulating controller for PMSMs confirm the effectiveness of the proposed simultaneous identification and control design methodology. While the focus of the chapter is on the application of the proposed adaptive excitation decoupling control methodology to PMSM torque regulation, the prospects of generalizing this methodology for overactuated systems are promising. However, this approach does have some drawbacks. Like the exact feedback linearization techniques [29,33], disturbance decoupling lacks robustness to unmodeled uncertainties. Additionally, the indirect design approach used to formulate the closed-loop adaptive excitation decoupling controller, pairing separately designed control law and parameter identifier, makes proving stability a challenge.

The 2 degree-of-freedom (DOF) Lyapunov design presented in Chapter 4, takes a different approach to achieving the simultaneous identification and control objective. By directly regulating the state to the output zeroing manifold, and ensuring that the invariance condition is satisfied, we are able to achieve the SIC objective by varying the state within this set (the output zeroing manifold) to ensure the system remains excited for identification. To do this, we develop an adaptive control law, using a Lyapunov stability analysis, which ensures that reference trajectories produced by a reference model are tracked asymptotically. Using the torque output mapping (i.e., state to regulated output mapping), we generate the command currents which are fed to the reference models by solving for the required (i.e., command) quadrature-axis current given torque and excitation input commands. The advantages of this approach are that closed-loop stability of the adaptive controller is proven in the design process, as well as the direct regulation of the states.

The SIC approaches presented in Chapters 3 and 4 did not consider optimization of the excitation signal introduced to the system for parameter identification. Additionally, they fixed the allocation of the applied control inputs based on predetermined control input(s), excitation input(s), and regulated output(s). In Chapter 5, we addressed these limitations by modifying the Lyapunov-based design in Chapter 4 to used an optimization-based "front-end". Specifically, the command currents fed to the inner-loop reference models are generated by a receding-horizon control allocation (RHCA), which includes in its cost function a metric to promote the generation of persistently exciting signals. The RHCA considers the output error-zeroing manifold by including it in the constraints. Additionally, the importance of considering past data in the generation of persistently exciting signals is discussed and demonstrated using simulations.

6.2 Future Work

6.2.1 Offline Identification of Induction Machine Parameters

Future work specific to offline identification of induction machine parameters which could be of interest, and potentially improve the performance of the proposed technique, are as follows:

- *Improved inverter models for compensation of additional nonideal effects.* While our use of first-harmonic dead-time compensation partially compensated non-ideal inverter behavior, additional efforts to characterize and compensate dead-time effect, as well as other effects such as conduction losses, would improve the accuracy even further. Additionally, control techniques which require accurate knowledge of the terminal voltages would benefit from such research efforts. Adaptive parameter estimation and sensorless control techniques are particularly sensitive to such discrepancies between the actual and command voltages.

- *Investigation into improved algorithms for circular data fits.* An issue which was observed while testing the parameter identification technique on simulation data was that the sensitivity of the cost function being minimized to variations in the different free variables (horizontal offset, vertical offset, and radius) is highly dependent on the distribution of data around the circular locus. The nature of our application is such that we only get data on the left side of the circular current locus, and often we are not able to span much of the locus before we hit the current limits of the machine. As a result, the computed sensitivities of the horizontal offset and the radius are considerable higher than that of the vertical offset; meaning that the horizontal offset and radius influence the data fit more than the vertical offset. While this isn't a problem for estimating the magnetic parameters (which are derived from the horizontal offset and radius) or rotor resistance (which is computed based on the individual locations of locus points), it did mean that using the estimated center of a fitted circle to compute the core loss conductance would not yield sufficiently accurate results. While we found that using the zero-slip data point alone would yield sufficiently accurate estimates of the core loss conductance, it is possible that introducing weighting into the cost function for the circular fit could improve the accuracy of the estimated core loss conductance.

6.2.2 Simultaneous Identification and Adaptive Control

Future work specific to simultaneous identification and control, for PMSMs and in general, which is of interest is as follows:

- *A generalized methodology for simultaneous identification and control of overactuated systems.* Using the knowledge and intuition gained via case studies, develop a general simultaneous identification and control methodology for some class (or classes) of overactuated systems. While the Adaptive Excitation Decoupling approach proposed and explored in Chapter 3 could be promising for generalization, a closed-loop stability proof remains a challenging result to obtain. Additionally, while we had intuition to guide our selection of excitation and control inputs for the PMSM, this choice is not as straightforward for more general plants. The RHCA-SIC approach presented in Chapter 5, inherently addresses this issue of allocating the excitation (for parameter identification) and control effort via the optimization problem formulation. It therefore likely, that the RHCA-SIC approach is the most promising starting point for developing a generalized methodology. Particularly, if an inner-loop adaptive controller is utilized to ensure closed-loop stability of the plant under control.

- *Application to other overactuated plants of interest.* In this dissertation, we focused on the application of the proposed simultaneous identification and control techniques to torque regulation in PMSMs. While these case studies provided the opportunity to try out ideas on a real system and gain a better understanding of the challenges involved, it would nonetheless be informative to consider other applications as well. For instance, the air-path control problem for turbocharged diesel engines with variable geometry turbines/compressors [86] presents a challenging overactuated control problem of practical interest. Simultaneous identification and control could help improve performance over the lifetime of an engine, while also providing more reliable parameter estimates which could be used for condition monitoring, e.g., indicating mechanical wear in the turbocharger. Inevitably, the consideration of alternative plants will provide additional insight that is likely to motivate improvements to the methodology.

- *Investigation into the influence of horizon window length and position on the generation of persistently exciting inputs and parameter identification.* In Chapter 5, we used a past-data horizon, N_p, which was equal to the prediction horizon, N_f, in our evaluation of the Fisher information matrix. However, this

decision was made somewhat arbitrarily. In fact, the Fisher matrix may be evaluated over any interval of interest, independent of the control allocation prediction horizon. Intuitively, we expect past data to be more valuable than future (i.e., predicted) data in our evaluation of the Fisher matrix for the reasons discussed in Chapter 5. It is therefore of interest, to investigate the influence that the selection of this time interval, its length and positioning (i.e., how much past and future data is included), has on the generation of persistently exciting reference trajectories and parameter identification.

- *Experimental verification of the RHCA-SIC approach for PMSMs.* To better understand the challenges of fielding the RHCA-SIC algorithm, experimental validation is needed. In the simulation results presented in Chapter 5, we had the luxury of "pausing" to solve the optimization problem at each time step. In practice, this optimization problem will have to be solved quickly in real-time. To do so will require an investigation into numerical solution techniques for the constrained optimization problem at hand.

- *Incorporation of voltage constraints in RHCA for PMSMs.* While the case study for PMSMs in Chapter 5 did not include voltage constraints in the problem formulation, it should be straightforward to include them. The voltage constraints on a voltage-source inverter form a convex set, and including them will ensure that the actuation provided by the inverter is fully utilized. Additionally, including voltage constraints in the RHCA will lead the controller to automatically perform field weakening at high-speeds when the drive system is voltage constrained.

BIBLIOGRAPHY

BIBLIOGRAPHY

[1] Tesla Motors. `https://my.teslamotors.com/roadster/technology/motor`. Accessed: 2015-12-02.

[2] Ieee standard test procedure for polyphase induction motors and generators. *IEEE Std 112-2004 (Revision of IEEE Std 112-1996)* (2004).

[3] Abdelhadi, B., Benoudjit, A., and Nait-Said, N. Application of genetic algorithm with a novel adaptive scheme for the identification of induction machine parameters. *Energy Conversion, IEEE Transactions on 20*, 2 (June 2005), 284–291.

[4] Alturas, A., Gadoue, S., Zahawi, B., and Elgendy, M. On the identifiability of steady-state induction machine models using external measurements. *Energy Conversion, IEEE Transactions on PP*, 99 (2015), 1–9.

[5] Aswani, A., Gonzalez, H., Sastry, S. S., and Tomlin, C. Provably safe and robust learning-based model predictive control. *Automatica 49*, 5 (2013), 1216 – 1226.

[6] Bodson, M. Evaluation of Optimization Methods for Control Allocation. *Journal of Guidance, Control, and Dynamics 25*, 4 (July 2002), 703–711.

[7] Bose, B. *Modern Power Electronics and AC Drives*. Prentice Hall PTR, New Jersey, New Jersey, 2002.

[8] Chatterjee, D. Impact of core losses on parameter identification of three-phase induction machines. *Power Electronics, IET 7*, 12 (2014), 3126–3136.

[9] Chen, C.-T. *Linear System Theory and Design*. Holt, Rhinehart, and Winston, New York, 1984.

[10] Chen, Y., and Wang, J. Adaptive vehicle speed control with input injections for longitudinal motion independent road frictional condition estimation. *Vehicular Technology, IEEE Transactions on 60*, 3 (March 2011), 839–848.

[11] Cheng, Y., Haghighat, S., and Di Cairano, S. Robust dual control mpc with application to soft-landing control. In *American Control Conference (ACC), 2015* (July 2015), pp. 3862–3867.

[12] Chiasson, J. *Modeling and High Performance Control of Electric Machines*. IEEE Press Series on Power Engineering. Wiley, 2005.

[13] Delpoux, R., Bodson, M., and Floquet, T. Parameter estimation of permanent magnet stepper motors without mechanical sensors. *Control Engineering Practice 26*, 0 (2014), 178 – 187.

[14] Duesterhoeft, W., Schulz, M. W., and Clarke, E. Determination of instantaneous currents and voltages by means of alpha, beta, and zero components. *American Institute of Electrical Engineers, Transactions of the 70*, 2 (July 1951), 1248–1255.

[15] Feldbaum, A. Dual control theory. *Automation and Remote Control 21*, 9 (1960), 874–1039.

[16] Filatov, N., and Unbehauen, H. *Adaptive Dual Control: Theory and Applications*. Lecture Notes in Control and Information Sciences. Springer Berlin Heidelberg, 2004.

[17] Fitzgerald, A., C. Kingsley, J., and Umans, S. *Electric Machinery*, 6th ed. McGraw-Hill, New York, 2003.

[18] Franklin, G. F., Powell, D. J., and Emami-Naeini, A. *Feedback Control of Dynamic Systems*, 5th ed. Prentice Hall PTR, Upper Saddle River, NJ, USA, 2006.

[19] Genceli, H., and Nikolaou, M. New approach to constrained predictive control with simultaneous model identification. *AIChE Journal 42*, 10 (1996), 2857–2868.

[20] Gonzlez, A., Ferramosca, A., Bustos, G., Marchetti, J., Fiacchini, M., and Odloak, D. Model predictive control suitable for closed-loop re-identification. *Systems and Control Letters 69* (2014), 23–33.

[21] He, Y., Wang, Y., Feng, Y., and Wang, Z. Parameter identification of an induction machine at standstill using the vector constructing method. *Power Electronics, IEEE Transactions on 27*, 2 (Feb 2012), 905–915.

[22] Heirung, T. A. N., Ydstie, B. E., and Foss, B. An adaptive model predictive dual controller. In *Adaptation and Learning in Control and Signal Processing* (2013), vol. 11, pp. 62–67.

[23] Hofmann, H. F., Sanders, S. R., and El-Antably, A. Stator-flux-oriented vector control of synchronous reluctance machines with maximized efficiency. *Industrial Electronics, IEEE Transactions on 51*, 5 (2004), 1066–1072.

[24] Hofmann, H. F., Sanders, S. R., and Sullivan, C. R. Stator-flux-based vector control of induction machines in magnetic saturation. *Industry Applications, IEEE Transactions on 33*, 4 (1997), 935–942.

[25] Holtz, J., and Thimm, T. Identification of the machine parameters in a vector-controlled induction motor drive. *Industry Applications, IEEE Transactions on 27*, 6 (Nov 1991), 1111–1118.

[26] Hou, J., Reed, D. M., Zhou, K., Hofmann, H., and Sun, J. Modeling and test-bed development for an electric drive system with hybrid energy storage. In *ASNE Electric Machines Technology Symposium (EMTS)* (2014).

[27] Ichikawa, S., Tomita, M., Doki, S., and Okuma, S. Sensorless control of permanent-magnet synchronous motors using online parameter identification based on system identification theory. *IEEE Transactions on Industrial Electronics 53*, 2 (April 2006), 363 – 372.

[28] Ioannou, P., and Sun, J. *Robust Adaptive Control*. Prentice Hall, New Jersey, 1996.

[29] Isidori, A. *Nonlinear Control Systems*. Communications and Control Engineering. Springer, 1995.

[30] Jansson, H., and Hjalmarsson, H. Input design via lmis admitting frequency-wise model specifications in confidence regions. *Automatic Control, IEEE Transactions on 50*, 10 (Oct 2005), 1534–1549.

[31] Johansen, T. A., and Fossen, T. I. Control allocationa survey. *Automatica 49*, 5 (2013), 1087–1103.

[32] Kenne, G., Simo, R., Lamnabhi-Lagarrigue, F., Arzande, A., and Vannier, J. An online simplified rotor resistance estimator for induction motors. *Control Systems Technology, IEEE Transactions on 18*, 5 (Sept 2010), 1188–1194.

[33] Khalil, H. *Nonlinear Systems*. Prentice Hall, New Jersey, 2002.

[34] Kim, H., and Lorenz, R. Improved current regulators for ipm machine drives using on-line parameter estimation. In *Industry Applications Conference, 2002. 37th IAS Annual Meeting. Conference Record of the* (Oct 2002), vol. 1, pp. 86–91.

[35] Kojooyan-Jafari, H., Monjo, L., Corcoles, F., and Pedra, J. Parameter estimation of wound-rotor induction motors from transient measurements. *Energy Conversion, IEEE Transactions on 29*, 2 (June 2014), 300–308.

[36] Kokotovic, P., Khalil, H., and O'Reilly, J. *Singular Perturbation Methods in Control Analysis and Design*. SIAM, Pennsylvania, 1999.

[37] Kolmanovsky, I., and Filev, D. Optimal finite and receding horizon control for identification in automotive systems. In *Identification for Automotive Systems*, Lecture Notes in Control and Information Sciences. Springer London, 2012, pp. 327–348.

[38] Kral, C., Habetler, T., Harley, R., Pirker, F., Pascoli, G., Oberguggenberger, H., and Fenz, C.-J. M. Rotor temperature estimation of squirrel-cage induction motors by means of a combined scheme of parameter estimation and a thermal equivalent model. *IEEE Transactions on Industry Applications 40*, 4 (July/August 2004), 1049 – 1057.

[39] Krishnan, R. *Permanent Magnet Synchronous and Brushless DC Motor Drives*. CRC Press, Boca Raton, 2010.

[40] Krishnan, R., and Bharadwaj, A. S. A review of parameter sensitivity and adaptation in indirect vector controlled induction motor drive systems. *IEEE Transactions on Power Electronics 6*, 4 (October 1991), 695–703.

[41] Krishnan, R., and Doran, F. C. Study of parameter sensitivity in high-performance inverter-fed induction motor drive systems. *Industry Applications, IEEE Transactions on IA-23*, 4 (July 1987), 623–635.

[42] Kwon, C., and Sudhoff, S. An on-line rotor resistance estimator for induction machine drives. In *Electric Machines and Drives, 2005 IEEE International Conference on* (May 2005), pp. 391–397.

[43] Kwon, Y.-S., Lee, J.-H., Moon, S.-H., Kwon, B.-K., Choi, C.-H., and Seok, J.-K. Standstill parameter identification of vector-controlled induction motors using the frequency characteristics of rotor bars. *Industry Applications, IEEE Transactions on 45*, 5 (Sept 2009), 1610–1618.

[44] Lee, K.-W., Jung, D.-H., and Ha, I.-J. An online identification method for both stator resistance and back-emf coefficient of pmsms without rotational transducers. *IEEE Transactions on Industrial Electronics 51*, 2 (April 2004), 507 – 510.

[45] Leve, F., and Jah, M. Spacecraft actuator alignment determination through null motion excitation. In *Proceedings of 62nd International Astronautical Congress* (2011).

[46] Lin, W.-M., Su, T.-J., and Wu, R.-C. Parameter identification of induction machine with a starting no-load low-voltage test. *Industrial Electronics, IEEE Transactions on 59*, 1 (Jan 2012), 352–360.

[47] Liu, K., Zhang, Q., Chen, J., Zhu, Z., and Zhang, J. Online multiparameter estimation of nonsalient-pole pm synchronous machines with temperature variation tracking. *IEEE Transactions on Industrial Electronics 58*, 5 (May 2011), 1776 – 1788.

[48] Liu, L., and Cartes, D. Synchronisation based adaptive parameter identification for permanent magnet synchronous motors. *IET Control Theory Applications 1*, 4 (July 2007), 1015 – 1022.

[49] Lobo, M., and Boyd, S. Policies for simultaneous estimation and optimization. In *American Control Conference, 1999. Proceedings of the 1999* (Jun 1999), vol. 2, pp. 958–964 vol.2.

[50] Lorenz, R. A simplified approach to continuous on-line tuning of field-oriented induction machine drives. *IEEE Trans. on Industry Application 26*, 3 (Mar 1990), 420 – 424.

[51] Luo, Y., Serrani, A., Yurkovich, S., Doman, D., and Oppenheimer, M. Dynamic control allocation with asymptotic tracking of time-varying control input commands. In *American Control Conference, 2005. Proceedings of the 2005* (June 2005), pp. 2098–2103 vol. 3.

[52] Maciejowski, J. *Predictive Control: With Constraints*. Pearson Education. Prentice Hall, 2002.

[53] Manchester, I. Input design for system identification via convex relaxation. In *Decision and Control (CDC), 2010 49th IEEE Conference on* (Dec 2010), pp. 2041–2046.

[54] Marafioti, G., Bitmead, R., and Hovd, M. Persistently exciting model predictive control using fir models. In *International Conference Cybernetics and Informatics* (2010).

[55] Marino, R., Peresada, S., and Tomei, P. On-line stator and rotor resistance estimation for induction motors. *Control Systems Technology, IEEE Transactions on 8*, 3 (May 2000), 570–579.

[56] Mohamed, Y. A.-R. I. Design and implementation of a robust current-control scheme for a pmsm vector drive with a simple adaptive disturbance observer. *IEEE Transactions on Industrial Electronics 54*, 4 (August 2007), 1981 – 1988.

[57] Mohan, N., Undeland, T., and Robbins, W. *Power Electronics: Converters, Applications, and Design*, 3rd ed. Wiley, 2003.

[58] Monjo, L., Kojooyan-Jafari, H., Corcoles, F., and Pedra, J. Squirrel-cage induction motor parameter estimation using a variable frequency test. *Energy Conversion, IEEE Transactions on 30*, 2 (June 2015), 550–557.

[59] Park, R. Two-reaction theory of synchronous machines, generalized method of analysis - part 1. *A.I.E.E. Transactions 48* (1929), 81–95.

[60] Proakis, J. G., and Manolakis, D. K. *Digital Signal Processing (4th Edition)*. Prentice-Hall, Inc., Upper Saddle River, NJ, USA, 2006.

[61] Ranta, M., and Hinkkanen, M. Online identification of parameters defining the saturation characteristics of induction machines. *Industry Applications, IEEE Transactions on 49*, 5 (Sept 2013), 2136–2145.

[62] Rathouskỳ, J., and Havlena, V. Mpc-based approximate dual controller by information matrix maximization. *International Journal of Adaptive Control and Signal Processing 27*, 11 (2013), 974–999.

[63] Reed, D., and Hofmann, H. Direct field-oriented control of an induction machine using an adaptive rotor resistance estimator. In *Energy Conversion Congress and Exposition (ECCE), 2010 IEEE* (Sept 2010), pp. 1158–1165.

[64] Reed, D., Zhou, K., Hofmann, H., and Sun, J. A stator current locus approach to induction machine parameter estimation. In *Transportation Electrification Asia-Pacific (ITEC Asia-Pacific), 2014 IEEE Conference and Expo* (Aug 2014), pp. 1–6.

[65] Reed, D. M. Direct field-oriented control of an induction machine using an adaptive rotor resistance estimator. Master's thesis, The Pennsylvania State University, 2009.

[66] Reed, D. M., Sun, J., and Hofmann, H. F. A robust adaptive controller for surface-mount permanent magnet synchronous machines. In *American Control Conference (ACC), 2014* (June 2014), pp. 5236–5241.

[67] Reed, D. M., Sun, J., and Hofmann, H. F. Simultaneous identification and torque regulation of permanent magnet synchronous machines via adaptive excitation decoupling. In *American Control Conference (ACC), 2015* (July 2015), pp. 3224–3229.

[68] Ruan, J., and Wang, S. A prediction error method-based self-commissioning scheme for parameter identification of induction motors in sensorless drives. *Energy Conversion, IEEE Transactions on 30*, 1 (March 2015), 384–393.

[69] Sanders, S., Noworolski, J., Liu, X., and Verghese, G. C. Generalized averaging method for power conversion circuits. *Power Electronics, IEEE Transactions on 6*, 2 (Apr 1991), 251–259.

[70] Shaw, S., and Leeb, S. Identification of induction motor parameters from transient stator current measurements. *Industrial Electronics, IEEE Transactions on 46*, 1 (Feb 1999), 139–149.

[71] Slotine, J.-J. E., and Li, W. *Applied Nonlinear Control*. Prentice Hall, New Jersey, 1991.

[72] Sotomayor, O. A., Odloak, D., and Moro, L. F. Closed-loop model re-identification of processes under {MPC} with zone control. *Control Engineering Practice 17*, 5 (2009), 551 – 563.

[73] Stephan, J., Bodson, M., and Chiasson, J. Real-time estimation of the parameters and fluxes of induction motors. *Industry Applications, IEEE Transactions on 30*, 3 (1994), 746–759.

[74] Tao, G. *Adaptive Control Design and Analysis*. Wiley, 2003.

[75] Toliyat, H., Levi, E., and Raina, M. A review of rfo induction motor parameter estimation techniques. *Energy Conversion, IEEE Transactions on 18*, 2 (June 2003), 271–283.

[76] Umbach, D., and Jones, K. A few methods for fitting circles to data. *Instrumentation and Measurement, IEEE Transactions on 52*, 6 (Dec 2003), 1881–1885.

[77] Underwood, S., and Husain, I. Online parameter estimation and adaptive control of permanent-magnet synchronous machines. *IEEE Transactions on Industrial Electronics 57*, 7 (July 2010), 2435 – 2443.

[78] Vermillion, C., Sun, J., and Butts, K. Model predictive control allocation for overactuated systems - stability and performance. In *Decision and Control, 2007 46th IEEE Conference on* (Dec 2007), pp. 1251–1256.

[79] Wade, S., Dunnigan, M., and Williams, B. Improving the accuracy of the rotor resistance estimate for vector-controlled induction machines. *Electric Power Applications, IEE Proceedings - 144*, 5 (Sep 1997), 285–294.

[80] Wang, K., Chiasson, J., Bodson, M., and Tolbert, L. A nonlinear least-squares approach for identification of the induction motor parameters. *Automatic Control, IEEE Transactions on 50*, 10 (Oct 2005), 1622–1628.

[81] Wang, K., Chiasson, J., Bodson, M., and Tolbert, L. An online rotor time constant estimator for the induction machine. *Control Systems Technology, IEEE Transactions on 15*, 2 (March 2007), 339–348.

[82] Weiss, A., and Di Cairano, S. Robust dual control mpc with guaranteed constraint satisfaction. In *Decision and Control (CDC), 2014 IEEE 53rd Annual Conference on* (Dec 2014), pp. 6713–6718.

[83] Weiss, A., Leve, F., Kolmanovsky, I., and Jah, M. Reaction wheel parameter identification and control through receding horizon-based null motion excitation. In *Advances in Estimation, Navigation, and Spacecraft Control*. Springer Berlin Heidelberg, 2015, pp. 477–494.

[84] Wittenmark, B. Adaptive dual control methods: An overview. In *In 5th IFAC symposium on Adaptive Systems in Control and Signal Processing* (1995), pp. 67–72.

[85] Zai, L.-C., DeMarco, C., and Lipo, T. An extended kalman filter approach to rotor time constant measurement in pwm induction motor drives. *Industry Applications, IEEE Transactions on 28*, 1 (Jan 1992), 96–104.

[86] Zhou, J., Fiorentini, L., Canova, M., and Serrani, A. Dynamic steady-state allocation for over-actuated turbocharged diesel engines. In *Decision and Control (CDC), 2013 IEEE 52nd Annual Conference on* (Dec 2013), pp. 6843–6848.